Hydropower Generation Optimization in the Era of Renewables and Climate Change

By

Mustafa Sahin Dogan

Dissertation

Submitted in partial satisfaction of the requirements for the degree of

Doctor of Philosophy

in

Civil and Environmental Engineering

in the

Office of Graduate Studies

of the

University of California

Davis

Approved:

Jay R. Lund, Chair

Jonathan D. Herman

Josué Medellín-Azuara

Committee in Charge

2019

To my family
İyi ki varsınız...

Contents

List of Figures

List of Tables

Abstract

Hydropower Generation Optimization in the Era of Renewables and Climate Change

Effects of expanding solar energy and non-stationary climate conditions on hydropower generation are explored with a hybrid linear programming-nonlinear programming (LP-NLP) hydropower optimization model. Additional operating algorithms are developed for pumped-storage hydropower optimization. The hybrid LP-NLP model is a reservoir operations model with an objective to maximize overall hydropower revenue. LP models are fast but less accurate, while NLP models are slow but have better nonlinear system representation. In a sequential optimization, the model solves the problem first with a linear approximation, then initializes the NLP model with the LP solution to reduce NLP iterations and runtime. LP and NLP models also can be used stand-alone.

Energy prices are highly correlated with net energy load. Starting 2013, California's solar generation has been increasing to meet its renewable energy targets. As solar generation increases, net load decreases, reducing energy prices during solar generation hours. As a result, dispatchable hydropower becomes less profitable during mid-day hours, shifting hydropower generation to hours 6-10 in the morning and increasing evening peak generation. In the dry season with less inflow availability and higher evening peak prices, operations focus mostly on evening peak hours.

Climate change effects on long-term hydropower planning from 2015 to 2100 with monthly time-step are evaluated with the LP model only as runtime of the NLP model significantly increases with large model sizes of this period. With climate change, temperature increases, more winter precipitation falls as rainfall rather than snowfall, and timing of snowmelt runoff shifts earlier. These changes slightly increase winter hydropower generation, while decreasing spring and early summer generation for hydropower plants with sizable storage capacities, which adds some operating flexibility and adaptability to changing conditions. Plants without storage capacities are more directly affected from climatic changes.

Two algorithms are developed for pumped-storage hydropower (PSH) operations. The first algorithm uses a price-duration curve to find optimal pump and generate thresholds, while the second algorithm uses numerical reservoir system modeling, accounting for water mass balance. The second algorithm also is used to evaluate solar generation effects on PSH operations. With the expansion of solar generation, water is pumped into the upper reservoir during night and solar generation hours with low energy prices, and energy is generated during the morning and evening peak hours with high energy prices.

Acknowledgments

Many people have contributed to this dissertation with ideas and moral support throughout this journey. I would first like to thank my advisor, Dr. Jay Lund, for his advice, mentorship, and insights throughout this dissertation. Thanks also for giving me many other opportunities, including teaching a class, leading workshops, and giving presentations, all of which have contributed to this doctoral research. I am grateful to have him as an advisor. Thanks to Dr. Jon Herman for editorial comments and for introducing Python programming language and data visualization. Since then, I have been enjoying them a lot. Thanks also to Dr. Josué Medellín-Azuara for answering all my questions and providing funding for several research occasions and conferences.

Special thanks to all members of Center for Watershed Sciences and old and current members of Water Systems Research group for providing this wonderful research environment.

I am grateful to my parents, sisters, and nephews, Ali Deniz, Sirac and Cagan. Thanks for your support and patience. I am so lucky to have you all.

This research is financially supported by US-China Clean Energy Research Center, Water Energy Solutions and Technologies (CERC-WET) Program Grant #DE-1A0000018, Associate Instructor funding from CEE department, and Graduate Student Researcher Awards from Jay Lund, Josué Medellín-Azuara, and Jon Herman. Thanks to the Ministry of National Education of the Republic of Turkey for providing me with full scholarship to pursue my academic goals.

Acronyms and Abbreviations

MCM: million cubic meters
BCM: billion cubic meters
MW: megawatt
MWh: megawatt hours
LP: linear programming
NLP: nonlinear programming
CDWR: California Department of Water Resources
CEC: California Energy Commission
CDEC: California Data Exchange Center
CAISO: California Independent System Operator
RCP: representative concentration pathway
GCM: general circulation model or global climate model
VIC: Variable Infiltration Capacity Hydrologic Model
RPS: Renewable Portfolio Standards
PSH: Pumped-storage hydropower

Chapter 1

Introduction and Literature Review

Ranging from small to large-scale, reservoirs can serve single or multiple objectives, including water supply, flood control, environmental protection, recreation, and hydropower. Reservoirs store and regulate water releases for various demands, such as irrigation water during the dry season or hydropower during peak energy demands.

As a limited resource, optimal water allocation is critical. However, optimal multi-stage water allocation is complex and often nonlinear, particularly due to the stochastic nature of reservoir inflows (Mariño & Loaiciga, 1985; Pereira & Pinto, 1985; Kelman et al., 1990; Kim & Palmer, 1997). Inflows vary within and between years (Faber & Stedinger, 2001). There are also uncertainties in water demands, as addressed in Karimanzira et al. (2016), whose predictabilities, however, are sometimes better than hydrologic variables, such as precipitation and runoff. Developing effective operating policies can be challenging when uncertainties affect performance (Tejada-Guibert et al., 1995). Many researchers have focused on evaluating hydrologic uncertainties and reservoir inflow forecasts (Kim & Palmer, 1997; Rangarajan & Simonovic, 1999; Faber & Stedinger, 2001; Hamlet et al., 2002; Tang et al., 2010; Rheinheimer et al., 2016; Wang et al., 2017). Considering all drivers, including inflow, demand and energy prices, the decision criteria in reservoir operations become when and how much to release in the current time-step and store water for later stages, as releasing too much water can cause future shortages and high storages may spill water, depending on hydrology (Pereira & Pinto, 1985).

For hydropower, reservoirs store energy, as higher-elevation water. Using potential energy difference (water head) between reservoir intake and tailwater levels, power is generated by vertical movement of water. Hydropower's lower operating cost (Madani et al., 2014) than most other power sources gives incentive to maximize hydropower generation in a power system with mixed generation sources (Hamlet et al., 2002). Hydropower also can provide operational flexibility by generating power on short notice (Chatterjee et al., 1998; Côté & Leconte, 2016) and additional ancillary services, such as peak and frequency regulation, and spinning reserve (Li et al., 2013). Hydropower plants usually are classified into three forms: a) large-storage, b) low-storage or run-of-river, and c) pumped-storage plants (Pérez-Díaz & Wilhelmi, 2010; Madani et al., 2014), with some plants overlapping these general types. Run-of-river plants run continuously and usually supply base power load, while plants with more storage capabilities and pumped-storage plants are more

dispatchable and regulated for peak demands (Pérez-Díaz & Wilhelmi, 2010).

Despite its advantages and ability to reduce CO_2 emissions, hydropower has ecological and environmental impacts (Bratrich et al., 2004; Viers, 2011). Large dams modify stream flow regimes, block fish migration routes, trap nutrients and sediments, and affect river ecosystems (Bratrich et al., 2004). Studying environmental impacts of hydropower and trade-offs between environmental and hydropower objectives are important tasks, but beyond the scope of this research, even though the developed model, discussed later, can be modified to include environmental in-stream flow requirements.

Figure 1.1 shows California's in-state electric generation capacity (a) and annual average generation (b) portfolios between 2001 and 2017. California, as of 2017, has an in-state installed hydropower capacity of 14 GW, which is roughly 18% of total state installed energy capacity of 80 GW (California Energy Commision, 2018). Most of California's hydropower plants are in the Sierra Nevada (east) and Cascade Range (north) and shown in Figure 1.3. Hydropower generation varies between years, depending on water availability. 2001-2017 annual in-state hydropower generation averages to 31 TWh (California Energy Commision, 2018). Ziaja (2017) discusses California's hydropower system policies and compares of rules and models.

Many algorithms have been developed for reservoir operations and water allocation. Martin (1983); Yeh (1985); Wurbs (1993); Labadie (2004); Ahmad et al. (2014) review reservoir optimization and compare techniques. Similar techniques are applied to hydropower reservoir operations. Most common applications use linear (LP) (Madani & Lund, 2009; Vicuna et al., 2011; Rheinheimer et al., 2016), nonlinear (NLP) (Tejada-Guibert et al., 1990) and dynamic programming (DP) (Grygier & Stedinger, 1985; Mariño & Loaiciga, 1985; Afshar et al., 1990; Zhao et al., 2012; Li et al., 2013) to solve hydropower optimization problems. Stochastic dynamic hydropower optimization models often better represent inflow uncertainty (Pereira & Pinto, 1985; Trezos & Yeh, 1987; Kelman et al., 1990; Tejada-Guibert et al., 1995; Kim & Palmer, 1997; Faber & Stedinger, 2001; Tang et al., 2010; Côté & Leconte, 2016). Turgeon (2007) proposes different solution methods for hydropower reservoir optimization. Turgeon's method is called optimal reservoir trajectory and solves based on raising reservoir storage to be profitable so long as gain from higher head exceeds loss from additional spill. This method, however, is limited to reservoirs on the same river system. Heuristic methods, such as evolutionary algorithms, also are used to optimize hydropower operations (Wu et al., 2016; Wang et al., 2017).

Although dynamic programming (DP) and its variation stochastic dynamic programming (SDP) are popular for hydropower system optimization, the curse of dimensionality (Yakowitz, 1982; Zhao et al., 2012; Feng et al., 2017) and its suitability to a generalized hydropower network solver remain challenging. Linear programming (LP) has advantages of a fast evaluation and finding a globally optimal solution, but nonlinear hydropower optimization problem needs to be simplified to fit a LP formulation, reducing the accuracy of results. NLP needs less simplification, and nonlinear hydropower operations can be well-represented. However, computing time increases exponentially with the number of decision variables. Chapter 2 presents a hybrid linear programming-nonlinear programming (LP-NLP) hydropower optimization model for California.

California generates electricity from various sources (Figure 1.1), with most in-State

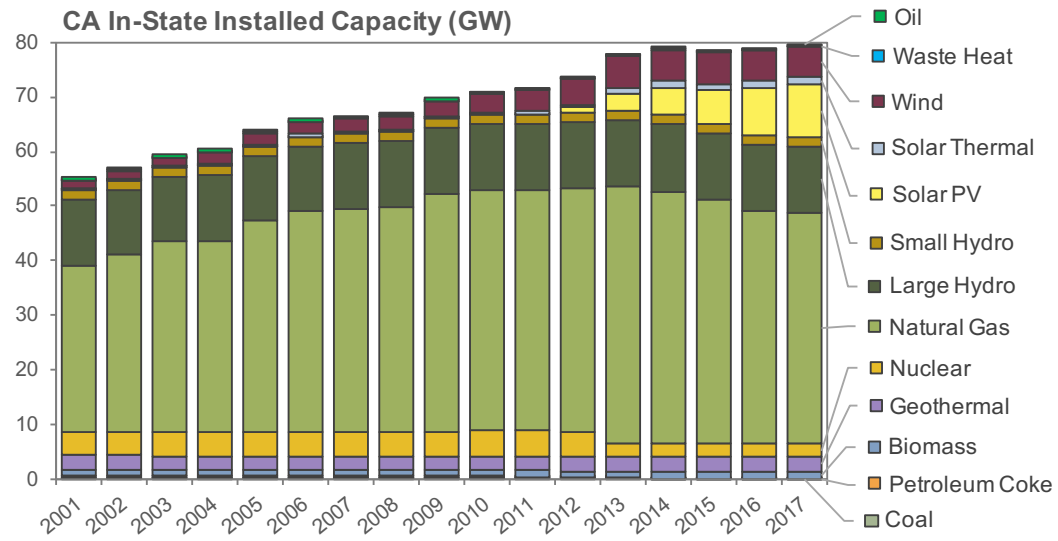

(a) In-state installed capacity (GW)

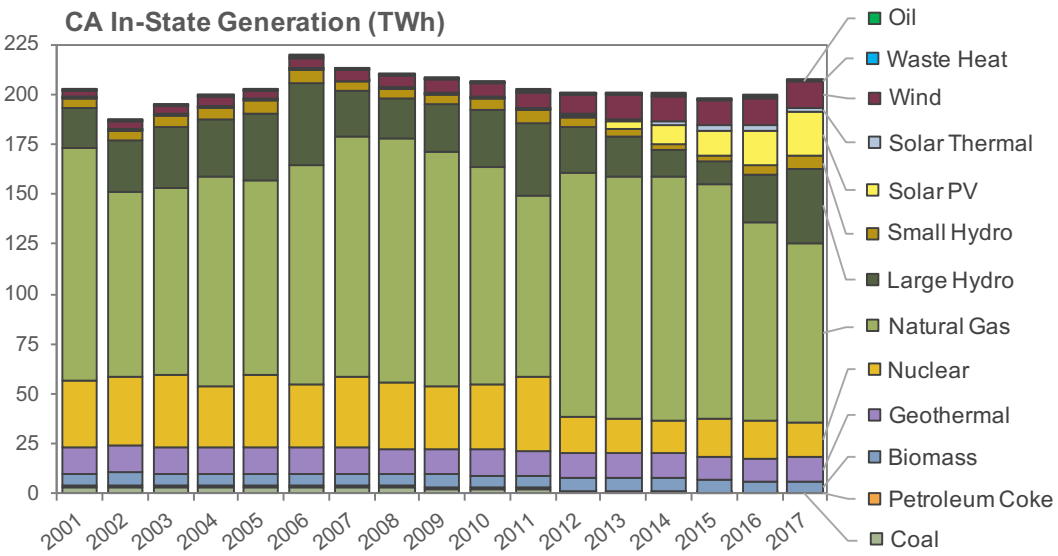

(b) In-state annual average generation (TWh)

Figure 1.1: California's in-state installed energy capacity (a) and annual average generation (b) between 2001 and 2017 (Data source: CEC Energy Almanac)

generation from natural gas. Starting 2012, natural gas and nuclear generation have been declining, while wind and especially solar generation have been increasing. These are all part of California's ambitious clean energy goals, called Renewable Portfolio Standard (RPS) targets, where the state had a renewable generation target of 20% and 25% of total generation in 2013 and 2016, respectively, and the next targets are 33%, 40%, 45%, and 50% by the years 2020, 2024, 2027, and 2030, respectively (California Energy Commision, 2017). In an earlier study, Eichman et al. (2013) show that 50/50 mix of additional solar and wind installation would provide the highest system-wide capacity factor, where large

wind farms provide low cost generation and solar provides more predictable generation. Most of these RPS targets, however, have been met by solar photovoltaic (PV) generation, which significantly affects hourly net load and energy prices with a so-called 'duck demand pattern' (Figure 1.2) for non-solar energy (Denholm et al., 2015). Increased solar generation lowers the back of the duck curve, when solar generation peaks, converting the system from one-daily peak to two-daily peaks. This new price pattern from renewable expansion significantly affects hourly hydropower reservoir operations (Chang et al., 2013). Chapter 3 evaluates effects of this new price pattern on dispatchable hydropower generation and presents adaptations using the hydropower optimization model developed in Chapter 2.

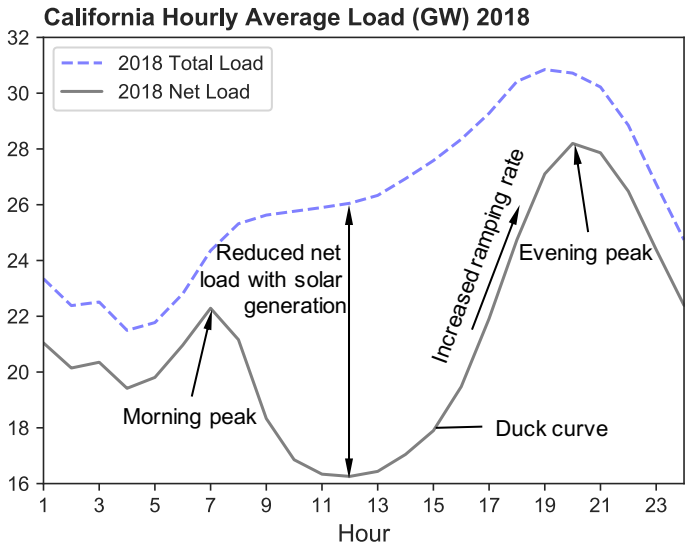

Figure 1.2: Total and net load (total - (solar + wind)) in 2018. Net load is called 'duck curve' due to its shape. (Data source: CAISO)

California's Fourth Climate Assessment Report states that by the end of this century, temperature will increase, sea level will rise and snowpack will decline with "very high" confidence, and frequency of droughts and the intensity of extreme precipitation events will increase with "medium-high" confidence (Bedsworth et al., 2018). This non-stationary climate is expected to shift the timing and magnitude of water availability (Lettenmaier & Sheer, 1991; Miller et al., 2003; Vicuna et al., 2007; Cayan et al., 2008; Vicuna et al., 2010; Dettinger, 2016; Swain et al., 2018). Snowmelt timing is important in California's water operations as snowpack in the Sierra Nevada stores water for water supply and energy demands during summer (Forrest et al., 2018). More precipitation as rainfall and earlier melting of the snowpack from higher temperatures is projected (Pierce et al., 2018), requiring adapting management to these changing conditions (Hanak & Lund, 2012; Herman et al., 2018).

Hydropower generation strictly depends on water availability and is susceptible to any change in runoff timing and magnitude from changed air temperature and precipitation (Mukheibir, 2013; Lanini et al., 2014; Boehlert et al., 2016). When water shortages occur

due to climate change or increased water demand, users will compete for limited water, including hydropower uses (Lin et al., 2013). Optimal water allocation and adaptation to changing conditions are key to maximizing overall objectives and system effectiveness. Climatic changes also should be considered when making investment decisions for new or existing hydropower facilities (Kim et al., 2017).

Madani and Lund (2009), Vicuna et al. (2011), Madani et al. (2014), Rheinheimer et al. (2014), and Rheinheimer and Viers (2015) study effects of climate change focusing on high-elevation hydropower generation with small-storage capacity plants and found that snowmelt runoff shift and precipitation mostly as rainfall rather than snow will have economic and environmental impacts and alter operations. Boehlert et al. (2016) and Forrest et al. (2018) show that hydropower generation in California will increase in winter and decrease in summer with climate change. To evaluate climate change impacts, especially on hydropower plants with sizable storage capacities, which are also more adaptable, the hydropower optimization model developed in Chapter 2 is run for several climate projections with hydropower generation, reservoir operations and investment results, presented in Chapter 4.

Pumped-storage hydropower (PSH) stores water in an upper reservoir during low demand and price hours to generate energy during high demand and price hours (Figueiredo & Flynn, 2006; Bozorg Haddad et al., 2014; Pérez-Díaz et al., 2015; Yang, 2016). Although some energy is lost during pumping and generation, energy price variability makes these plants profitable. PSH systems are dispatchable and improve power reliability in addition to their ancillary services (Figueiredo & Flynn, 2006; Kougias & Szabó, 2017). Barbour et al. (2016) provides a review of PHS development in major energy markets, including Europe, USA, and China. PHS operations are driven solely by hourly energy price variability, but unlike other hydropower types, are less dependent to water availability. The major operating decision is when to pump and generate given efficiencies of pump and turbine and capacities. Chapter 5 presents two algorithms that optimize short-term hourly operations of PSH plants. The first algorithm uses price-duration curves to find optimal operating duration, pump and generate price thresholds, and provides analytical solution to the problem. The second algorithm is more sophisticated and is modified from the reservoir operations model developed in Chapter 2.

This research develops an efficient and flexible hydropower operation and planning model using state-of-the-art optimization modeling techniques. The model is then used to evaluate solar PV and changed price pattern effects on short-term hydropower operations, and climate change effects on long-term hydropower planning and management. Also, separate algorithms are developed for pumped-storage hydropower operations. Research questions of this dissertation include:

- (*Chapter 2*) How to incorporate recent advances in optimization to develop a hybrid model that utilizes advantages of different techniques? Assuming NLP best represents operations, can LP reduce the number of NLP iterations? LP accuracy losses are quantified and discussed.

- (*Chapter 3*) How does solar photovoltaic (PV) generation-changed energy price patterns affect short-term hydropower operations in California?

- (*Chapter 4*) How do future climate projections affect California's long-term hydropower generation and management?

- (*Chapter 5*) How to generate optimum operation (energy generation vs. pumping) strategies for pumed-storage hydropower (PSH)? How does solar generation affect PSH decisions?

The hybrid hydropower optimization model described in Chapter 2 is run for short-term reservoir operations with an hourly time-step to evaluate solar generation effects on hydropower, discussed in Chapter 3. The hybrid model also is run for long-term hydropower planning with a monthly time-step to evaluate climate change impacts, presented in Chapter 4. Finally, a modified version of the hybrid model is applied to PSH, and is compared with another algorithm. This comparison and solar generation effects on PSH are discussed in Chapter 5.

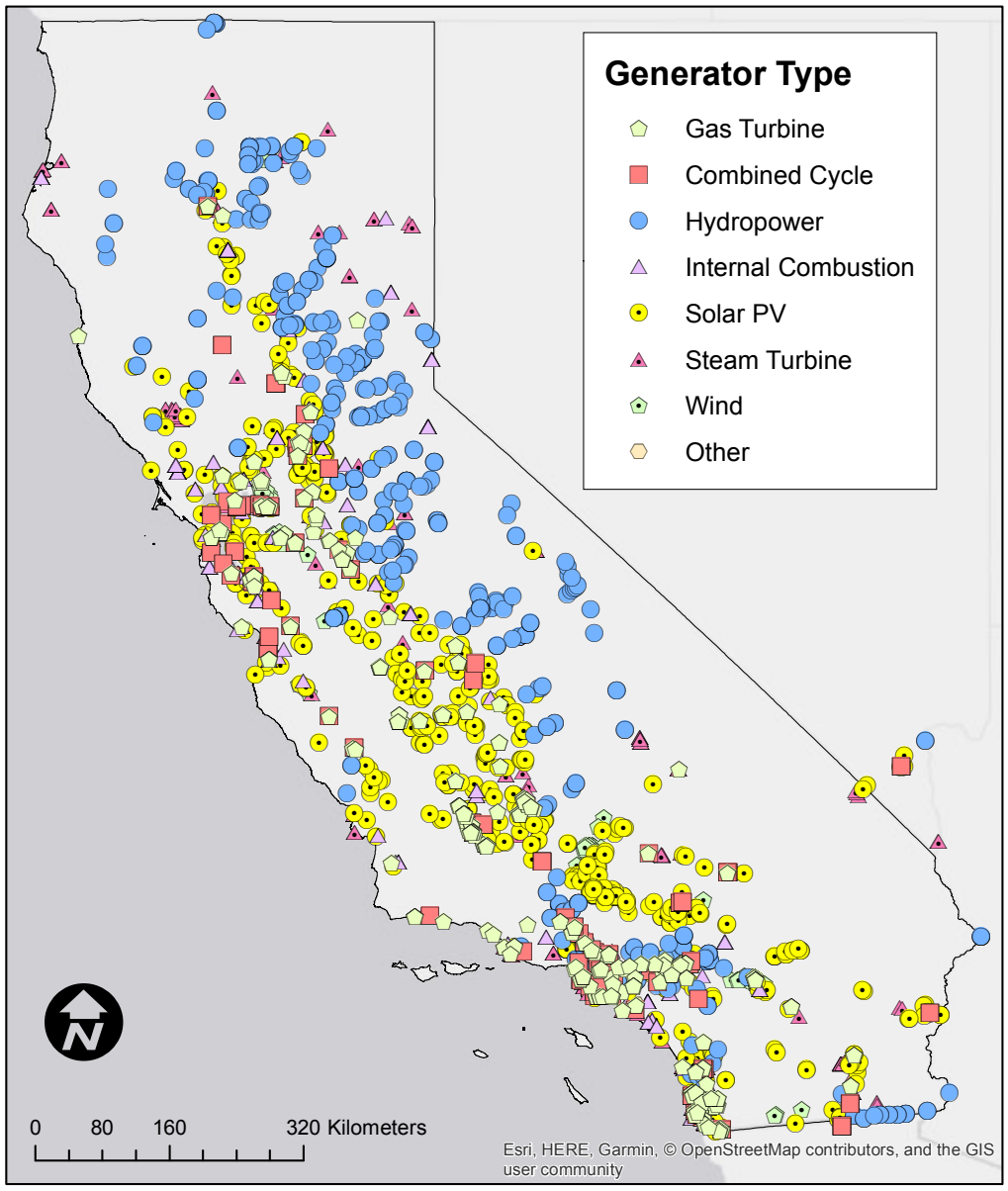

Figure 1.3: California's power generation by source (Data source: CEC)

Chapter 2

Hybrid Linear Programming - Nonlinear Programming for Hydropower Optimization

2.1 Introduction

In a decentralized (or deregulated) energy market, an independent hydropower plant operator seeks to maximize profit (Li et al., 2009). This is done by storing limited water and generating energy during most beneficial hours within available storage capacity (Bushnell, 2003; Olivares & Lund, 2012). Optimizing storage and release schedules of hydropower plants with reservoirs is critical for operational decisions. Plants without sizable storage capability are called run-of-river (Anderson et al., 2015). Run-of-river plants divert a fraction of flow and operate continuously depending on water availability (Garrido et al., 2009; Lazzaro & Botter, 2015). This chapter discusses hydropower optimization with linear and nonlinear programming using the network-flow reservoir system modeling and quantifies accuracy losses and runtime benefits of LP, NLP, and the hybrid LP-NLP models.

2.2 Hydropower Optimization

Hydropower optimization requires representing two key inputs in addition to plant characteristics: reservoir inflow and energy prices. The latter is assumed exogenous, that hydropower operations do not affect energy prices. Inflow and price are assumed to be known with certainty in a deterministic model. Equation 2.1 shows total power generated (Watts) as a function of density of water, ρ (kg/m^3); gravitational constant, g (m/s^2); plant efficiency, η (constant); water head, $H(t)$ (m); and flow through turbines, $Q(t)$ (m^3/s):

$$Power = \rho g \eta H(t) Q(t) \tag{2.1}$$

Integrating power over time, t (hour), in a given period, ΔT, yields generation (Wh):

$$Generation = \int_0^T \rho g \eta H(t) Q(t) dt \tag{2.2}$$

Multiplying generation with energy price, $p(t)$ (\$/Wh) results in hydropower revenue (\$):

$$Revenue = \int_0^T \rho g \eta H(t) Q(t) p(t) dt \tag{2.3}$$

For N power plants in a network, total hydropower revenue (Equation 2.3) from all plants and time-steps can be formulated as:

$$Total\ Revenue = \sum_i^N \sum_t^T \rho g \eta_i H_{i,t} Q_{i,t} p_t \Delta t \tag{2.4}$$

For constant head power plants, head H does not change for a given plant i in time t. However, for variable head power plants with large storage capacity, water head H van be written in terms of storage, resulting in two decision variables: turbine release Q and storage S.

$$Total\ Revenue = \sum_i^N \sum_t^T \rho g \eta_i H(S)_{i,t} Q_{i,t} p_t \Delta t \tag{2.5}$$

Hydropower optimization is a nonlinear problem since water head, H, changes nonlinearly with storage (Equation 2.1). Furthermore, multiplying two decision variables, head as a function of storage $H(S)$ and release Q, adds another layer of nonlinearity. The hybrid LP-NLP model developed in this chapter combines fast evaluation of LP and accurate representation of NLP. In a sequential optimization, a LP model is created and solved first, and then a NLP model of the same problem is solved using LP decision outputs as an initial solution, which reduce the number of iterations and computing time for slower NLP model. In both cases, the deterministic model maximizes hydropower revenue (Equation 2.5), given inflow and energy price. The following sections discuss hydropower optimization, LP and NLP model development, and its application to California's hydropower operations.

2.2.1 Storage-Head Relationship

For a plant with large storage capacity, water head changes with reservoir levels. Head increases if the plant stores water and decreases if storage decreases. Depending on a reservoir site's topography, there is a nonlinear relationship between reservoir water storage, elevation and energy storage. Water head is the difference between reservoir elevation and tailwater race, $H = E_{reservoir} - E_{tailwater}$. Figure 2.1 depicts the power storage and the head as a function of water storage for a rectangular and sloped (trapezoidal) reservoir. For the same water storage and capacity, surface area increases and head decreases with sloped reservoirs. The power storage and the head increases linearly as water storage increase for rectangular reservoirs, while the power storage and the head increases with marginal decrease for sloped reservoirs.

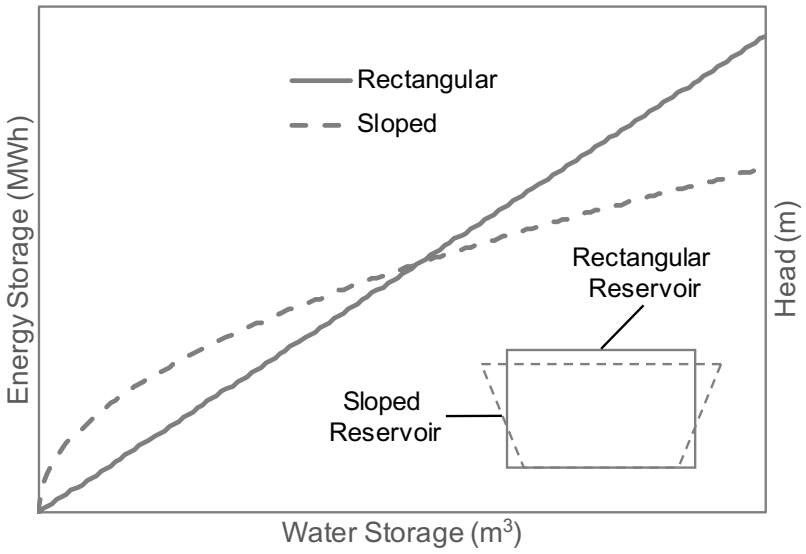

Figure 2.1: Rectangular vs. sloped reservoir power storage and head changes depending on water storage

A third-degree polynomial relationship, suitable for rectangular and sloped reservoirs, is used to represent head as a function of storage for variable head power plants. Polynomial parameters α, β, γ and c are specific for each power plant i and fit using observed storage and elevation data from the California Data Exchange Center (2018).

$$H = \alpha_i S^3 + \beta_i S^2 + \gamma_i S + c_i \tag{2.6}$$

Figure 2.2 shows polynomial relationship between storage and head for selected reservoirs. For large reservoirs, such as Shasta and New Melones, head variations are much higher with a change in storage. Small reservoirs, such as Keswick (downstream of Shasta) and Nimbus (downstream of Folsom), have less head variations. Even though head could be assumed fixed for those small reservoirs, a variable head function (Equation 2.6) is applied. Using polynomial parameters α, β, γ and c as inputs, head H is dynamically calculated as a function of storage. Substituting Equation 2.6 into Equation 2.5 becomes:

$$Total\ Revenue = \sum_{i}^{N} \sum_{t}^{T} \rho g \eta_i (\alpha_i S_{i,t}^3 + \beta_i S_{i,t}^2 + \gamma_i S_{i,t} + c_i) Q_{i,t} p_t \Delta t \tag{2.7}$$

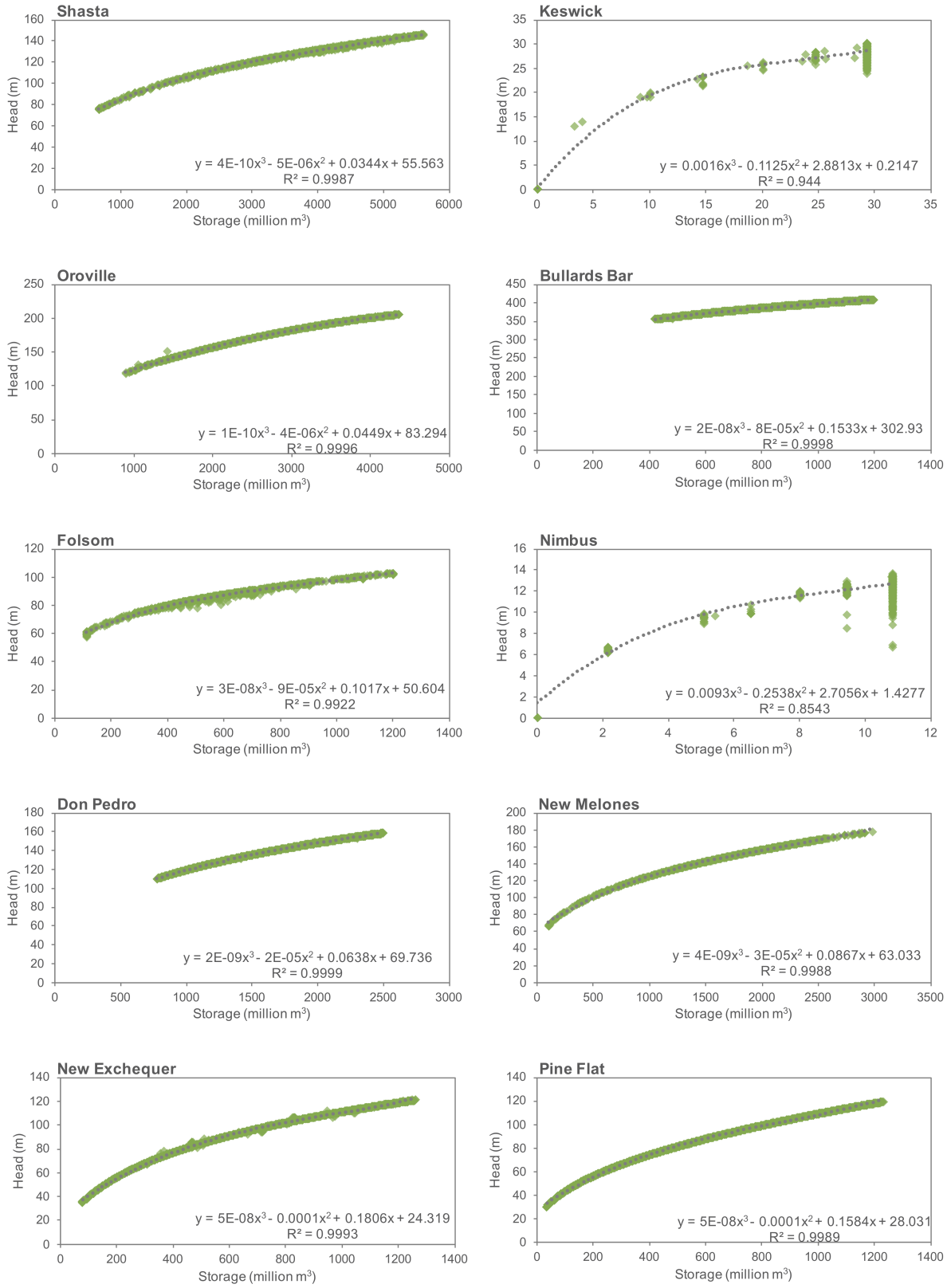

Figure 2.2: Relationship between head ($E_{reservoir} - E_{tailwater}$) and reservoir storage, and polynomial curves (Data source: CDEC)

2.2.2 Generalized Network Flow Representation

Network flow optimization models allocate a commodity carried in the network and common in transportation, transmission, and water resources (Draper et al., 2003, 2004; Bazaraa et al., 2010; Dogan et al., 2018). Optimality criteria can be to minimize the cost of commodity movement and losses or maximize flow and benefits. Since hydropower plants are often connected with streams or canals and water is allocated among them, multireservoir hydropower modeling fits a network flow framework. A typical hydropower network contains nodes and links, where nodes denote power plants and links denote streams, canals or pipelines. General representation of hydropower network flow representation contains objective function to be maximized.

$$\max_{X} \; z = \sum_{i} \sum_{j} f(X_{ij}) \tag{2.8}$$

subject to:

$$X_{ij} \leq u_{ij}, \forall (i,j) \in A \tag{2.9}$$

$$X_{ij} \geq l_{ij}, \forall (i,j) \in A \tag{2.10}$$

$$\sum_{i} X_{ji} - \sum_{i} a_{ij} X_{ij} = 0, \forall j \in N \tag{2.11}$$

where (i, j) indices represent origin and terminal nodes in time and space. X_{ij} is flow from node i to node j (decision variable). $f(X)$ in (Equation 2.8) can be linear or nonlinear objective function. Equations 2.9, 2.10 and 2.11 represent upper bound, lower bound and mass balance constraints, respectively. A denotes matrix of links (arcs), and N denotes matrix of nodes.

Figure 2.3 illustrates a simple hydropower network with two time-steps (t and $t + 1$) and two plants (i and $i + 1$) in serial. Flow carried in the network originates from an artificial node called 'Source' and goes into a node called 'Sink', for which Equation 2.11 is skipped as there are only outgoing links from 'Source' and incoming links to 'Sink.' Adding more physical elements, such as reservoirs and canals, increases the model network horizontally, and adding more time-steps to the network increases the network vertically, where physical network is replicated and only connection between time-steps is reservoir storage from one time-step to the other.

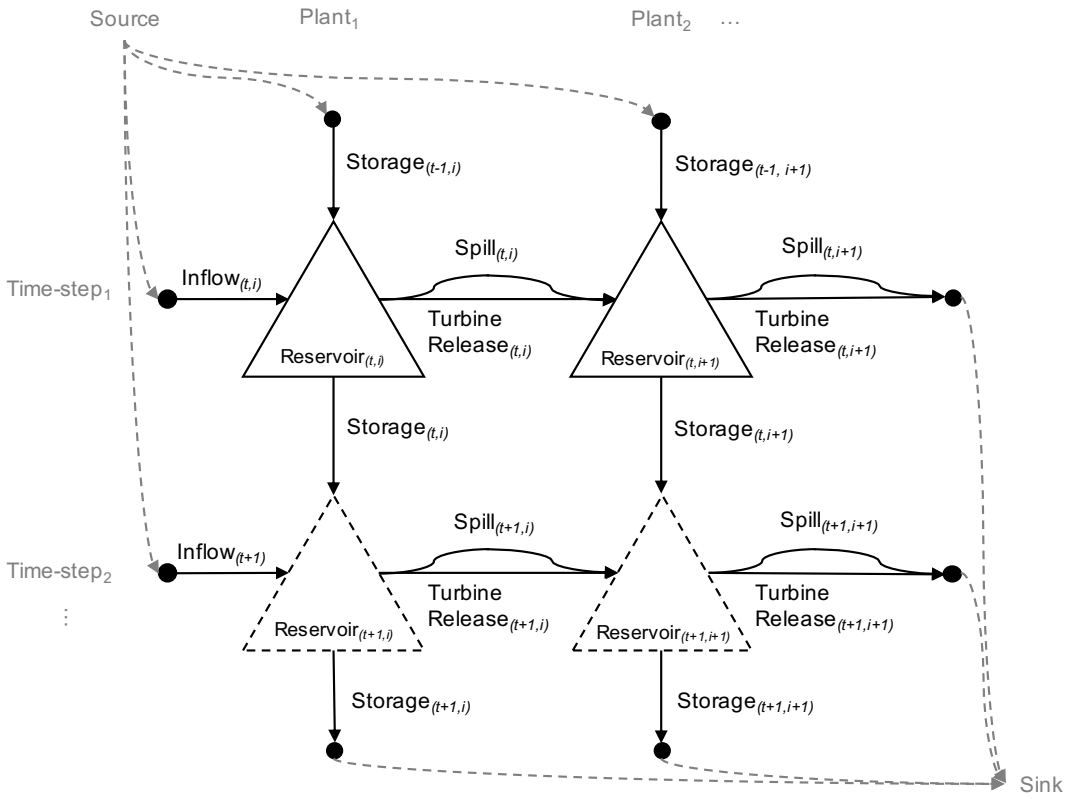

Figure 2.3: Generic network flow representation of the model with two time-steps (t and $t+1$) and two plants (i and $i+1$) in series

Most large-scale water resources models use linear programming, successive linear programming, or dynamic programming as nonlinear programming is computationally expensive (Martin, 1983). CALVIN, a large-scale hydroeconomic optimization model for California's water infrastructure, represents nonlinearities with piecewise linear penalty (or cost) curves, where multiple links are connected from origin node i to terminal node j with varying (convex) unit costs, which has accuracy losses than general linear programming (Draper et al., 2003; Dogan et al., 2018). Lund and Ferreira (1996) and Murk (1996) also use the similar piecewise linear programming to model Missouri and Columbia River system reservoirs.

2.2.3 Nonlinear Programming Model

Hydropower operations are substantially nonlinear, which occurs mostly from changing water head and storage. The Nonlinear Programming (NLP) model dynamically represents water head based on the polynomial relationship (Equation 2.6) and does not require simplifying the objective function or constraints. To calculate head from storage, the NLP model separates flow X and storage Y decision variables. Converting Equation 2.7 into network flow framework, objective function of NLP model becomes:

$$\max_{X,Y} \; z = \sum_{m \in A_F} \sum_{n \in A_S} \rho g \eta_n (\alpha_n Y_n^3 + \beta_n Y_n^2 + \gamma_n Y_n + c_n) X_m p_m \Delta t + \sum_{m \in A_F} p_m X_m \qquad (2.12)$$

subject to

$$X_{ij} \leq u_{ij}, \forall (i,j) \in A_F \tag{2.13}$$

$$Y_{ij} \leq u_{ij}, \forall (i,j) \in A_S \tag{2.14}$$

$$X_{ij} \geq l_{ij}, \forall (i,j) \in A_F \tag{2.15}$$

$$Y_{ij} \geq l_{ij}, \forall (i,j) \in A_S \tag{2.16}$$

$$[\sum_i X_{ji} + \sum_i Y_{ji}] - [\sum_i a_{ij} X_{ij} + \sum_i a_{ij} Y_{ij}] = 0, \forall j \in N_F, N_S \tag{2.17}$$

where m and n represent flow and storage links of the physical network; i and j are origin and terminal nodes in a given link; A_F and A_S are sets of flow and storage links; u is upper and l is lower bound constraints; and a is amplitude used to represent evaporation losses. η is overall plant efficiency. There are two parts in objective function (Equation 2.12): First part represents nonlinear hydropower revenue; the second (linear) part is used to penalize spills. Equations 2.13 - 2.16 enforce upper bound and lower bound constraints on flow and storage links, while 2.17 enforces mass balance at every flow (N_F) or storage (N_S) node j.

The NLP model is solved with IPOPT, an open-source large-scale nonlinear programming solver (Wächter & Biegler, 2006).

2.2.4 Linear Programming Model

The Linear Programming (LP) model simplifies the nonlinear objective function by linearizing Equation 2.7. Instead of dynamically calculating water head, power generation and eventually revenue, the LP model uses prescribed unit benefit values b. These unit benefit values are calculated by fitting a linear surface to nonlinear hydropower revenue curve at each plant and time-step, where coefficient of determination r^2 is maximized (minimizing residuals) shown in Equation 2.18.

$$r^2 = 1 - \frac{SSE}{SST} \tag{2.18}$$

where SSE is sum of squares of errors (or residuals), and SST is total sum of squares, which can be written in a general form as:

$$r^2 = 1 - \frac{\sum_i (y_i - f_i)^2}{\sum_i (y_i - \bar{y})^2} \tag{2.19}$$

$$r^2 = 1 - \frac{\sum_i (Benefit_{NLP,i} - Benefit_{LP,i})^2}{\sum_i (Benefit_{NLP,i} - \frac{1}{N} \sum_i Benefit_{NLP,i})^2} \tag{2.20}$$

where $Benefit_{NLP}$ is calculated using Equation 2.7, and $Benefit_{LP}$ is calculated by optimizing unit benefits (slopes) of flow and storage, b, to maximize r^2 for all plants

and time-steps i. Linear benefits with optimized b, nonlinear benefits and errors between nonlinear and linear benefits are simulated in Figure 2.4. Errors are highest at corner points where storage and releases are maximum (plant capacity). Despite errors in the LP model, both models try to reach maximum storage and release, where benefit is the highest.

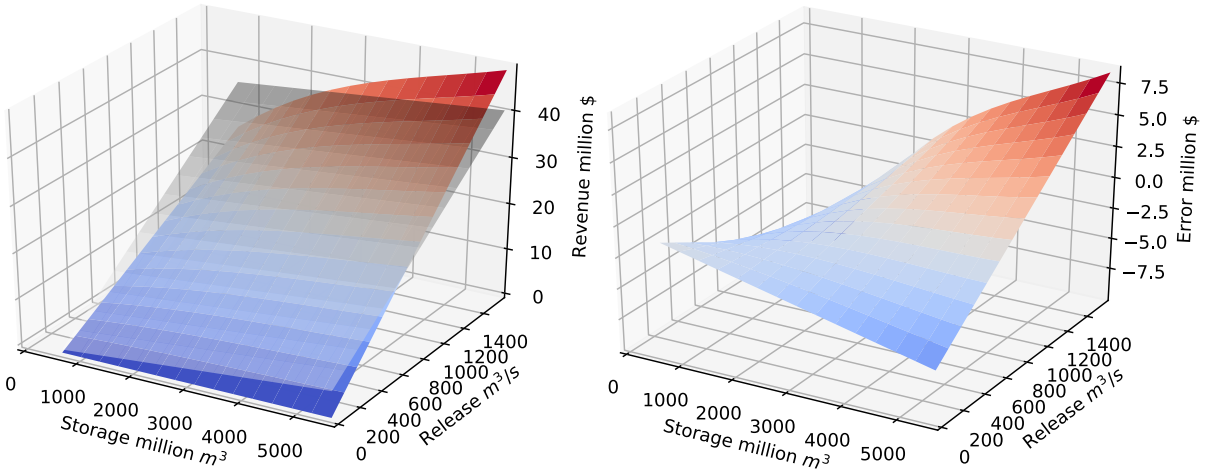

(a) Objective function surfaces

(b) Errors

Figure 2.4: Linear and nonlinear objective functions (benefit curves) and errors showing residuals between nonlinear and linear curves

After calculating b_{ij} by maximizing Equation 2.20, the LP model's objective function and constraints can be written as:

$$\max_{X} \; z = \sum_{i} \sum_{j} b_{ij} X_{ij} \tag{2.21}$$

subject to:

$$X_{ij} \leq u_{ij}, \forall (i,j) \in A \tag{2.22}$$

$$X_{ij} \geq l_{ij}, \forall (i,j) \in A \tag{2.23}$$

$$\sum_{i} X_{ji} - \sum_{i} a_{ij} X_{ij} = 0, \forall j \in N \tag{2.24}$$

where i and j are origin and terminal nodes in space and time; N and L are sets of nodes and links; X is flow (decision variable), b is unit benefit, u is upper, l is lower bound and a is amplitude used to represent losses such as evaporation. The parameter b (negative) also is used to penalize spills. The objective function (Equation 2.21) is a sum of benefits, and Equations 2.22 - 2.24 enforce upper bound, lower bound and mass balance constraints, respectively.

The LP model is solved with the GNU Linear Programming Kit (GLPK), an open-source, large-scale linear programming solver (Free Software Foundation, 2019).

2.3 Application: California

California relies on hydropower for 7% (in 2015) to 47% (in 1983), with an average of 19% (1983-2017), of in-state electricity generation, depending on hydrologic variability (Figure 2.5). Drought years, 1987-1992 and 2012-2015, have less, and wet years, 1983,1997, and 2016, have more hydropower generation. About 74% of California's hydropower is from high elevation plants (Madani & Lund, 2009) in northern and eastern California, and about 63% of total hydropower capacity of 14000 MW is in the Sierra Nevada (Figure 2.6), driven mostly by (often stored) water from snowmelt (Rheinheimer et al., 2014). CEC considers small hydropower (turbine capacity < 30 MW) as a renewable energy source.

The developed model can represent fixed-head (high head, low storage) and variable head (low head, high storage) hydropower plants. As a proof-of-concept model, 11 plants are modeled (Table 2.1). Head is dynamically calculated using Equation 2.6. However, fixed plants could also be represented by eliminating all parameters except c in Equation 2.6. These plants are multipurpose and hydropower generation is often by-product of operations. However, only hydropower objectives are considered here.

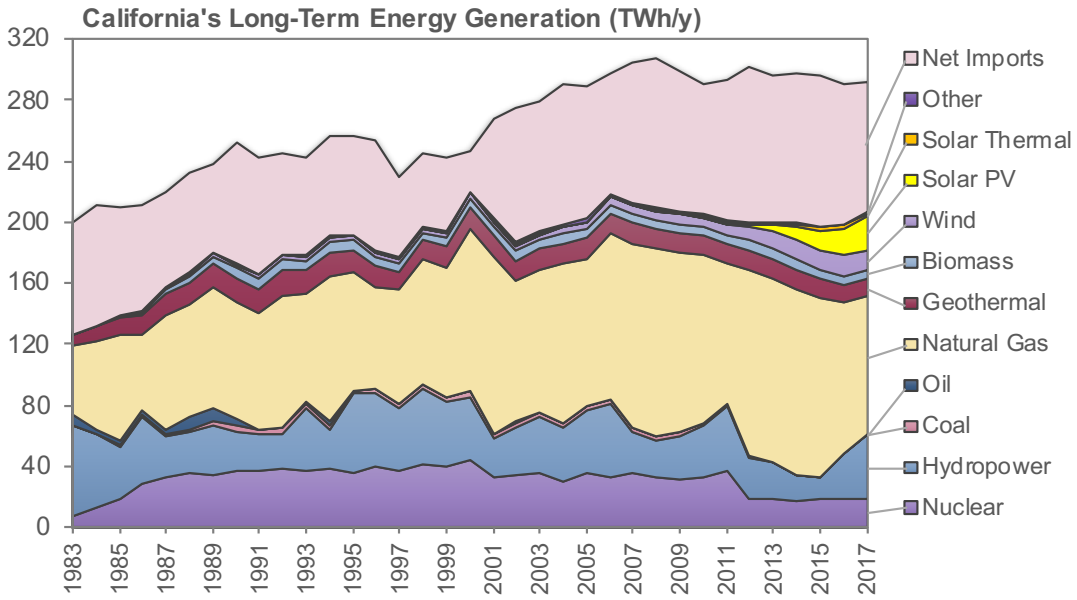

Figure 2.5: Long-term annual average energy generation portfolio of California and imports (Data source: CEC Energy Almanac)

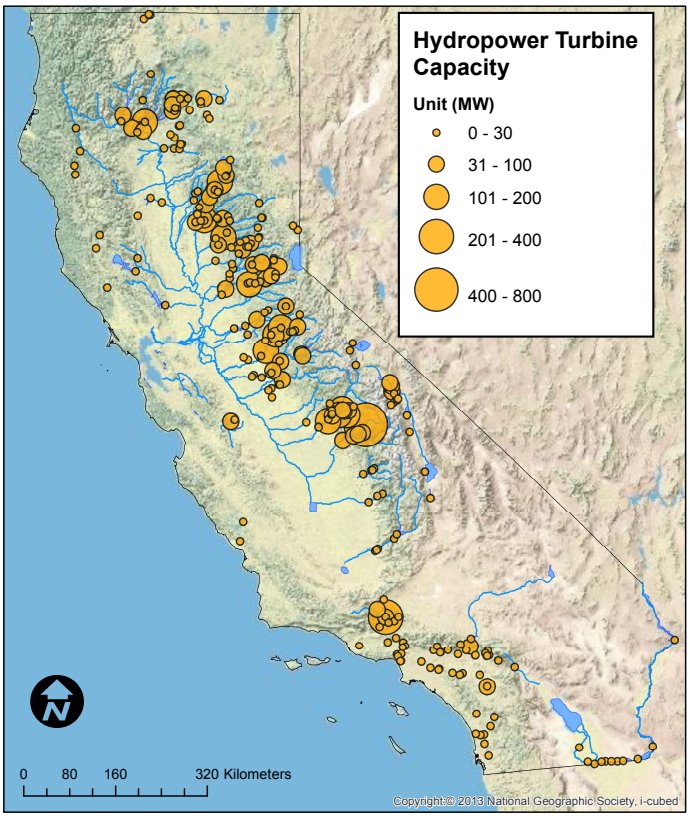

Figure 2.6: California's hydropower plants and capacities for a single turbine unit (Note: some plants have multiple units. Data source: CEC)

2.3.1 Energy Prices

Energy prices are the economic value of unit energy generation in the energy market. The energy market in California consists of an independent system operator (ISO), scheduling coordinators, power exchanges, utility distribution companies, retail marketers, customers and generators (Srivastava et al., 2011). The California Independent System Operator (CAISO) is a non-profit organization, which operates California's wholesale electricity market, where automated auctions are run every day and every five minutes, across 4600 price nodes (locations), dispatching the lowest cost generators to meet demand while ensuring transmission capacity (CAISO, 2018a).

Hourly average wholesale energy prices are obtained from CAISO (2018b). Locational marginal fifteen-minute energy prices are averaged to obtain statewide hourly average energy prices shown in Figure 2.7. Energy prices are lower during off-peak hours (0-6), when demand is lower, and higher during on-peak hours (18-22), when demand is higher. With a price-taking approach, these energy prices ($/MWh) are used as input to calculate hydropower revenues from generation (Equation 2.7).

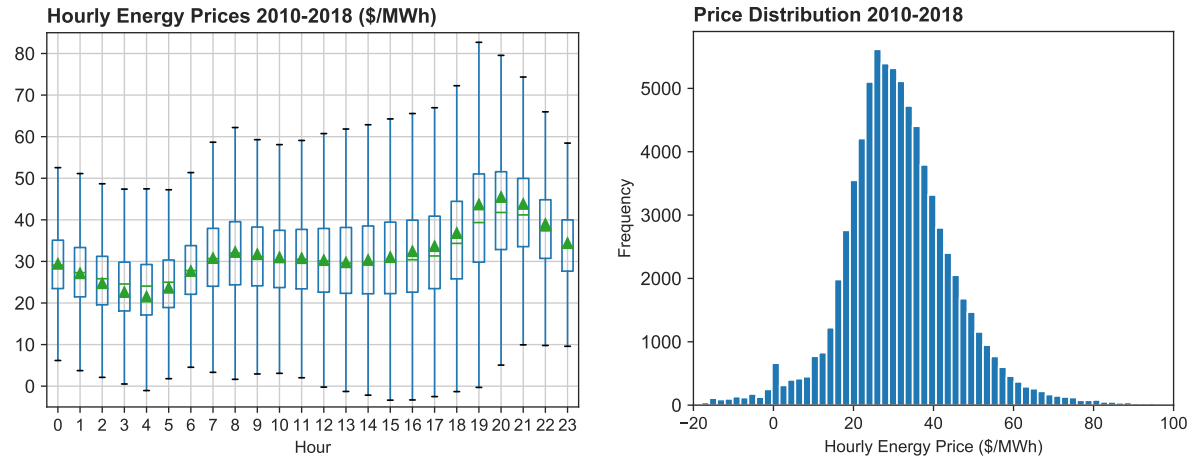

(a) Boxplot of energy prices

(b) Distribution of energy prices

Figure 2.7: Hourly statewide average marginal energy prices of California ($/MWh) between 2010 and 2018 (Data source: CAISO)

2.3.2 Hydrologic Inputs and Plant Characteristics

Hydropower plants operate depending on water availability. So, reservoir inflows are important for modeling. In the deterministic case, inflows are directly used as model inputs. Reservoir inflows represent hydrologic variability across a modeling period. Some models use historical hydrology to represent this variability; others use hydrologic forecasts. Planning models, such as CALVIN, usually use long-term historical hydrology, and operations models often use short-term future forecasts. The developed model can be used for both long-term planning and short-term operating decisions. The model can be run in several time-step lengths, including hourly, daily, weekly, monthly and annual, depending on data availability, and historical hydrology or future forecasts can be used as reservoir inflows. Reservoir inflows with hourly resolution are downloaded from the California Data Exchange Center (2018). Both historical and forecast inflows are represented deterministically in this modeling.

Table 2.1 shows modeled hydropower plants and their characteristics, such as storage and release capacity, deadpool storage, overall efficiency η and polynomial parameters α, β, γ used to dynamically calculate water head from storage.

Table 2.1: Network plants, their properties, and parameters used to dynamically calculate head as a function of storage

Plant	**Plant ID**	**Turbine Cap.** (MW)	**Storage Cap.** ($10^6 m^3$)	**Deadpool** ($10^6 m^3$)	**Release Cap.** (m^3/s)	η	α	β	γ	c
Shasta	SHA	714	5615	662	1584	0.92	3.97E-10	-5.47E-06	0.03	56
Keswick	KES	117	29	0	1703	0.77	1.62E-03	-1.12E-01	2.88	0.2
Oroville (Hyatt)	ORO	644	4364	867	1153	0.86	9.54E-11	-4.29E-06	0.04	83
Bullards Bar (Colgate)	BUL	315	1192	310	105	0.90	2.07E-08	-7.90E-05	0.15	303
Englebright (Narrows II)	ENG	47	86	62	96	0.90	1.2E-05	-4.45E-03	0.80	28
Folsom	FOL	207	1203	111	1109	0.83	3.21E-08	-8.67E-05	0.10	51
Nimbus	NIM	14	11	0	1112	0.78	9.27E-03	-2.54E-01	2.71	1.4
New Melones	NML	300	2985	99	224	0.90	4.33E-09	-2.87E-05	0.09	63
Don Pedro	DNP	203	2504	123	255	0.85	2.00E-09	-1.63E-05	0.06	70
New Exchequer	EXC	95	1264	142	88	0.85	4.98E-08	-1.45E-04	0.18	24
Pine Flat	PNF	165	1233	148	227	0.87	4.72E-08	-1.25E-04	0.16	28

2.3.3 Comparing LP and NLP Models

Both LP and NLP models use the same network structure, similar to Figure 2.3 but with slightly different representation of operations and equations. The NLP model separates flow and storage decisions and dynamically calculates head and hydropower revenue. The LP model has a single decision variable and uses unit benefit values b to calculate total benefit. If all nonlinearities of hydropower optimization can be represented, the NLP model is assumed to perfectly represent operations. With objective function linearization in the LP model, accuracy losses occur. This section compares LP and NLP model outputs to quantify errors and test the LP model.

The LP and NLP models are compared for dry and wet periods. The dry period, with 3,541 decision variables, is from June 1 to September 1, 2018 with a daily time-step and has an average of 23 m^3/s reservoir inflow. The wet period, with 3,466 decision variables, is from January 1 to April 1, 2017 with a daily time-step and has an average of 310 m^3/s reservoir inflow. Initial and ending storage values are set to half of the storage capacity for modeled reservoirs. Differences on decision variable outputs (Figure 2.8) are due to residuals (errors) shown in Figure 2.4-(b). Despite the same network and properties, different objective functions drive operations, resulting in output differences. The NLP model has a fuller system representation, while the LP model employs unit benefit values. Negative values in Figure 2.8 show that the LP model over-estimates storage and release decisions about 17% of the time for the dry period and 10% of the time for the wet period. Positive values show the LP model under-estimating at roughly 2% and 25% of time, for wet and dry periods, respectively. At the remaining times, the NLP and LP outputs are similar ($\pm E-05$). The LP model slightly over-estimates in dry periods and under-estimates in wet periods in both duration and magnitude. As the hydrology becomes wetter, the LP model's under-estimation increases, and with a drier hydrology, the LP model's over-estimation increases. The LP model is the least reliable in high storage and low release, and low storage and high release conditions.

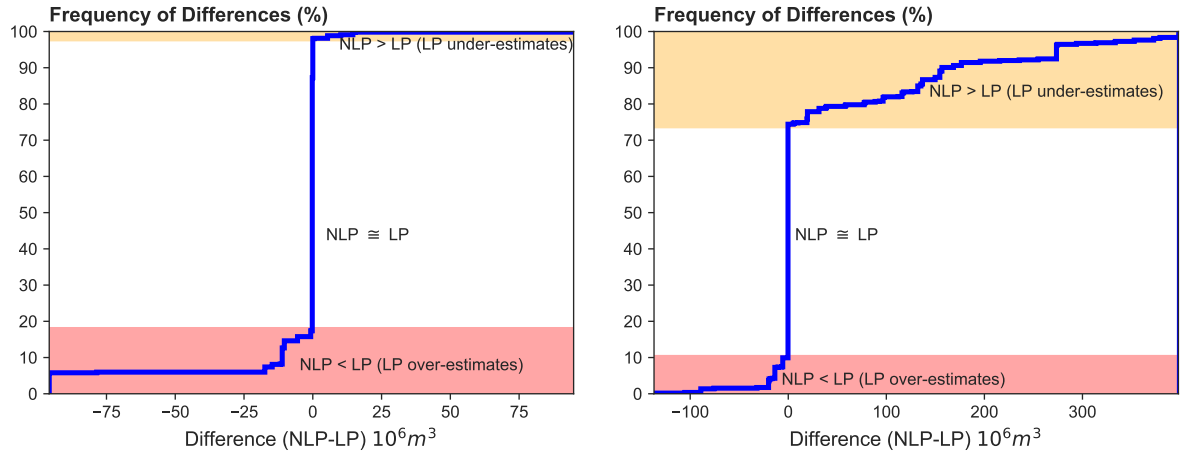

(a) Dry period

(b) Wet period

Figure 2.8: Percent frequency distribution of decision value (daily release and storage) differences between NLP and LP models for dry and wet periods

Figure 2.9 compares LP and NLP model outputs (daily flow and storage in million m^3) for dry and wet periods. Mostly due to less operational flexibility in the dry period, there is more agreement between LP and NLP model outputs. Wet period decisions cover wider range and LP model under-estimates some high storage decisions. Most large differences between the LP and NLP models are from only three reservoirs, under specific conditions. The LP decisions in the wet season are less reliable in two cases: a) The largest differences are from reservoirs with low deadpool and large head variations (New Melones and Pine Flat), where nonlinearities are higher; and b) reservoirs with large storage capacity (Shasta), where the LP model mostly underestimates storage.

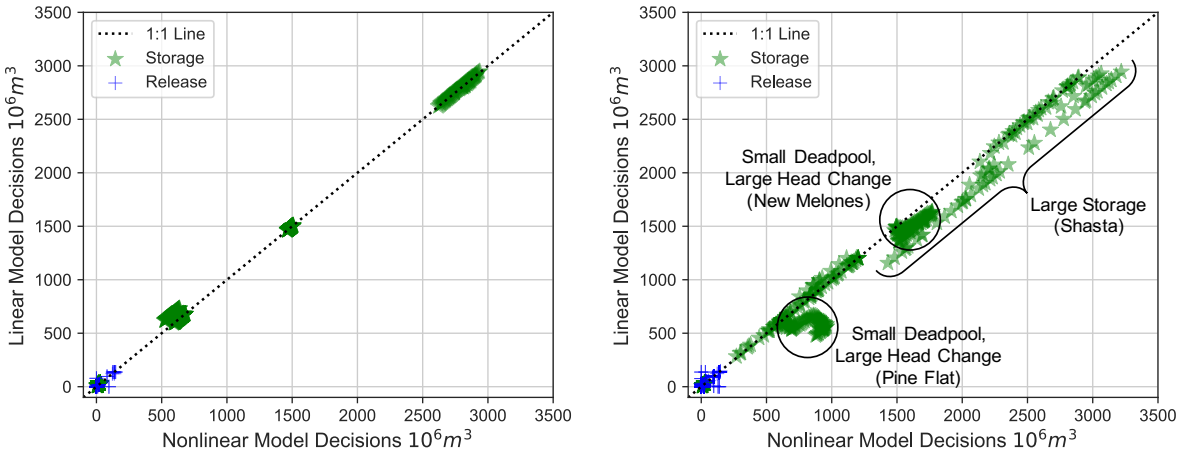

(a) Dry period

(b) Wet period

Figure 2.9: LP and NLP model decision variables (daily release and storage) comparison and marginal density distributions for dry and wet periods

Although operations for the LP model are driven by a linear objective function, power, generation and revenue results in Table 2.2 are postprocessed from the polynomial head function (Equation 2.6) after obtaining flow and storage decisions. the LP model over-estimates power and generation by 1% in dry period, and under-estimates by 2.3% in wet period. Given the model objective is to maximize total hydropower revenue, the LP model's revenue in wet period is quite close to the NLP model. In dry period, however, the LP model under-estimates revenue by about 2%. This could be partly due to multiple optimal solution or LP model's lower storage or release decisions during less available times in the wet period.

Table 2.2: Dry and wet period daily average hydropower load (MW/day), generation (MWh/day), and revenue ($/day)

	NLP Model	**LP Model**	**Difference**	**Difference (%)**
$\text{Power load}_{\text{dry period}}$	25.6	25.9	0.25	1%
$\text{Power load}_{\text{wet period}}$	327.1	319.4	-7.7	-2.3%
$\text{Generation}_{\text{dry period}}$	615	621	6	1%
$\text{Generation}_{\text{wet period}}$	7,850	7,666	-184	-2.3%
$\text{Revenue}_{\text{dry period}}$	32,235	31,622	-613	-1.9%
$\text{Revenue}_{\text{wet period}}$	232,725	232,731	6	0.002%

2.3.4 Hybrid LP-NLP Hydropower Optimization Model

The Hybrid LP-NLP model takes the fast calculation advantage of the LP model to reduce the number of iterations in the NLP model, which has fuller system representation but slow computing time. Both LP and NLP models use the same network, defined by

plants and time-step in the modeling horizon. Despite the LP model's accuracy losses and resulting errors, the LP can efficiently point to an optimal feasible region. In a sequential optimization, first the LP model is created and run. Then, LP decision outputs are used to initialize the NLP model's decision variables, called warmstart, to reduce number of NLP iterations for convergence.

Figure 2.10 compares accuracy and solver runtimes of LP, NLP and Hybrid LP-NLP models. Each model is run for three different model sizes, small, medium and large-scale with a number of decision variables of 502, 1376 and 3162, respectively. Accuracy losses in LP model result from residuals in the objective function and relative to the NLP model in Equation 2.25, where $\widehat{f}$ is the average objective function (revenue) value. Accuracy losses accumulate as size increases in the LP model. Runtime increases exponentially, however much faster for the NLP and Hybrid LP-NLP models. Hybrid model, where the NLP model is initialized with LP outputs, significantly reduce runtime of the NLP model without affecting accuracy.

$$Accuracy\ (\%) = 100 * (1 - \frac{|(\widehat{f}_{LP} - \widehat{f}_{NLP})|}{\widehat{f}_{NLP}}) \tag{2.25}$$

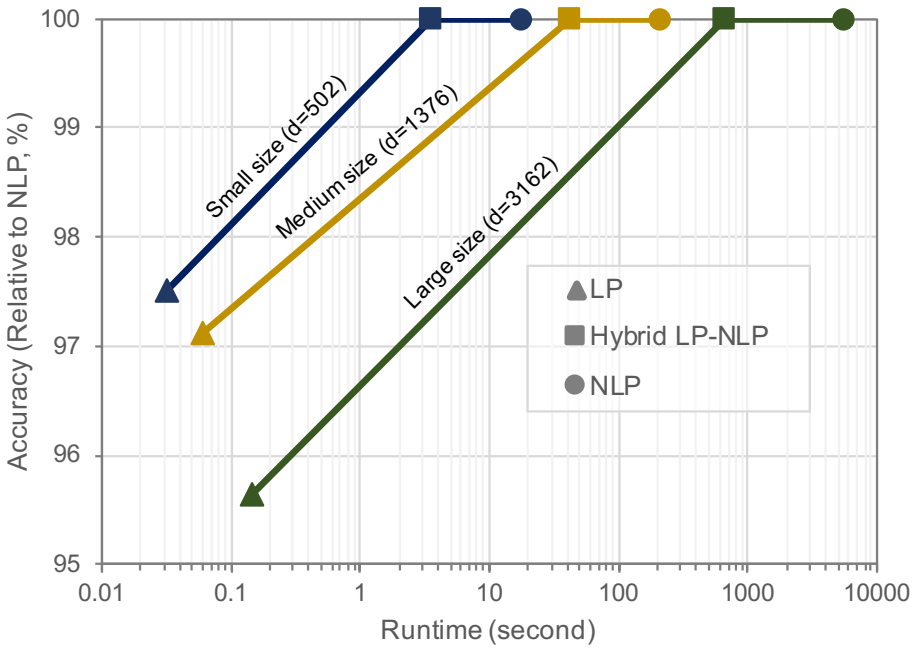

Figure 2.10: Result accuracies and solver runtimes of LP, NLP and Hybrid LP-NLP models with different model sizes (Small, medium, and large models have 502, 1376, and 3162 decision variables, respectively. Solver runtime does not include time for model creating and postprocessing)

The hybrid LP-NLP model, which initializes the NLP model with the LP model's solution, reduces runtime of the NLP model by about 80% in all model sizes (Figure 2.11). The NLP model also can be initialized with the NLP solutions (lower bound NLP)

after solving it to represent the lower bound for runtime improvement with a perfect initial solution. This is the time that the model takes to verify the optimal solution. There is still a room up to the lower bound NLP to further reduce the NLP iterations and runtime if a better initial solution (than LP) with less residuals is provided, such as piecewise LP or successive LP, especially for the large model size.

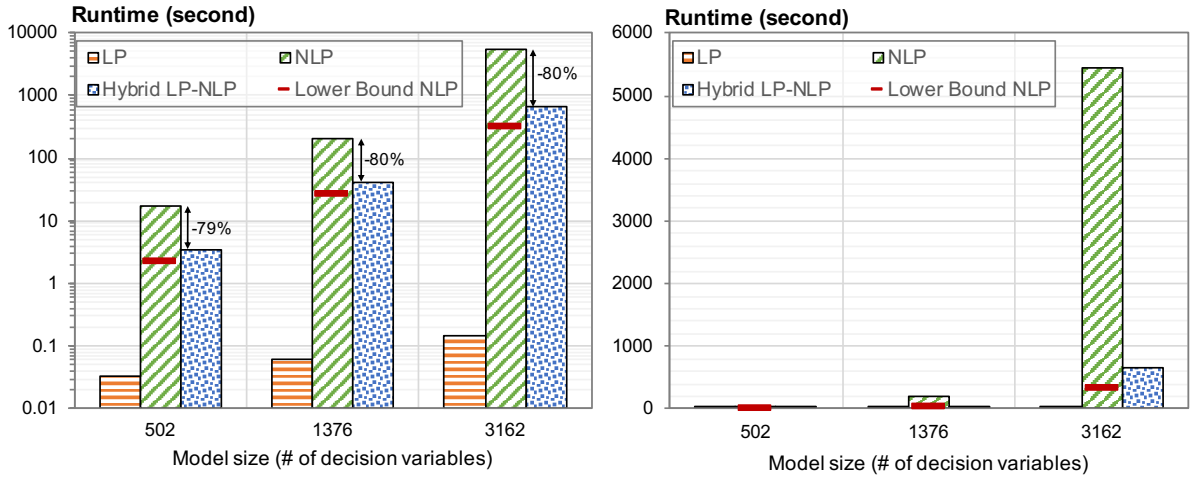

(a) Runtime (log-scale)

(b) Runtime (normal scale)

Figure 2.11: Solver runtimes of LP, NLP, and Hybrid LP-NLP models and lower bound NLP with different model sizes (Small, medium, and large model sizes. Solver runtime does not include time for model creating and postprocessing)

The initialization with the LP model reduces the number of NLP iterations, while runtime still increases exponentially and can be pose a problem for long-term operations with many decision variables. In addition, price and inflow uncertainties increase as the modeling horizon increase. So, the LP model's ability to run for long periods in a short duration of runtime can be favorable to the NLP model's better system representation of storage-dependent head.

2.4 Limitations

The model limitations include perfect hydrologic foresight, single revenue-maximizing objective, and the assumption that hydropower operation does not affect energy prices. For short-term operations, of a 1 to 3 day period with hourly time-step, operators usually have good hydrologic foresight. However, for long-term operations or highly variable and uncertain short-term conditions, perfect hydrologic foresight may result in too optimistic operations, flattening effects of extreme events, such as droughts and floods. However, for long-term operations and planning, hydrological uncertainties are much higher than limitations imposed by the perfect foresight. Most modeled reservoirs are multipurpose, but their short-term objective is often to maximize hydropower revenue within water supply release schedules and flood operations. Finally, the marginal cost of hydropower generation is much lower than fossil-fueled sources, so a price-taking approach is employed.

2.5 Conclusions

A hybrid hydropower optimization model was developed and applied to California's hydropower system. Taking advantage of fast calculation in the LP and a fuller system representation of a NLP model, the hybrid model runs the LP and NLP models sequentially, using LP outputs to initialize the NLP model and reduce number of iterations for convergence and runtime by 80%. This initialization, called warmstart, significantly reduces iterations and runtime for the NLP model without affecting accuracy of results. The hybrid LP-NLP runtime can be reduced up to lower bound NLP if a more accurate solution than LP, such as piecewise LP or successive LP, is provided. The LP and NLP models also can run separately. Despite reduction with warmstart, the hybrid LP-NLP model still requires much longer runtime than the LP model. So, for short-term operations, where a good system representation is important, the hybrid LP-NLP model can be used. For long-term planning and management decisions, where hydrologic and energy price uncertainties are higher, the LP model can be better. LP and NLP decisions are similar in the dry season, with less operational flexibility. As water availability increase in the wet season, differences between the LP and NLP models increase. The LP model is less reliable when water availability is higher, head changes nonlinearly with storage, and storage capacity is large.

Chapter 3

Solar Energy Effects on Short-term Hydropower Operations

3.1 Introduction

Hydropower with a sizable storage capacity is considered a dispatchable resource, where stored water stores energy when demand is low and is dispatched later to meet peak demands (Pérez-Díaz & Wilhelmi, 2010). These peak demands can be seasonal, such as summer demand for long-term operations, or daily peak-hour demands for short-term operations. In an economic equilibrium, load (supply) equals demand. On average, total demand is less at night and more during daytime (Figure 3.1). Nuclear, geothermal, small hydropower provide mostly base load supplies, and thermal (mostly natural gas), large hydropower and imports help meet both peak demands and base load. Although total demand remains unchanged, hourly breakdown of load sources has been changed significantly since 2010. This is because of California's ambitious Renewable Portfolio Standard (RPS) targets that the State wants to achieve 33%, 40%, 45%, and 50% of total generation from renewable sources, such as solar, wind, small hydro, biomass, biogas, and geothermal, by 2020, 2024, 2027, and 2030, respectively (California Energy Commision, 2017). Most of these goals are met by wind and solar photovoltaic (PV) generation, which are variable due to their intermittent nature (Chang et al., 2013). The difference between total load and variable supply is net load, and its curve is called a 'duck curve' due to its shape (Denholm et al., 2015). With increasingly variable supply, especially solar, this shape has notably transformed, lowering net load when solar power production peaks around noon and steeper ramping rates to meet the peak demand in the evening. The net load is highly correlated with wholesale energy prices. This chapter aims to quantify effects of changed price patterns on short-term hydropower reservoir operations, using the hybrid LP-NLP hydropower optimization model with an hourly time-step over a seasonal period from 2010 to 2018. Although the modeled reservoirs serve for multi-purposes, including water supply, environment, flood protection and recreation, their short-term objective often is to maximize hydropower revenue given release schedules.

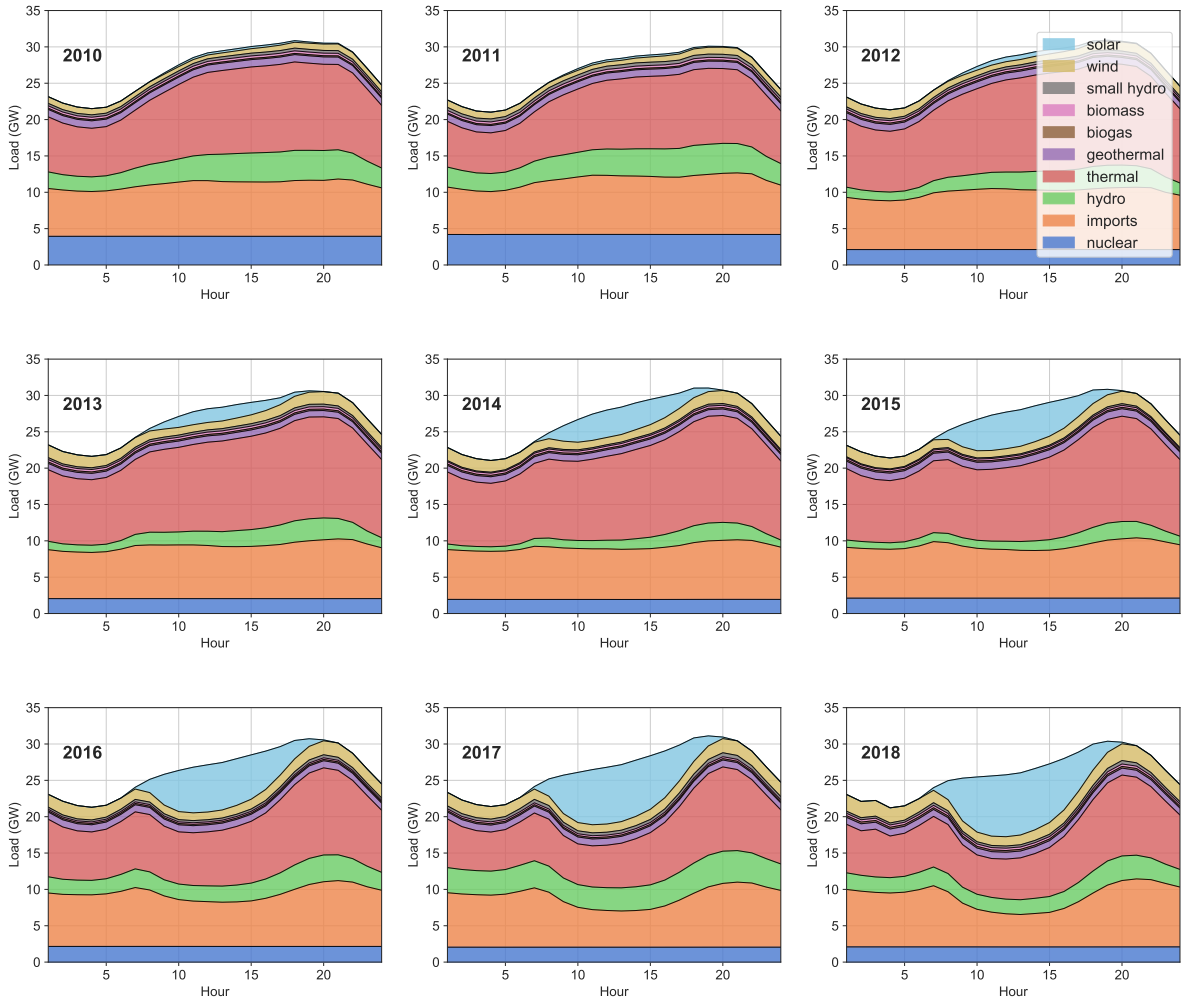

Figure 3.1: Hourly average load (GW) and sources between 2010 and 2018. The net load (total - (solar + wind)) curve is called a 'duck curve' (Data source: CAISO)

3.2 Reservoir Inflows

Five large-scale reservoirs with varying storage sizes and inflow rates are modeled (Table 3.1). The model is run for two seasons: wet and dry. The wet season is between January and June, and the dry season is between July and December of each year from 2010 through 2018. In the wet season, average reservoir inflows are much higher with precipitation and snowmelt runoff, giving operators more flexibility for dispatchable hydropower operations. In the dry season, with lower flows, priorities are given to the most valuable hours in terms of energy prices to maximize overall revenue. For initial and ending storage boundary conditions, half of the reservoir storage capacity is assumed for each season and year, without carryover storage.

Table 3.1: Modeled hydropower plants and observed mean (μ) and standard deviation (σ) of hourly inflows (m^3/s) in wet and dry seasons (Data source: CDEC)

Plant	**Plant ID**	**Capacity** (MW)	**Storage Capacity** (MCM)	**[1]Wet Season** μ	σ	**[2]Dry Season** μ	σ
Shasta	SHA	714	5615	281	309	134	153
Bullards Bar	BUL	315	1192	71	102	20	47
Folsom	FOL	207	1203	162	240	57	92
New Melones	NML	300	2985	64	79	30	33
Pine Flat	PNF	165	1233	91	109	34	56

[1]January-June, [2]July-December

The modeled reservoirs are on the lower foothills of the surrounding mountains, where there are several hydropower plants upstream with low-storage, owned by several agencies including Pacific Gas and Electric Company (upstream of Shasta, Folsom, New Melones, and Pine Flat), Sacramento Municipal Utility District (upstream of Folsom), and Northern California Power Agency (upstream of New Melones). Nevertheless, these upstream hydropower plants somewhat regulate hourly inflows with hydropower peaking releases to the modeled hydropower plants, as shown in Figure 3.2. With large storage capacity, modeled reservoirs can reduce upstream regulation effects, generating energy when it is most valuable. Also, hourly overall average inflows between 2010 and 2018 for dry and wet seasons are used to evaluate only energy price effects on operations, eliminating any hydrologic impacts.

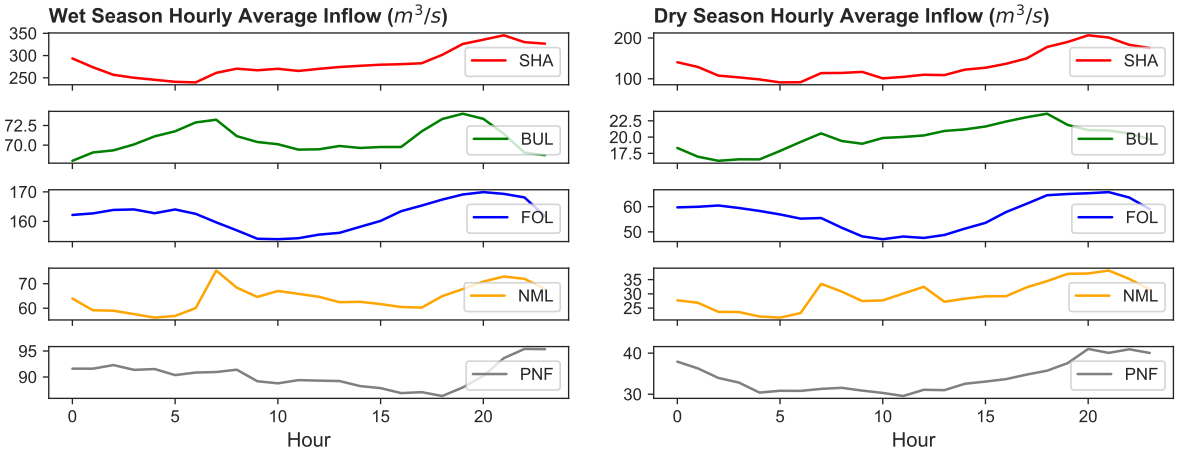

(a) Wet season hourly average plant inflows

(b) Dry season hourly average plant inflows

Figure 3.2: Wet and dry season hourly overall average reservoir inflows (m^3/s) affected by upstream hydropower peaking releases between 2010 and 2018 (Data source: CDEC)

3.3 Renewable Generation and Solar

Energy generation from renewable sources, including geothermal, biogas, biomass, small hydro (<30 MW), wind, and solar, are a significant portion of California's energy portfolio. Geothermal, biogas, biomass, and small hydro provide about 1500 MW hourly base load, while solar dominates the renewable portfolio when it peaks, especially in recent years (Figure 3.3-(a)). Solar and wind generation are intermittent and greatly vary across hours. Wind usually peaks around midnight and solar peaks around noon, somewhat and sometimes complementing each other. Starting 2013, as a part of RPS targets, solar generation has been booming, with modest increases in wind generation, while generation from the other renewables are mostly unchanged (Figure 3.3-(b)).

Solar energy converts the sun's directly radiated light into electricity (photovoltaics) or heat (thermal) (Labouret & Villoz, 2010; Pick, 2017). Electricity generation in solar PV occurs via cells or panels that directly transform the sun's energy into electricity, while solar thermal first heats fluids, such as water, air or other fluids, then generates electricity (Labouret & Villoz, 2010). Solar thermal is very small (Figure 1.1). So, total generation from solar PV and thermal is referred simply as solar generation here.

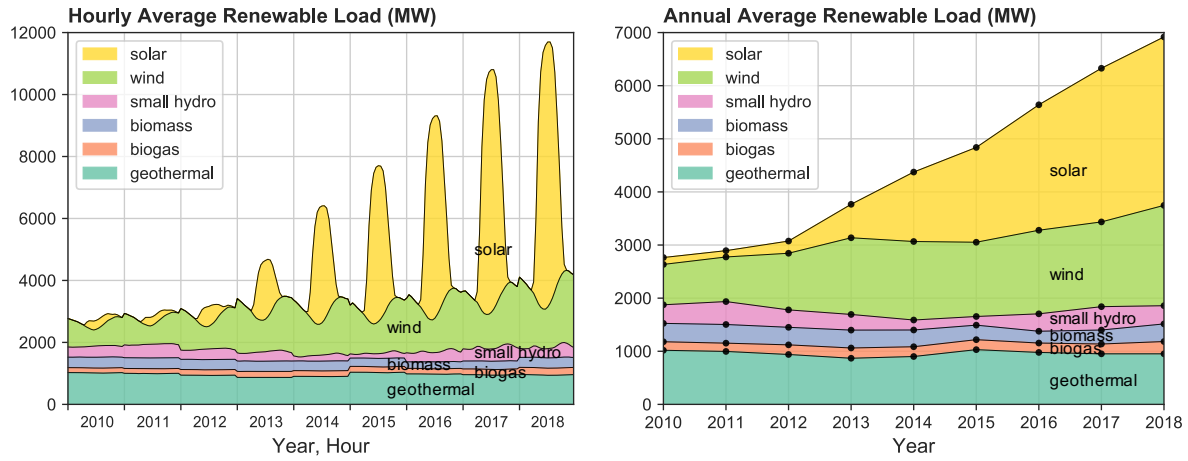

(a) Hourly average renewable load

(b) Annual hourly average renewable load

Figure 3.3: Hourly and annual average renewable loads (MW) between 2010 and 2018 (Data source: CAISO)

3.3.1 Renewable Goals

California's Renewable Portfolio Standard (RPS) establishes gradually increasing renewable targets, shown in Figure 3.4-(a), and requires at least 50% of total generation from renewable sources by 2030 (California Energy Commision, 2017). The State has met its first and second goals (20% and 25%), and in 2017, about 30% of total generation was from renewable sources. Small hydropower provides less than 5% of total generation and changes with water availability, decreasing in drought years between 2012 and 2016. Large-scale conventional hydropower, with capacity $\geq$ 30 MW, is not considered renew-

able. To met RPS target of 50%, the State needs additional 20% renewable generation. Figure 3.4-(b) shows that starting 2013, most increase in renewable generation is from solar (slope = 1.09), meaning solar is meeting most RPS targets. Thus for the 2030 goal, existing (2017) solar generation must be almost doubled. Since most significant solar generation increases occur starting 2013, years from 2010 through 2012 are considered pre-solar years, from 2013 through 2018 are considered post-solar years to study how the solar deployment is affecting hydropower operations.

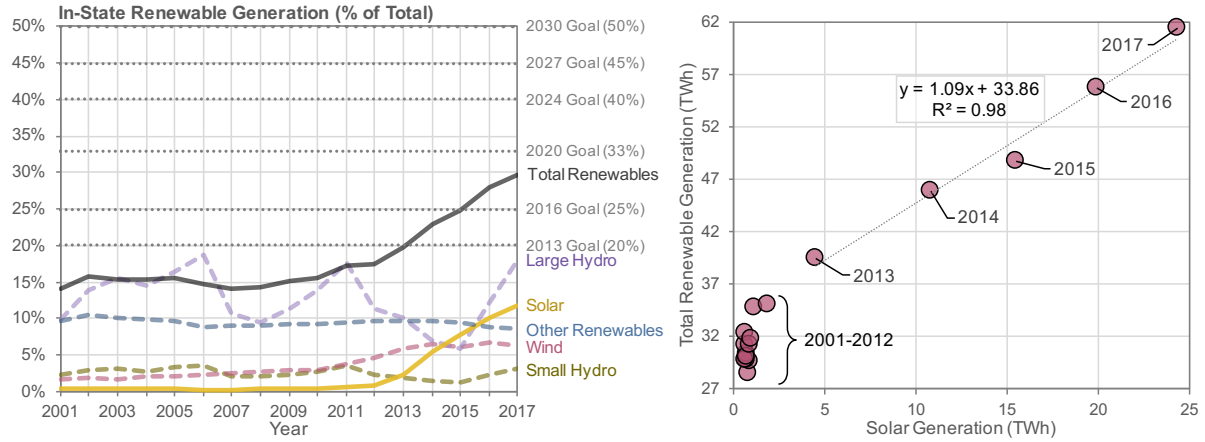

(a) Renewable generation (% of total)

(b) Total vs. solar generation

Figure 3.4: Annual average renewable generation (% of total), California's renewable goals, and total vs. solar generation comparison (Note: Large Hydro is not considered renewable. Data source: CEC Energy Almanac)

3.4 Demand-Energy Price Relationship

There is a strong relationship between demand (load) and energy prices. Energy prices are higher during on-peak hours and lower during off-peak hours. These prices are more correlated with the net load, the difference between total load and variable supply, shown in Figure 3.5. This difference is much higher during solar peaks. Load difference in off-peak and on-peak demands are mostly from wind generation, and larger differences are from solar generation. Prices increase with a steeper slope with off-peak demands, then slowly increase with average demand, then steeper increase again with on-peak demands. Around the average energy price and load, the unit increase in price (ΔP) is much greater with net load than the total load. As the variable supply increases, the gap between net load and total load grows, resulting in steeper increases in energy prices, especially in average demands, when solar generation peaks.

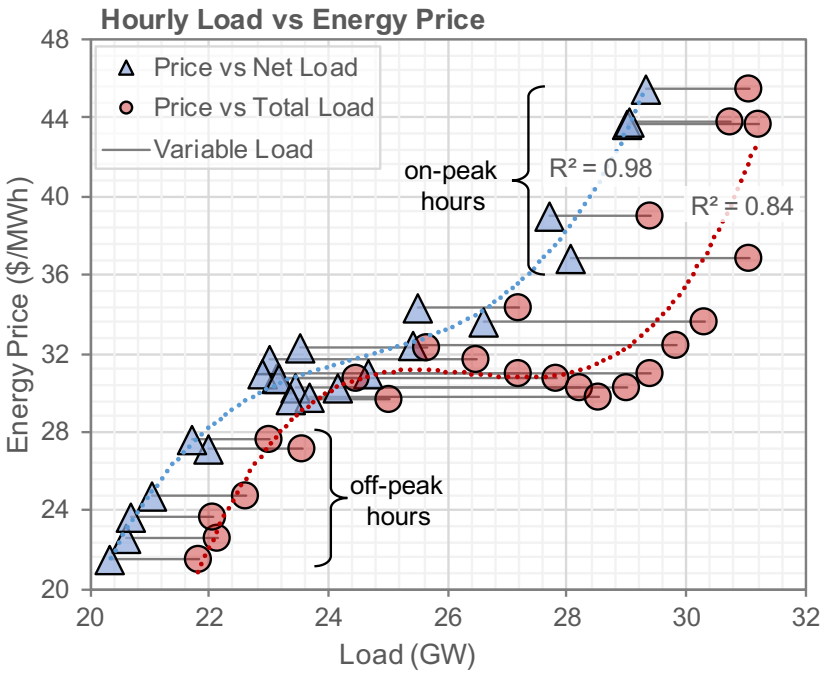

Figure 3.5: Hourly average (2010-2018) energy prices vs. total and net loads (Data source: CAISO)

3.5 Energy Prices and Changed Pattern

Hourly energy prices are obtained from CAISO (2018b), and reflect the market value of a unit of generation. These wholesale prices are different than retail electricity prices that utility companies charge their customers, where usually fixed plus tier-based tariffs are used (PGE, 2019). CAISO maintains the power grid and regulates market operations in California. Originally node-based, statewide average of hourly marginal energy prices are used. Figure 3.6 shows hourly average energy prices for each year between 2010 and 2018 and wet and dry seasons. Energy prices depend on several variables, such as natural gas prices, but usually are higher in dry season due to air conditioning use. Since energy prices change with the net load, as variable supplies, particularly solar, increase, net load decreases, which lowers energy prices between hours 8 and 18 in both seasons, resulting in twice-daily peaks. Also, in the dry season, the price difference between the first and second peaks is much higher, increasing price volatility.

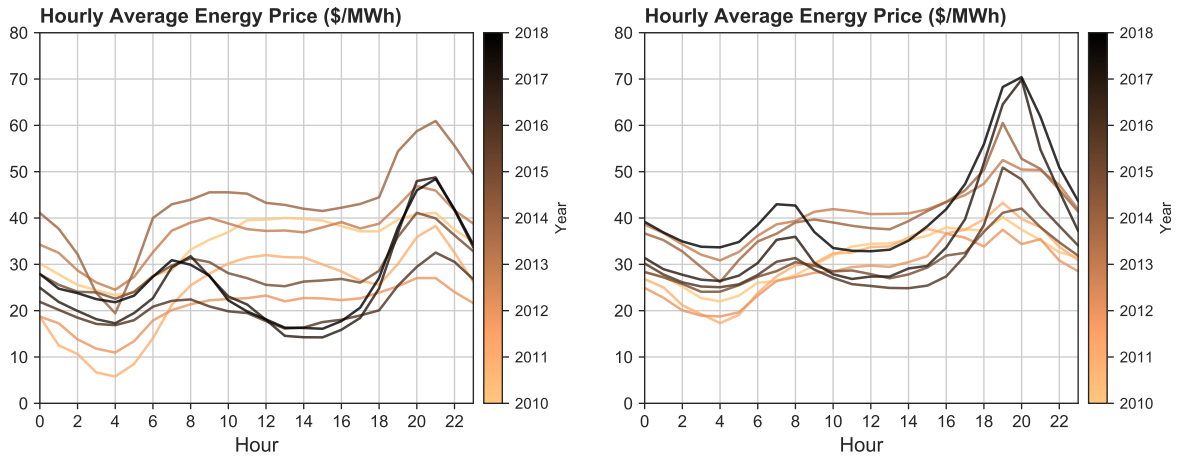

(a) Jan-Jun hourly average energy prices

(b) Jul-Dec hourly average energy prices

Figure 3.6: Hourly average (statewide average of all price nodes) marginal energy prices ($/MWh) between 2010 and 2018 in wet (Jan-Jun) and dry (Jul-Dec) seasons (Data source: CAISO)

Affected by solar generation, energy prices change considerably and reshape the price scheme. Figure 3.7 shows this transformation between 2010 and 2018 for wet and dry seasons with normalized energy prices between 0 and 1. The normalization (Equation 3.1) removes the magnitude of prices, which can differ each year, and better show the effects and price trends. Energy prices undergo a significant transformation during solar generation hours in both seasons. As solar generation increases, energy prices gradually decrease between hours 8 and 20, resulting in two daily peaks. In pre-solar years, 2010-2012, daytime prices are much higher, slightly increasing during evening peak. Price in these years are higher between 8 and 23, and lower the rest of the day. In the wet season (Jan-Jun) of 2016 through 2018, normalized energy prices are even lower during hours 10-18 than prices at night, where total demand is lower. For hydropower plants with sizable storage capacities, this new price scheme gives little incentive to generate hydropower during off-peak hours, focusing operations in a smaller time-frame during on-peak hours, with much increased pulse releases.

$$Price\ Normalized_{n,s} = \frac{(P_{n,s} - \min(P_{n,s}))}{(\max(P_{n,s}) - \min(P_{n,s}))}, \forall (n,s) \tag{3.1}$$

where P is an array of hourly average marginal energy prices in year n (2010-2018), and season s (wet, dry).

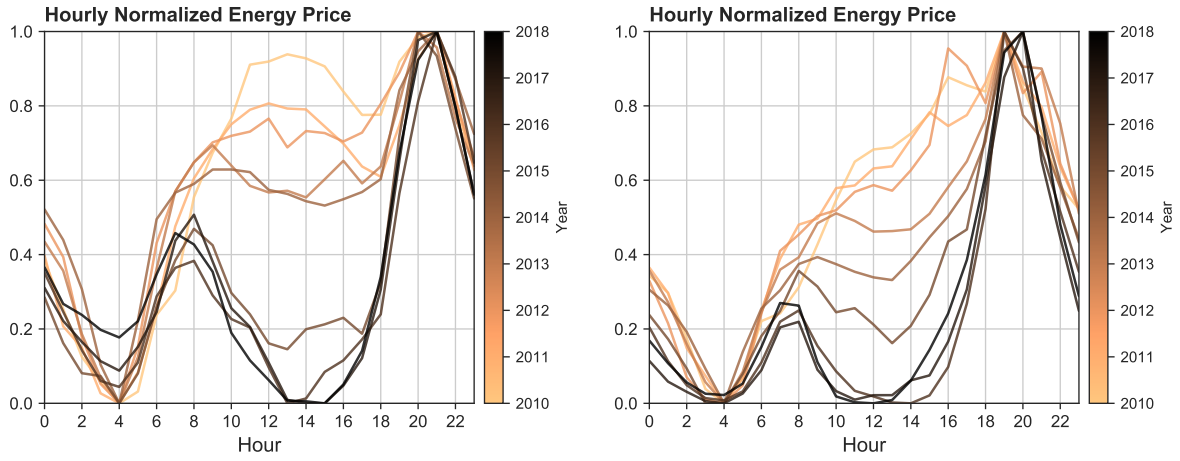

(a) Jan-Jun normalized hourly energy prices

(b) Jul-Dec normalized hourly energy prices

Figure 3.7: Normalized hourly energy prices in wet and dry seasons

Negative energy prices usually occur due to over-generation when the demand is low. While shifted slightly to earlier months in recent years, negative prices are mostly in the wet season and wetter years, such as 2011 and 2017, resulting mostly from low-storage (run-of-river) hydropower generation (Figure 3.8-(a)). Another important transformation can be observed in hourly negative price trends. Solar deployment shifts months with negative prices earlier, but more importantly it affects the hourly timing of these prices (Figure 3.8). In the pre-solar period, negative prices occur during low demand hours, between 0 and 8. As solar generation increases, lowering net hourly load, negative prices shift to hours between 8 and 18 in the post-solar period. Negative prices are not desirable for hydropower plants without much storage capacity. In contrast, hydropower plants with storage capacities, can store water during those low-valued hours, gaining head, and release water during profitable hours. This negative price scheme is economically favorable for pumped-storage hydropower plants, which pumps water to an upper reservoir during low-valued hours to release and generate electricity during higher-valued hours.

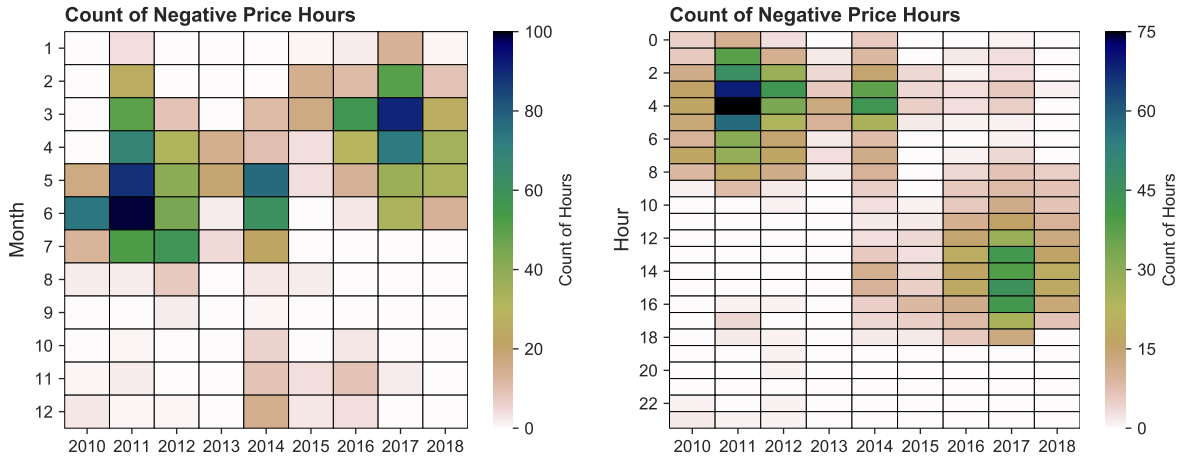

(a) Count of hours with negative prices by month (b) Count of hours with negative prices by hour

Figure 3.8: Count of negative energy price occurring hours between 2010 and 2018 (Data source: CAISO)

3.6 Results

The hybrid LP-NLP hydropower optimization model is run for several energy price patterns to evaluate effects of solar generation on short-term hydropower operations with hourly time-steps for each wet and dry season from 2010 to 2018. Results include hydropower generation, reservoir storage and release, and revenue difference in wet and dry seasons, and are discussed below. Also, adaptations to the new energy price pattern are explored.

3.6.1 Hydropower Generation

Hydropower generation is controlled by water storage and release decisions, driven by energy prices. Hydropower generation meets the demand since energy price and demand are highly correlated. As storage increases, the potential energy difference between storage elevation and tailwater (head) increases. Increased storage also sustains hydropower generation for longer periods. However, hydropower is not generated until the stored water is released through turbines. So, the decision becomes how much to store and release and when to do so. Figure 3.9 shows hourly average hydropower generation (MWh) for pre-solar (2010-2012) and post-solar (2013-2018) periods as seasonal and annual overall hourly averages. Since energy prices decrease from hours 9 through 18, generation during these hours shifts to earlier peaking hours of 8 in the wet season. Also, generation for the evening peak hours starts earlier, extending through midnight. In the dry season, all hydropower generation is in the evening peak hours in a smaller time-frame, as unit price of energy is much higher in these hours. In addition, water is limited so, it is saved for peak hours to maximize revenue. The average reservoir operating rule becomes to generate hydropower first during evening peak, and only if there is enough water, release during the morning peak, with reduced hydropower generation during solar generation

hours (9-18).

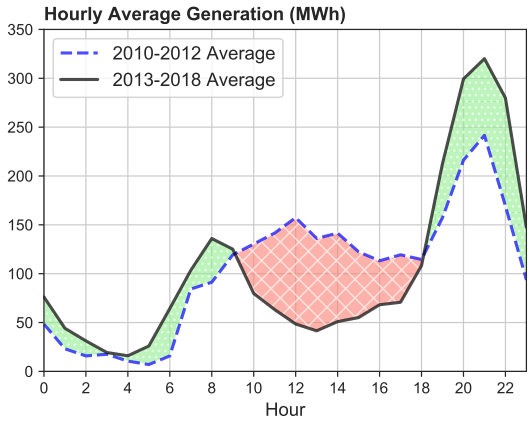

(a) Jan-Jun generation

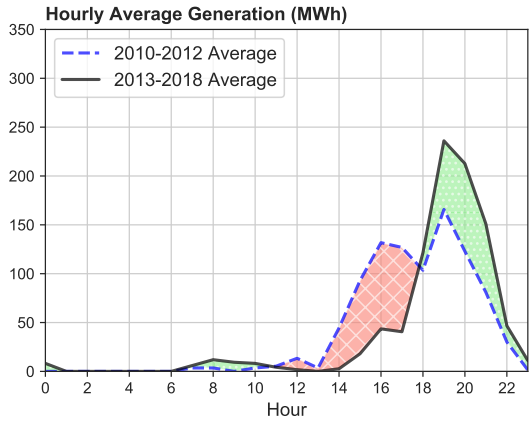

(b) Jul-Dec generation

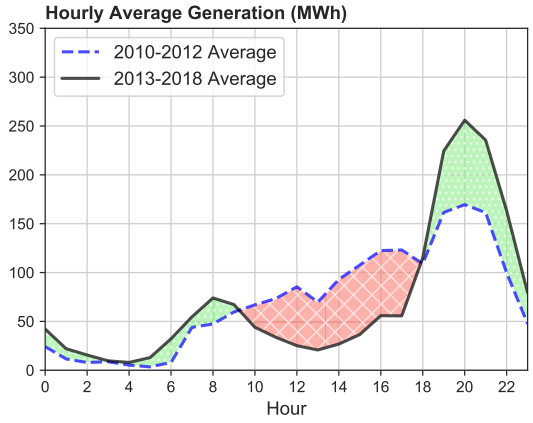

(c) Annual average generation

Figure 3.9: Hourly average hydropower generation (MWh) for pre and post-solar periods in wet (Jan-Jun) and dry (Jul-Dec) seasons and annual average

Operations vary for plants as each has different storage and turbine capacities and inflow rates (Figure 3.10). Shasta and Folsom generate small amounts in morning peak hours, while remaining plants generate during both morning and evening peaks with large amounts in the post-solar period in the wet season. Bullards Bar generates hydropower during most hours. This is because its head does not change significantly with storage (Figure 2.2), so it does not have to wait long to store water and gain head. New Melones and Pine Flat generate hydropower during both peaks with similar morning and evening peak generation amounts. All plants in the wet season reduce hydropower generation for hours between 9 and 18 in the post-solar period.

Generation focuses mostly on evening peak hours in the dry season due to less water availability and much higher energy prices during the evening peak. All plants significantly reduce pre-solar period hydropower generation during solar generation hours, with

small morning peak generation, and extend the duration of evening peak generation. Hydropower plants can start operations more quickly than thermal plants, but increased ramping rates in the post-solar period can cause harm downstream. In addition, minimum in-stream flow requirements downstream of these plants often affect optimized releases. Most large reservoirs, such as Shasta, Bullards Bar, and Folsom, have smaller reservoirs downstream, which can act as afterbays to alleviate negative impacts of pulse releases and help meet environmental targets. Water availability, storage capacity and storage-head relationship result in different plant operations.

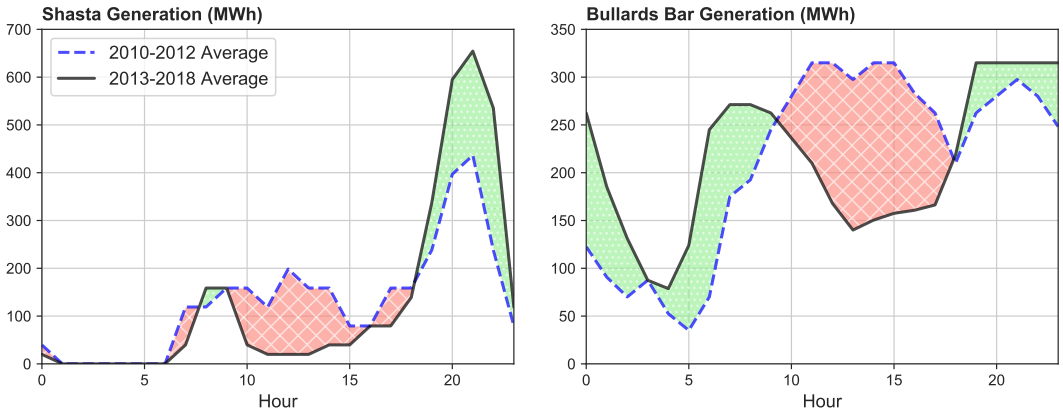

(a) Shasta

(b) Bullards Bar

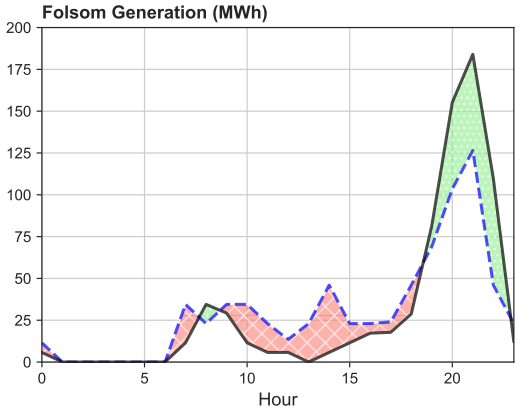

(c) Folsom

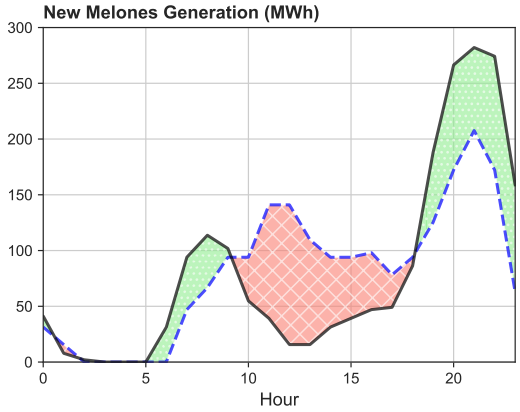

(d) New Melones

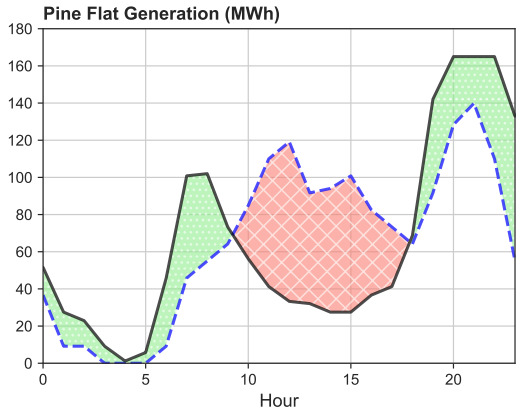

(e) Pine Flat

Figure 3.10: Hourly average generations (MWh) of modeled plants in the wet season (Jan-Jun) for pre and post-solar energy price periods.

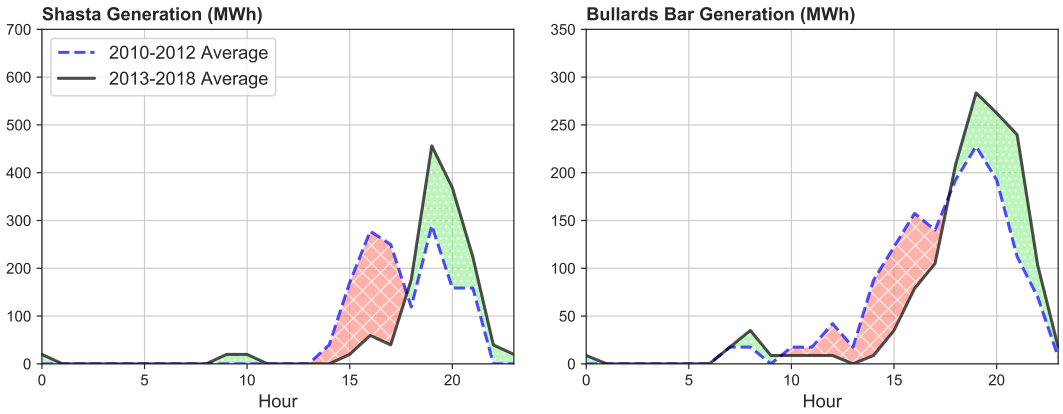

(a) Shasta

(b) Bullards Bar

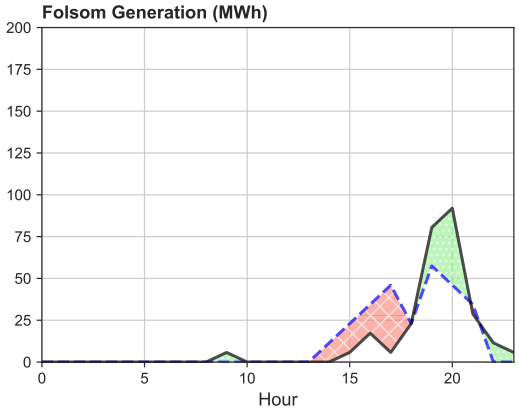

(c) Folsom

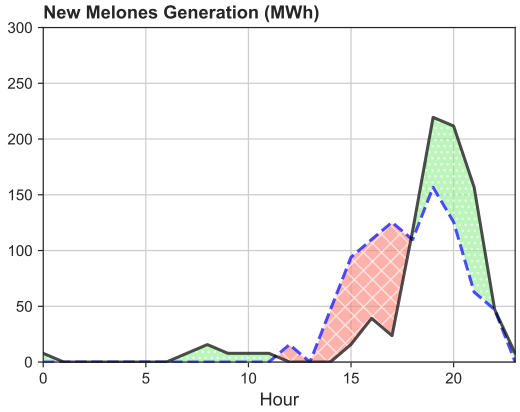

(d) New Melones

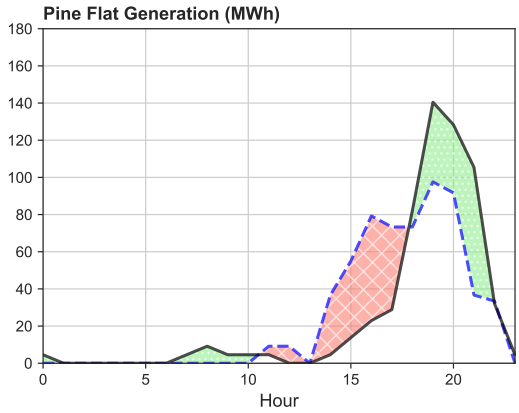

(e) Pine Flat

Figure 3.11: Hourly average generations (MWh) of modeled plants in the dry season (Jul-Dec) for pre and post-solar energy price periods

3.6.2 Reservoir Storage and Release

Reservoir storage increases with inflows and decreases with generation releases. The slope of the rising limb of the storage curve gives average inflow rate, and similarly the slope of the recession limb equals the average turbine discharge rate. Spills are penalized to minimize foregone energy, and no significant spills occur during any hourly time-step with overall average inflows. The pre-solar period storage peaks earlier in the day in the wet season, occurring around hours 6 and 10 (Figure 3.12-(a)). Storage slightly decreases during hours around 7-8 with morning peak releases in the post-solar period of the wet season, but a much greater daily peak occurs at 18 and falls with evening peak generation releases. In the dry season (Figure 3.12-(b)), normalized storage does not change significantly with solar development. Peak storage of the post-solar period shifts about 3 hours later, occurring around 18.

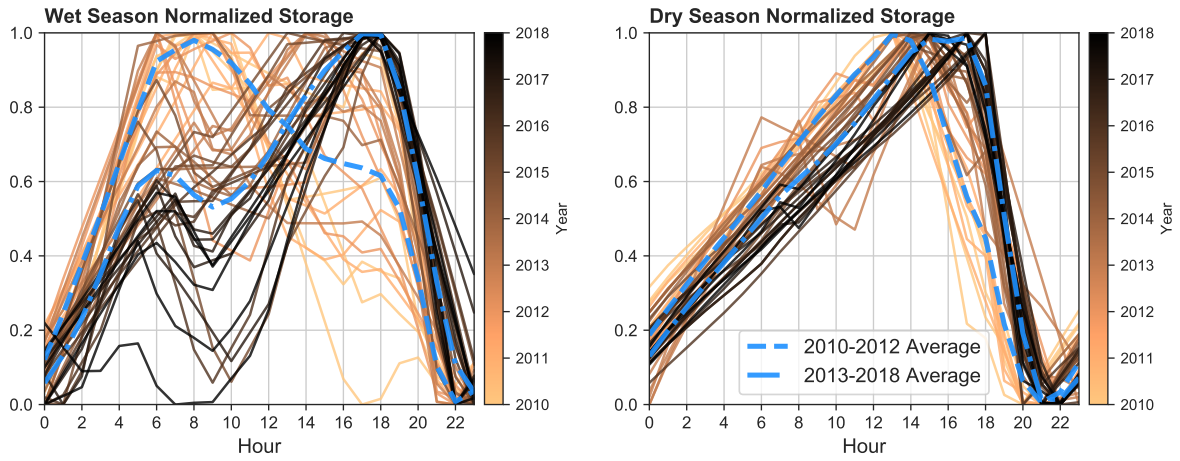

(a) Jan-Jun hourly normalized storage

(b) Jul-Dec hourly normalized storage

Figure 3.12: Normalized reservoir storage of 5 modeled plants for pre and post-solar periods in wet (Jan-Jun) and dry (Jul-Dec) seasons

Since overall average inflows are used for pre- and post-solar periods to eliminate inter-annual hydrologic variability, total release volume does not change (the area under the release curve is the same for both periods shown in Figure 3.13). In the wet season of the pre-solar period, some releases on hours between 9 and 18 move to earlier hours, forming the morning peak releases. The remaining releases move to later hours, extending the duration and amount of evening peak releases in the post-solar period. Plants make little releases during morning peak hours in the dry season, and concentrate all operations to evening peak hours. Some pre-solar period releases, between 13 and 18 hours shift to later hours, increasing evening peak releases in the post-solar period.

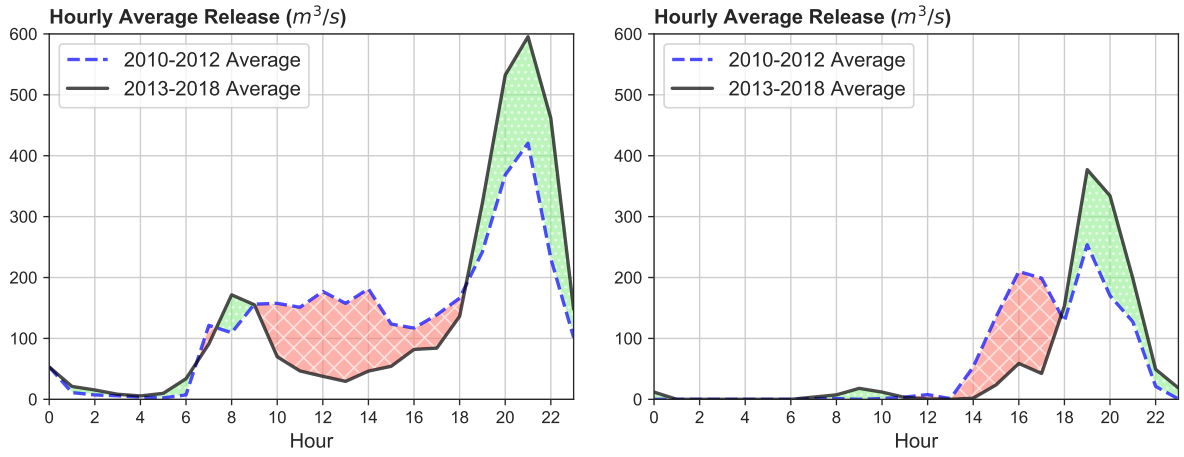

(a) Jan-Jun hourly average release

(b) Jul-Dec hourly average release

Figure 3.13: Hourly average turbine releases (m^3/s) of all plants for pre and post-solar periods in wet (Jan-Jun) and dry (Jul-Dec) seasons

3.6.3 Hydropower Revenue

The hybrid LP-NLP hydropower optimization model maximizes hydropower revenue across all plants i and time-steps t. Hydropower revenue (R) is obtained by multiplying hydropower generation (G) with unit energy prices (p), shown in Equation 3.2. To maximize revenue, the model generates hydropower during the most profitable hours. Generation in less profitable hours are only made when enough water is available.

$$R_{i,t} = p_{i,t} * G_{i,t} \tag{3.2}$$

Table 3.2 shows hourly average modeled revenue in wet and dry seasons between 2010 and 2018, denoting how the revenue changes with the solar induced energy price changes. Overall, hydropower revenue increases proportionally with increased (mean) energy prices and are higher in the wet season and lower in the dry season. As the solar development increases between 2010 and 2018, price range increases significantly, causing twice-daily peaks. This range is measured as the energy price difference between hours 20, evening peak demand and price hour, and 13, solar generation peak hour. Given those changes and similar amounts of hydropower generation on average, with seasonal average reservoir inflows, hydropower revenue increases in the post-solar period. For example, wet season of 2016 and 2012 have the same average price (21 $/MWh), but hourly average revenues in these years are 2,842 and 2,706 $/h, respectively. Similar, the dry seasons of 2016 and 2011 have the same average price (31 $/MWh), but price range and hourly revenue of 2016 (23 $/MWh and 1,846 $/h) is much more than revenue of 2011 (6 $/MWh and 1,765 $/h). Similar comparisons can be made for other years and seasons between pre- and post-solar periods, showing the effect of the new price pattern on hydropower revenue. Years from 2013 to 2015 are transitioning years from 1-daily to 2-daily energy price peaks, so revenue comparison in these years may not give the same results (for example 2010 and 2013 wet seasons).

Figure 3.14 shows how hourly average revenue ($K/h) changes with hourly energy price and generation. Revenue changes linearly with energy prices and hydropower generation (Equation 3.2). However, the slope of this linear relationship varies at each generation level, becoming steeper as generation increases. In years between 2010 and 2012, although average revenues differ between wet and dry seasons (Table 3.2), peak hourly revenues are around 10-20 $K per hour. The seasonal peak price differences are much greater in years between 2016 and 2018, with peak generation hourly revenues around 10-20 $K in the wet season and 15-35 $K in the dry season. Hourly revenues are also much higher in this period than 2010-2012 for two reasons: first, energy prices differ between these two periods (slightly higher in the dry season of 2016-2018) (Figure 3.6); and second with adaptations to the energy price changes, more hydropower revenue is gained.

Table 3.2: Average energy price, price range, and hourly average modeled revenue (Energy price data source: CAISO)

			Energy Price ($/MWh)		**Average Revenue**
Period	**Year**	**Season**	**Average**	**Range**[1]	($/h)
Pre-solar	2010	Wet	34	1	4,585
	2010	Dry	31	3	1,665
	2011	Wet	24	4	3,490
	2011	Dry	31	6	1,765
	2012	Wet	21	5	2,706
	2012	Dry	28	5	1,653
Post-solar	2013	Wet	37	10	4,447
	2013	Dry	41	10	2,190
	2014	Wet	43	16	5,724
	2014	Dry	40	15	2,209
	2015	Wet	29	16	3,708
	2015	Dry	30	15	1,636
	2016	Wet	21	13	2,842
	2016	Dry	31	23	1,846
	2017	Wet	25	33	3,891
	2017	Dry	36	43	2,550
	2018	Wet	27	30	3,933
	2018	Dry	43	37	2,761

[1]Energy price difference between hours 20 and 13, which are evening energy price peak and mid-day solar generation peak hours

Note: hourly overall average (2010-2018) inflows for each season are used

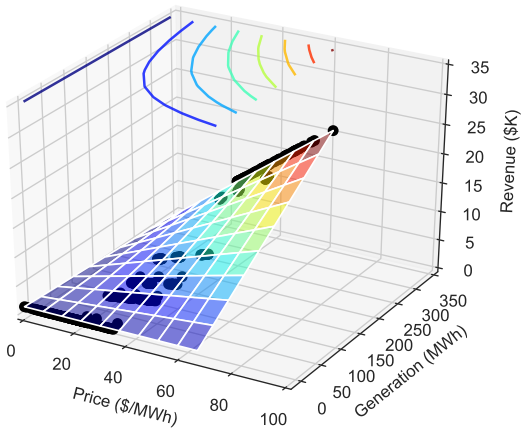

(a) 2010 through 2012, wet season

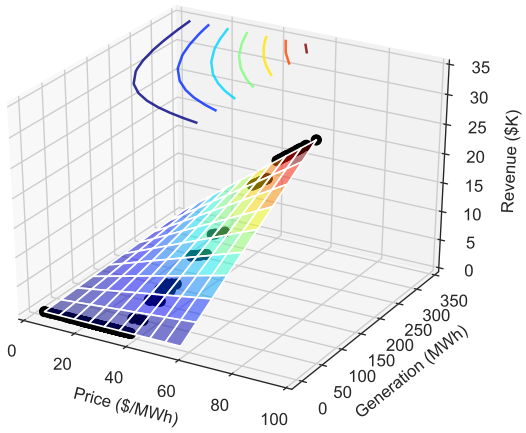

(b) 2010 through 2012, dry season

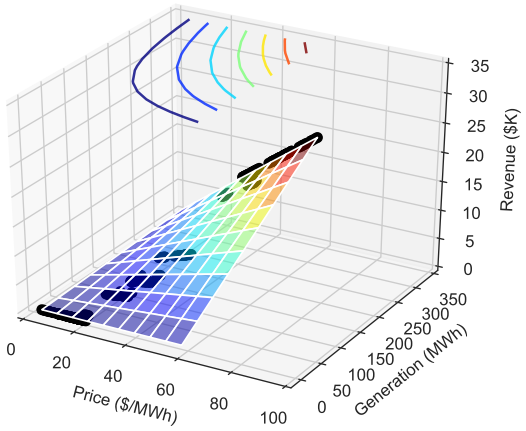

(c) 2016 through 2018, wet season

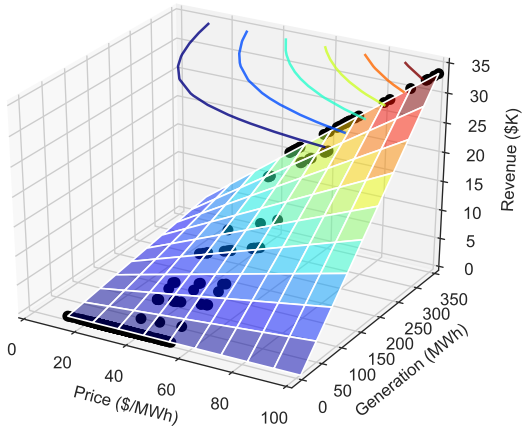

(d) 2016 through 2018, dry season

Figure 3.14: Hourly average revenue ($K) from generation in wet and dry seasons of years 2010-2012 and 2016-2018 energy prices with fitted contour surfaces

Figure 3.15 shows hourly revenue differences between pre-solar (2010-2012) and post-solar (2013-2018) period averages. Although a total of roughly 18.2 $K revenue is lost due to less hydropower generation during solar generation hours between 11 and 17, roughly 30.1 $K of revenue is gained in the other hours in wet season, with a net increase of 11.9 $K. The dry season has less operational flexibility. In this season, roughly 12.9 $K of revenue is lost between hours 12 and 17, but a total of 25 $K is gained during hours between 18 and 22, totaling the net difference to 12.1 $K. The adaptation to new conditions of the post-solar period results in an additional net daily benefit of 24 $K per plant.

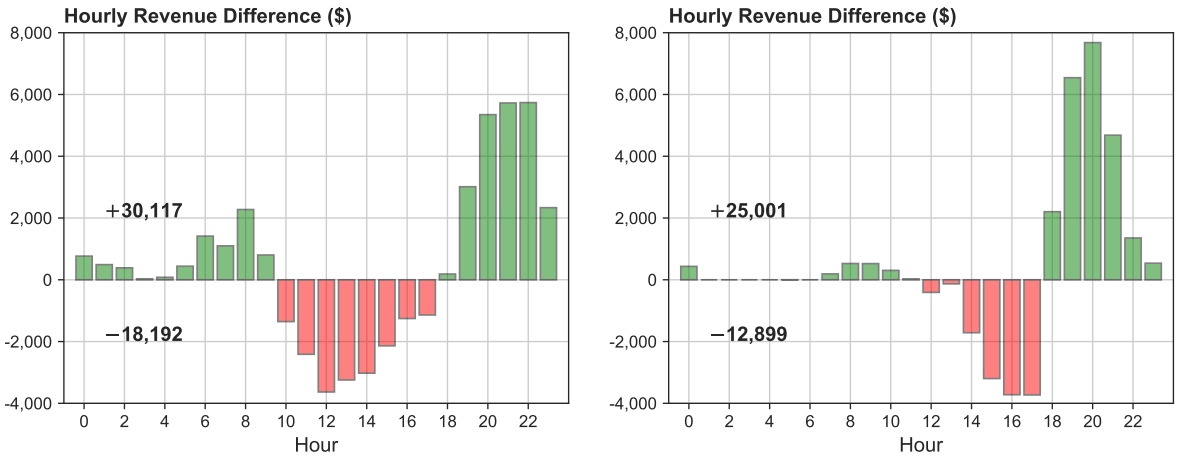

(a) Jan-Jun hourly average revenue difference

(b) Jul-Dec hourly average revenue difference

Figure 3.15: Hourly average revenue difference ($) between pre and post-solar periods in wet (Jan-Jun) and dry (Jul-Dec) seasons

3.7 Summary and Adaptations

The new energy price pattern increases overall hydropower revenue with adaptations, although most hours between 10 and 18 are less profitable due to solar generation, especially in wet seasons with more water availability. Figure 3.16 summarizes annual average operations with normalized values (between 0 and 1) for pre-solar and post-solar periods and wet and dry seasons. The normalized values of energy prices were much lower due to less net load during hours between 9 and 18 in the post-solar period, creating two daily peaks occurring hours 7-9 in the morning and 19-21 in the evening in both seasons. The magnitude of the latter is much greater than former. Since the model is driven by energy prices, subject to water availability, operations significantly adapt to these new energy price conditions. Reservoir storage peaks daily during hours 6-9 in wet season and 13-14 in dry season in the pre-solar period, then decreases with hydropower releases. These storage peaks move hours 16-18 in wet season and 15-17 in dry season in the post-solar period, before the evening peak releases start. Peak releases of the post-solar period concentrates to smaller time-frame of the evening peak hours. Plants generate some hydropower during the morning peak hours in the post-solar period, mostly in the wet period, but most generation and revenue is from hours between 19 and 21.

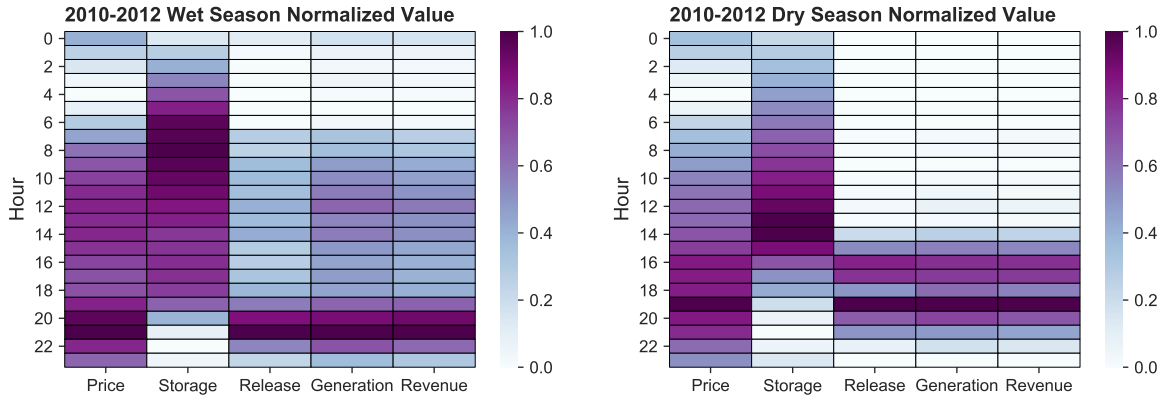

(a) Wet season of the pre-solar period

(b) Dry season of the pre-solar period

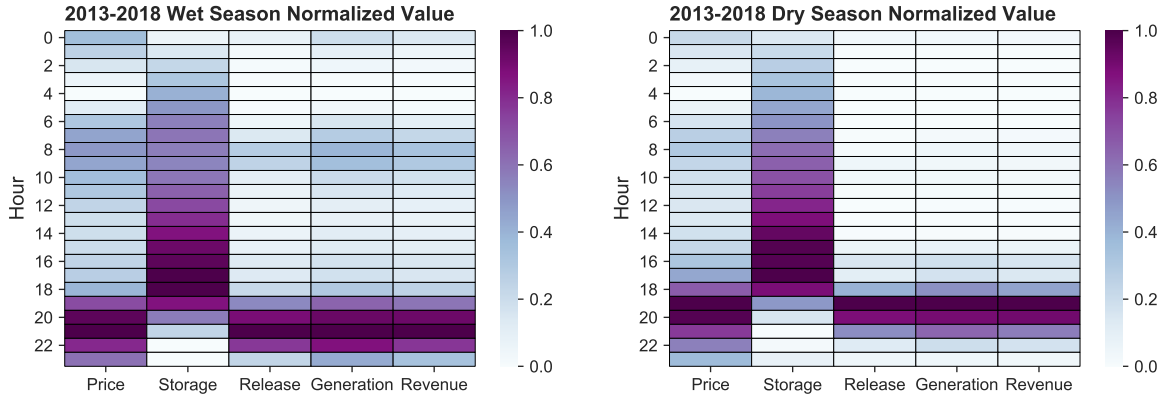

(c) Wet season of the post-solar period

(d) Dry season of the post-solar period

Figure 3.16: Summary of annual operations with normalized values for pre-solar (2010-2012) and post-solar (2013-2018) periods

Water resources system management evolves as policies, operating rules, environmental regulations, and climatic conditions change. Adaptive management is key for robust, reliable, and resilient water resources system management, including flood, water supply, ecosystem, and hydropower, and to use limited resources efficiently (Medellín-Azuara et al., 2008; Connell-Buck et al., 2011; Hanak & Lund, 2012; Lund & Moyle, 2013; Ahmadi et al., 2014; Hui et al., 2018). Adapting short-term hydropower reservoir operations to the new price scheme increases overall hydropower revenue. Figure 3.17 compares actual hourly reservoir outflows of Shasta and Pine Flat for pre-solar and post-solar periods in wet and dry seasons. Based on these reservoir release records, Shasta seems to follow the hourly price curve for its release decisions, releasing more when energy prices are higher and less with lower prices to increase overall hydropower revenue. Pine Flat, on the other hand, does not optimize short-term operations for hydropower, and release decisions do not change across hours. Although Shasta's operations are good for increasing hydropower revenue, it can do better with adapted operations by reducing generation releases in solar generation hours and increasing the evening peak generation. Using

mathematical optimization modeling, both plants can increase their hydropower revenues with release schedules discussed before. Pine Flat has a much more room for a better short-term hydropower operations in terms of allocating releases to more profitable hours and increasing hydropower revenue.

Useful adaptations include:

- Hydropower releases are not valuable or optimal in hours when solar generation is higher in either season.
- If water availability is greater (in the wet season), releases are made twice a day to generate during on-peak hours in the morning and evening.
- If water is more scarce, generate only during the most valuable hours (the evening peak).
- Storing water during less profitable hours and energy generation during the evening peak for extended durations increases overall hydropower revenue.

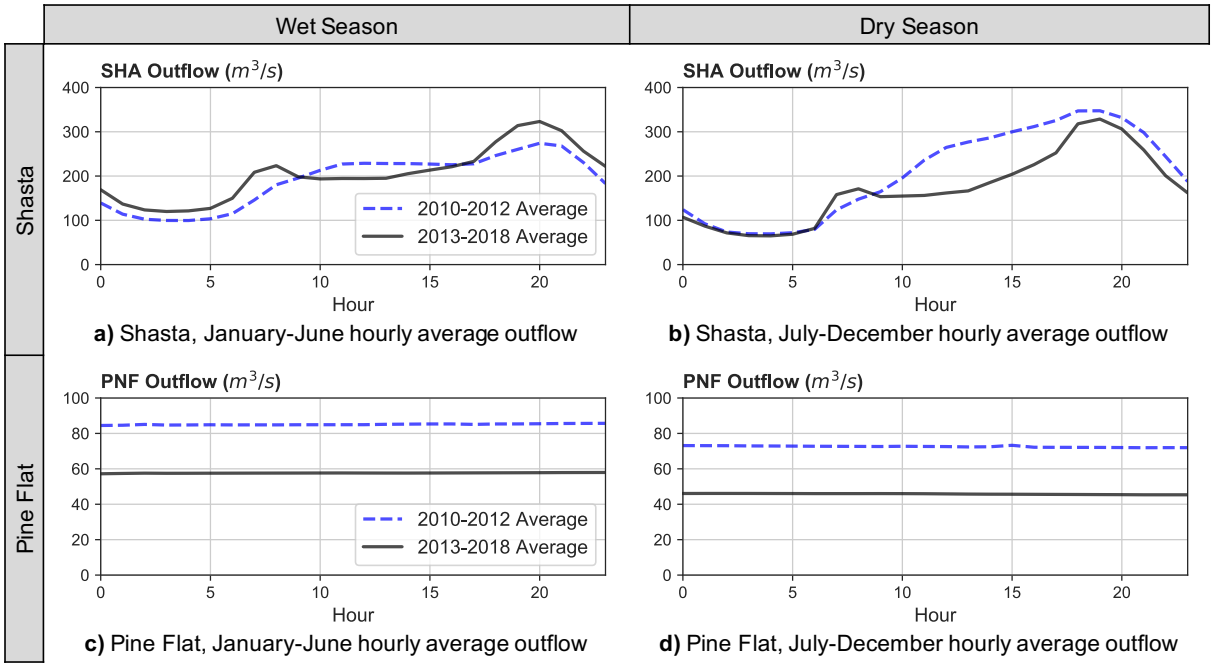

Figure 3.17: Hourly average actual reservoir outflows of Shasta (SHA) and Pine Flat (PNF) in wet (Jan.-Jun.) and dry (Jul.-Dec.) seasons (Data source: CDEC)

3.8 Conclusions

This chapter presented effects of new energy price patterns from renewable generation, particularly solar energy, on short-term hydropower operations, using a hybrid LP-NLP hydropower optimization model. The expansion of solar generation, as part of California's renewable goals, decreased energy prices significantly during daylight hours, when

solar generation peaks, resulting in a two-peak net demand and energy price pattern. The first peak occurs around 8 in the morning, and the second peak occurs around 20 in the evening. This new energy price pattern considerably affects dispatchable hydropower operations. The new price pattern, if adapted to, is more profitable for short-term hydropower operations. In the wet season, twice-daily hydropower pulse releases, without much generation between 10 and 18, increase hydropower revenue. In the dry season, the evening price peak is much greater than the morning. With more limited water availability in this season, operations concentrate on the evening peak hours with a shorter duration. Large hydropower pulse releases in a smaller duration of time can potentially harm downstream ecosystems, but most reservoirs have a small afterbay which can reduce the impacts of these pulses. California will increase renewable generation to meet its RPS target of 50% by 2030. Given most of this target is from solar generation, the State might double current solar generation. This will continue to lower energy prices during solar hours and reshape energy price pattern, giving more opportunities for operational optimization of dispatchable hydropower.

Chapter 4

Climate Change Effects on Long-term Hydropower Planning

4.1 Introduction

Climate change impacts in water resources planning are usually evaluated by applying projected climate variables, temperature and precipitation, derived from general circulation models (GCM) to a hydrologic model, which outputs variables, such as runoff (Kopytkovskiy et al., 2015). Each GCM is considered as a different climate scenario. Scenario-based approaches reflect system performance under different uncertain conditions and benefit decision makers by looking at operations from different perspectives, where mean and median impacts are more relevant for risk-neutral decisions, such as hydropower planning, whereas extreme conditions might be more relevant for risk-averse decisions, such as floods and droughts (Brekke et al., 2009).

The LP hydropower optimization model is run for several climate projections, ranging wetter to drier, but all are warmer than the historical climate. The downscaled climate projections and hydrologic variables are developed as a part of California's Fourth Climate Assessment and publicly available (cal-adapt.org). This dataset also includes routed stream flow for selected locations shown in Table 4.2. For two plant locations, Sacramento River at Shasta and Kings River at Pine Flat, available routed stream flow locations do not overlap with the hydropower model. Thus, a routed stream flow predicting model is developed for those locations, discussed in subsequent sections.

Figure 4.1 shows analytical modeling process for this chapter. The Variable Infiltration Capacity (VIC) hydrologic model (Liang et al., 1994) is run with downscaled GCM variables (Pierce et al., 2014) under 20 future climate scenarios (10 models and 2 rcps: medium and high CO_2 cases), producing hydroclimatic data, including routed stream flows (Cal-Adapt, 2018). Routed stream flow predicting model is run for two plant location, where VIC routed runoff is now available. Then the hydropower optimization model is run with predicted stream flows and energy prices from CAISO (2018b). Hydropower generation is evaluated under historical and 20 future climate projections, and results are presented.

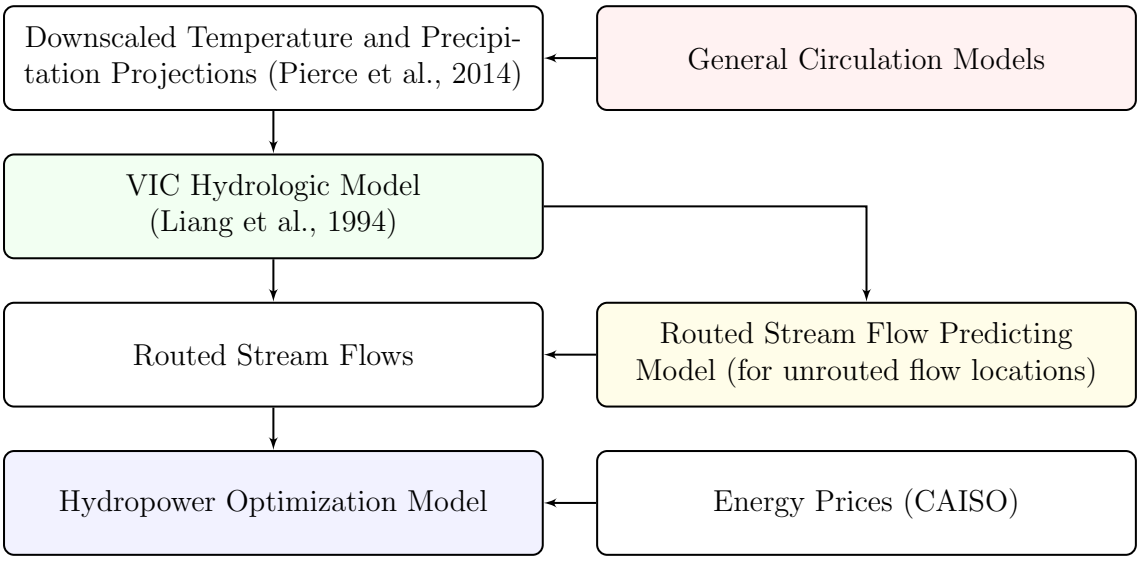

Figure 4.1: Analytical modeling framework

Monthly average energy prices (a) and demands (b) are shown in Figure 4.2. Due to California's climatic conditions, energy demand is much higher in summer (air conditioning), peaking marginal wholesale energy prices in August. Cheaper hydropower generation, especially from high-elevation plants, reduces energy prices in spring. The hydropower optimization model is driven energy prices and constrained by water availability and physical capacities. The model only considers hydropower objectives (Equations 2.21 and 2.12). Many modeled plants are operated mainly for water supply with hydropower generated as byproduct. However, higher energy prices in summer somewhat coincide with irrigation season water demand.

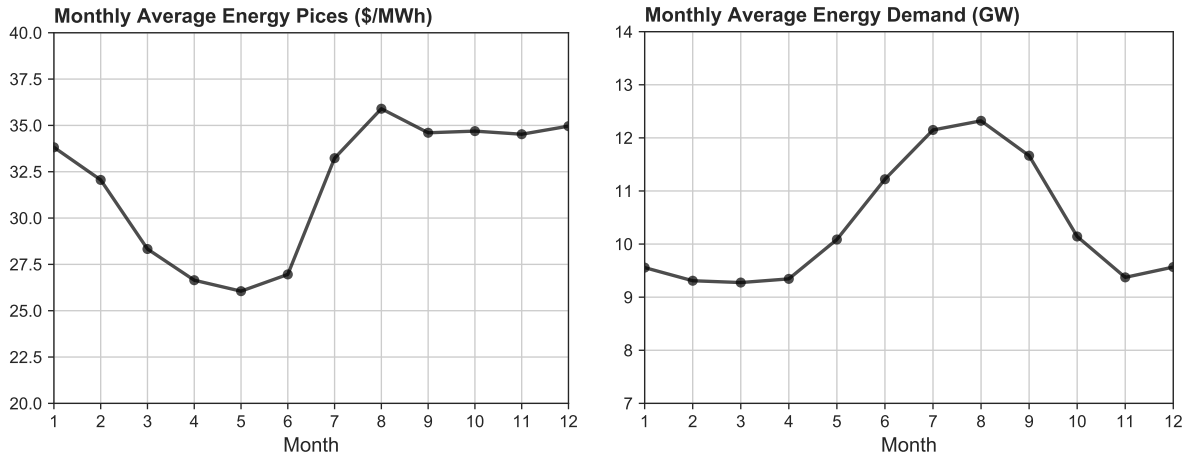

(a) Energy price ($/MWh)

(b) Energy demand (MW)

Figure 4.2: Monthly average marginal energy prices between 2010 and 2018 (Data source: CAISO)

4.2 Modeled Hydropower Plants

Modeled hydropower plants (Figure 4.3) can be categorized based on their historical hydrographs (Figure 4.4) into three groups: Cascade Range (CR); Northern Sierras (NS); and Southern Sierras (SS). CR plants (Shasta and Keswick) are fed mostly by rainfall, which peaks in winter, with some baseflow during summer. NS plants (Oroville, Englebright, Folsom and Nimbus) are considered mixed rainfall and snowmelt-fed plants, where average stream flow peaks in May due to snowmelt. There is also considerable stream flow during winter and some baseflow during summer, but much lower than CR plants. The third category SS plants (New Melones, Don Pedro, New Exchequer and Pine Flat) are mostly fed by snowmelt and have significant flow variations between months with very low summer baseflow. All these plants are in the lower foothills of surrounding mountains with large storage capacities, which give them some operational flexibility, facilitating climate adaptation, unlike high-elevation low storage (run-of-river) plants with little operational flexibility and adaptability.

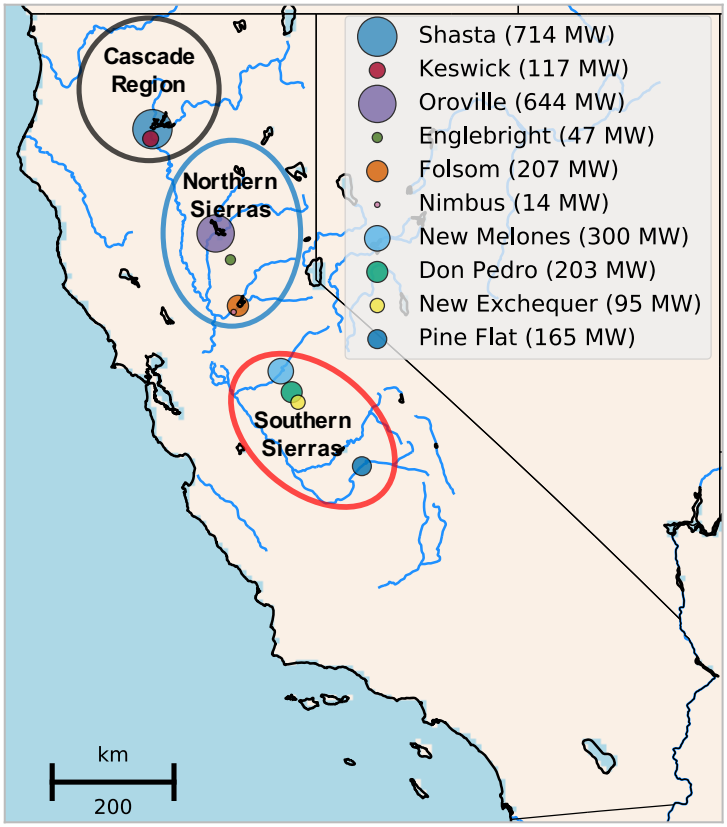

Figure 4.3: Modeled hydropower plants for long-term climate scenarios

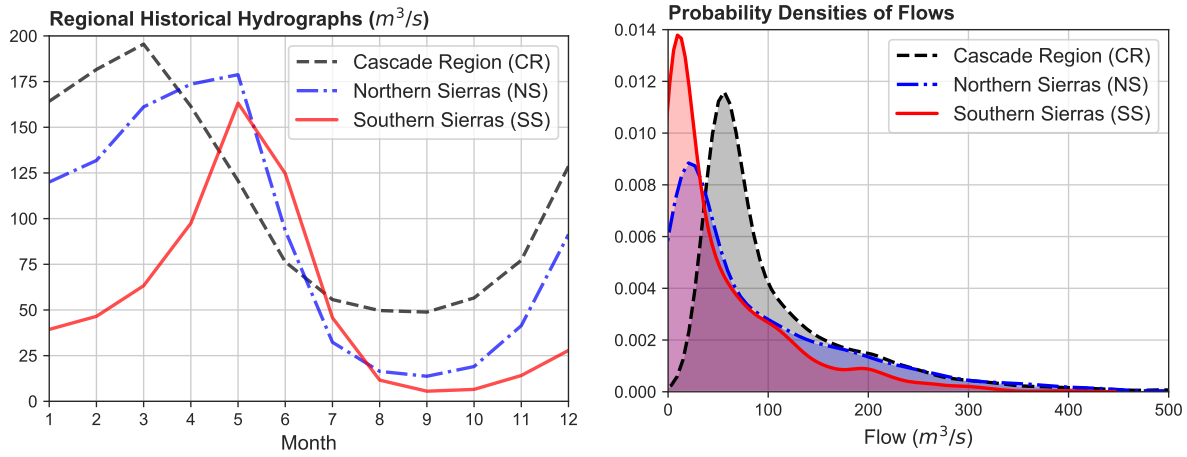

(a) Monthly average inflows (m^3/s)

(b) Probability (kernel) densities of inflows

Figure 4.4: Regional monthly historical (1922-2014) hydrographs and probability densities of three systems with flow regimes historically dominated by mostly rainfall runoff (CR), mixed rainfall and snowmelt runoff (NS) and mostly snowmelt runoff (SS) (Data source: CDWR)

4.3 Climate Scenarios

All climate models (Table 4.1) predict warmer air temperatures for California, with an average increase of 1.5-2 ^oC under medium (rcp 4.5) and 2-3 ^oC under high or business-as-usual (rcp 8.5) CO_2 emission cases. Precipitation predictions vary among the models. Some models, such as CanESM2 and CNRM-CM5, predict a wetter future with an average increase of 14-25% by the end of this century, while others models, such as ACCESS1-0, HadGEM2-ES and MIROC5, predict a drier climate with an average reduction of 1-4.5%. Ensemble average and ensemble median of 20 climate scenarios are 4.7 and 1.6 % increase than historical conditions. So, on average the climate is expected to become slightly wetter.

Table 4.1: Changes in average daily air temperature and precipitation between 2014-2100 downscaled over California under 20 climate projections (10 models and 2 rcp scenarios) compared to historical climate (1950-2013) (Data source: cal-adapt.org)

		Change in Average			
		Temperature (Δ°C)		**Precipitation** (%)	
Model	**Institution**	RCP 4.5[1]	RCP 8.5[2]	RCP 4.5	RCP 8.5
ACCESS1-0	CSIRO, and Bureau of Meteorology, Australia	1.78	2.48	-1.1	-4.5
CanESM2	CCCMA, Canada	2.02	2.81	14.3	22.8
CCSM4	NSF, Department of Energy, and NCAR, USA	1.56	2.29	4	6.1
CESM1-BGC	NSF, Department of Energy, and NCAR, USA	1.49	2.12	5.7	10.8
CMCC-CMS	Centro Euro-Mediterraneo per i Cambiamenti, Italy	1.51	2.24	0.6	0.9
CNRM-CM5	CNRM Meteo-France, and CERFACS, France	1.64	2.31	16	19
GFDL-CM3	NOAA Geophysical Fluid Dynamics Laboratory, USA	1.95	2.63	2.9	0.6
HadGEM2-CC	Met Office Hadley Centre, UK	1.79	2.79	2.3	0
HadGEM2-ES	Met Office Hadley Centre, UK	1.95	2.78	-1.1	-0.2
MIROC5	JAMSTEC, AORI, and NIES, Japan	1.68	2.14	-2.6	-1.4
	Ensemble Average	1.74	2.46	4.1	5.4
	Ensemble Median	1.73	2.40	2.6	0.8

[1]Medium and [2]High (business-as-usual) CO_2 emission scenarios

Changes in precipitation and temperature are not uniformly distributed throughout the state. Figure 4.5 shows the spatial distribution of daily average historical (1950-2014) and ensemble average (2015-2100) rainfall and snowfall (mm/day), and percent differences on precipitation (rainfall + snowfall). Rainfall slightly increases in northern parts of the state and Sierra Nevadas. Snowfall, however, slightly decreases with changing climate. While northern parts of the state receive increased average precipitation, southern California becomes drier, which can exacerbate historical mismatch with water availability in the north and demand in the south and increase the southern California's dependence on imported water. Historically, temperature is higher in the Central Valley and desert inlands of the southern California and lower in mountainous parts of the state (Figure 4.6). Temperature increases are slightly less in coastal areas and higher inland parts of the state. Increased temperature and reduced snowfall affect timing and magnitude of snowmelt runoff, which implies significant changes into California's snowmelt-driven reservoir operations.

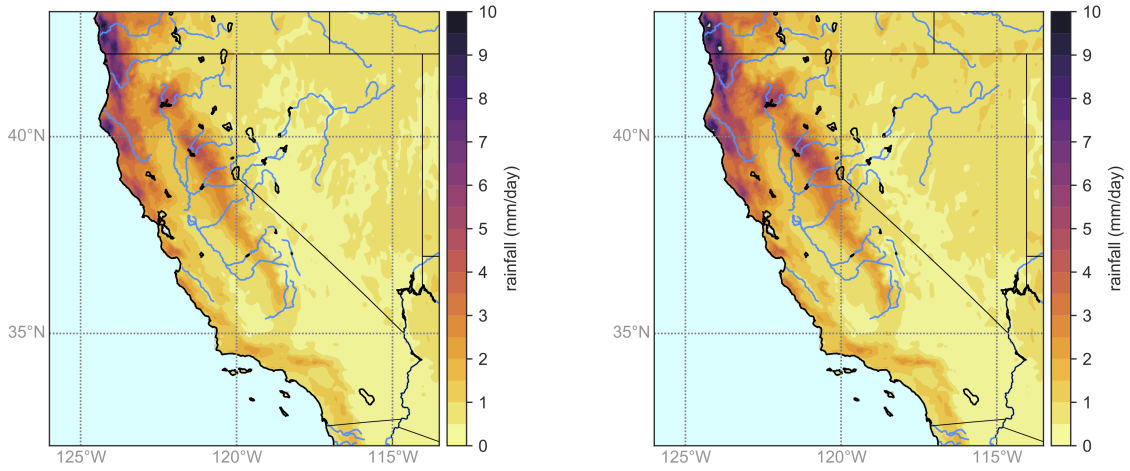

(a) Historical average rainfall (mm/day)

(b) Ensemble average rainfall (mm/day)

Figure 4.5: Historical average (1950-2014) and ensemble average across all scenarios (2015-2100) rainfall and snowfall, and change in precipitation (rainfall + snowfall) (Data source: cal-adapt.org)

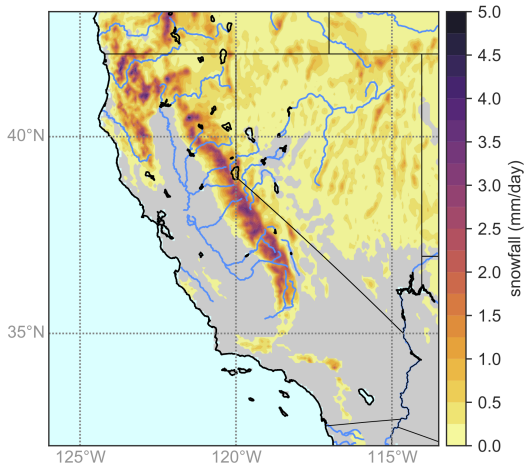

(c) Historical average snowfall (mm/day)

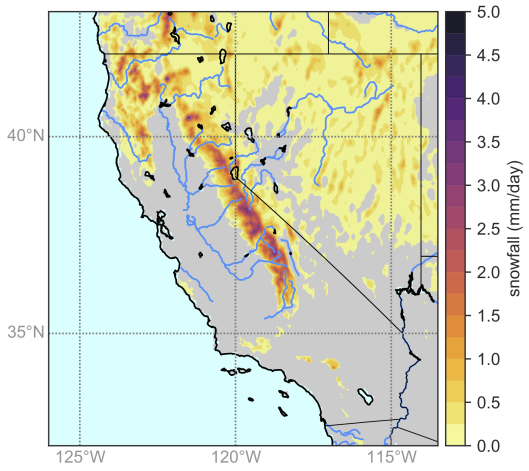

(d) Ensemble average snowfall (mm/day)

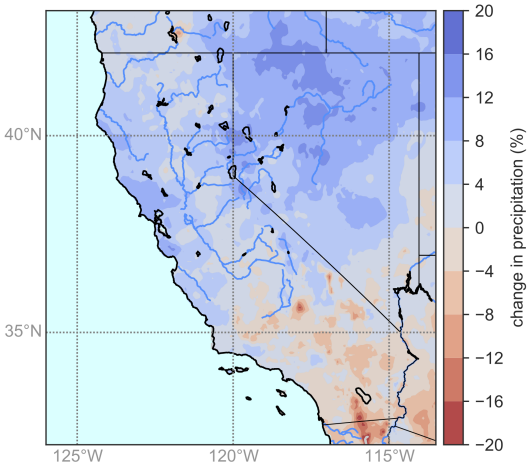

(e) Change in precipitation (%)

Figure 4.5: Historical average (1950-2014) and ensemble average across all scenarios (2015-2100) rainfall and snowfall, and change in precipitation (rainfall + snowfall) (Data source: cal-adapt.org)

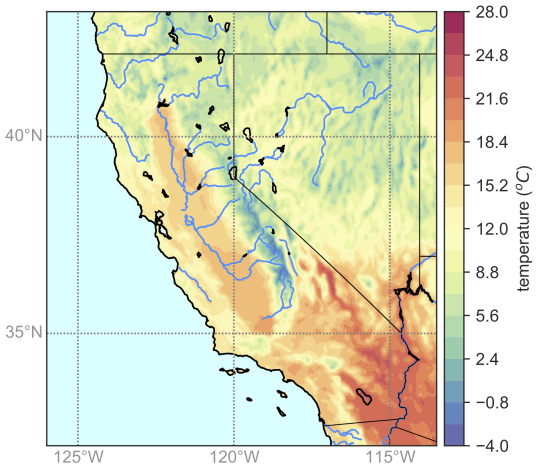

(f) Historical average temperature (^oC)

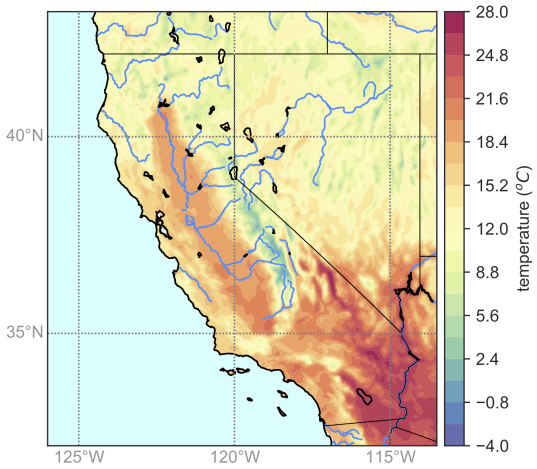

(g) Ensemble average temperature (^oC)

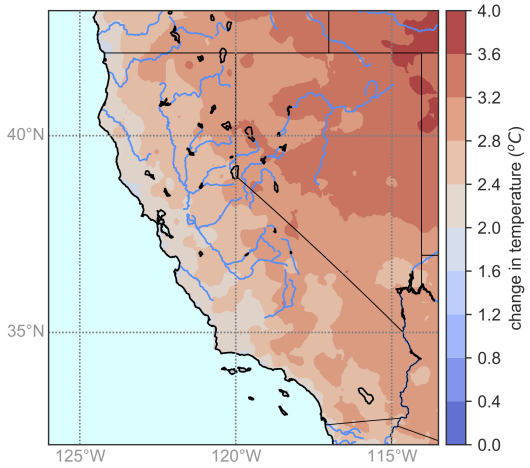

(h) Change in temperature (^oC)

Figure 4.6: Historical average (1950-2014) and ensemble average across all scenarios (2015-2100) daily temperature, and change in temperature (Data source: cal-adapt.org)

4.4 Routed Stream Flow Predicting Model

The fourth climate assessment dataset includes routed stream flows for several locations (Cal-Adapt, 2018). But two plant locations, Sacramento River at Shasta and Kings River at Pine Flat, of the hydropower optimization model are not included. A statistical model is developed to predict routed stream flows for those missing locations. Routed stream flow predicting model (RSFPM) takes VIC variables and VIC routed flows shown in Table 4.2 and makes predictions using Random Forest method (Breiman, 2001). Random Forest is a tree-based ensemble method and uses patterns and relationships between input and predictor variables to make predictions.

Table 4.2: VIC variables and VIC routed stream flows used to predict routed stream flow

VIC Variable	**VIC Routed Stream Flow**
- Rainfall (mm/day)	- Sacramento River at Red Bluff
- Snowfall (mm/day)	- Feather River at Oroville
- Precipitation (mm/day)	- Yuba River at Smartville
- Snowmelt (mm/day)	- Bear River at Wheatland
- Unrouted baseflow & runoff (mm/day)	- American River at Fair Oaks
- Incoming & net radiation (W/m^2)	- Mokelumne River at Pardee
- Soil moisture (mm)	- Stanislaus River at New Melones
- Air temperature (^oC)	- Calaveras River at Jenny Lind
- Relative humidity (%)	- Tuolumne River at Don Pedro
- Total evapotranspiration (ET) (mm/day)	- Merced River at New Exchequer
- Potential ET (mm/day)	- San Joaquin River at Millerton

The RSFPM generates decision trees using input variables shown in Figure 4.7. The model determines split points that minimize mean squared error for each estimator at each depth. The bottom layer has the final values of decisions. Once the tree structure is formed based on a training dataset, the model predicts routed flows using VIC variables for each climate scenario, performing 'true' and 'false' operations starting from the top of the tree. If the statement is true, then the left branch, if false, then the right branch is followed until the bottom of the tree is reached, where final values (routed stream flow predictions) are located. The RSFPM creates many decision trees, forming the forest, and takes the ensemble average for the final decision. The ensemble average of N number of regression trees with each $T(x)$ prediction is:

$$\widehat{f}^N(x) = \frac{1}{N}\sum_{n=1}^{N} T(x) \tag{4.1}$$

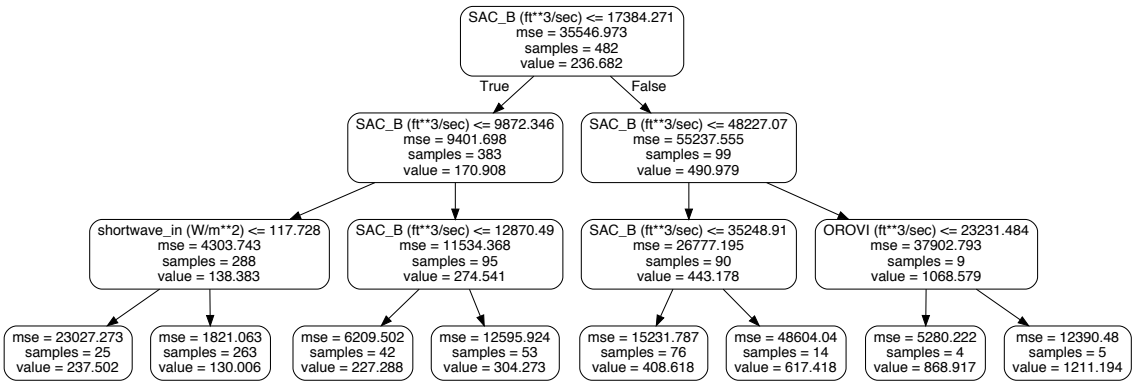

Figure 4.7: An example (simple) decision tree with a depth of 3

4.4.1 Model Testing and Prediction

The RSFPM is calibrated and tested for historical period (1950-2014) and applied to 20 climate scenarios for the future period (2015-2100). Figure 4.8 compares observed and predicted stream flows. The model predicts with reasonable accuracy. Although Kings River routed flow predictions better align on the perfect fit line (1:1), Sacramento River predictions are close to the perfect fit. Figure 4.9 shows time-series plots of observed and predicted stream flows. 90 individual trees are grown for each river location and ensemble averages are taken for the final prediction. 90 trees of the random forest is a calibrated parameter. As more trees are grown, better correlation between observed and predicted flow is achieved. But, after 90 trees, the correlation benefit (greater Pearson's r) does not change and runtime increases as more trees are grown. Finally, before making predictions, RSFPM is tested for Feather River at Oroville, where VIC routed flows are available. Figure 4.10 compares VIC routed and RSFPM routed (predicted) flows for HadGEM-ES rcp 4.5 scenario between 2015-2100. Random forest predictions reduce variance due to decision tree and ensemble averaging. RSFPM peak flows are usually slightly lower, and low flows are greater than VIC routed flows. After testing the model, Sacramento River at Shasta and Kings River at Pine Flat routed flows are predicted under 20 climate scenarios (Figure 4.11).

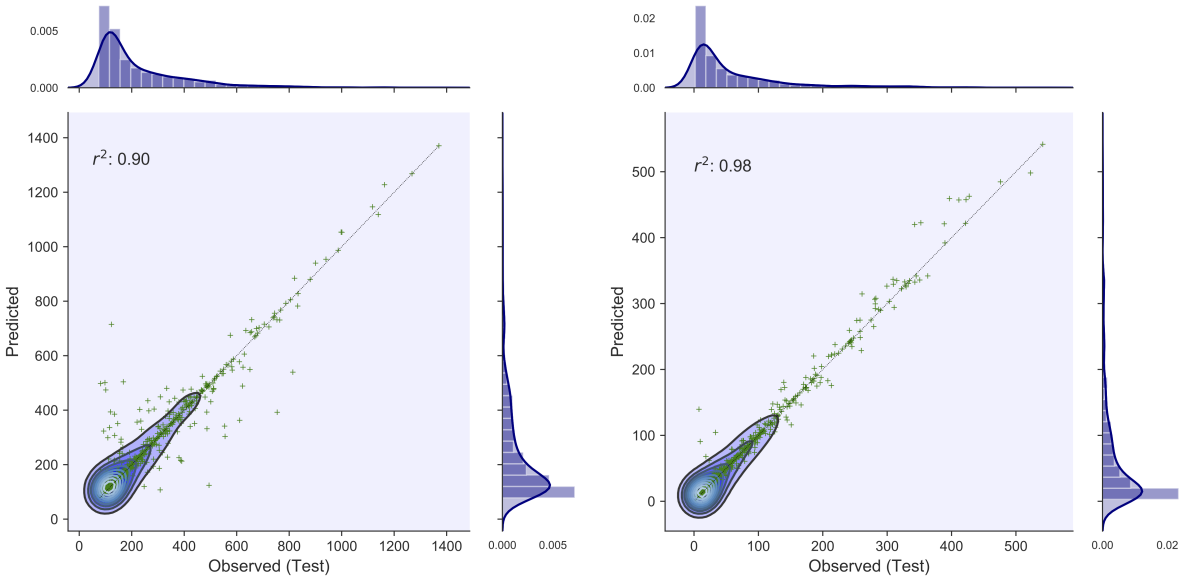

(a) Sacramento River at Shasta

(b) Kings River at Pine Flat

Figure 4.8: Observed vs. RSFPM flow prediction (m^3/s) with marginal and joint probability densities for routed flow locations

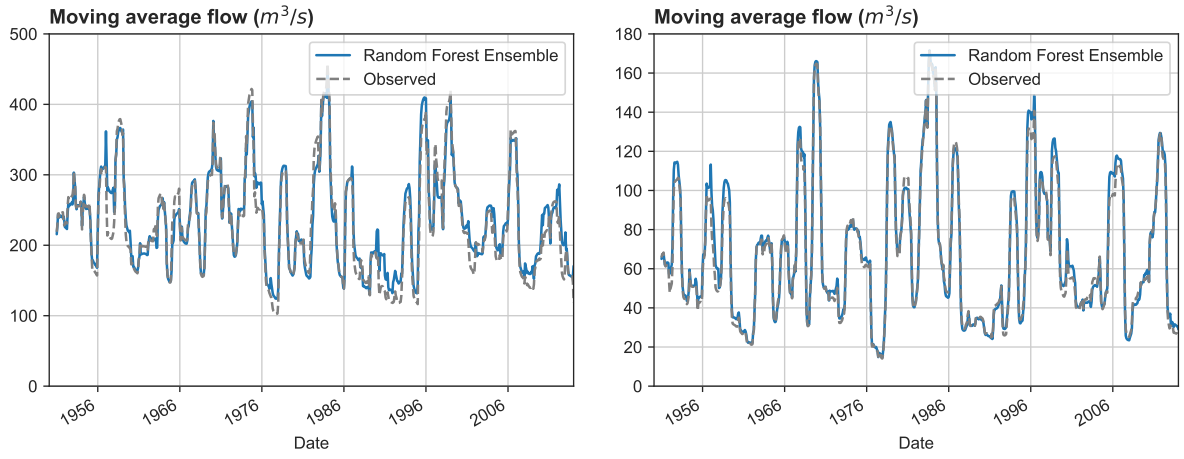

(a) Sacramento River at Shasta

(b) Kings River at Pine Flat

Figure 4.9: Time-series of observed and RSFPM predictions for routed flow locations

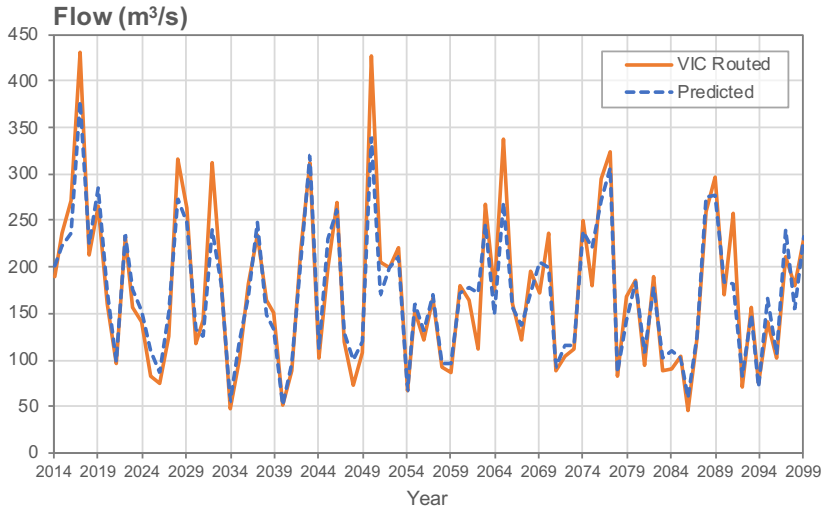

Figure 4.10: Comparison of VIC routed and RSFPM predicted flows for Feather River inflows into Oroville

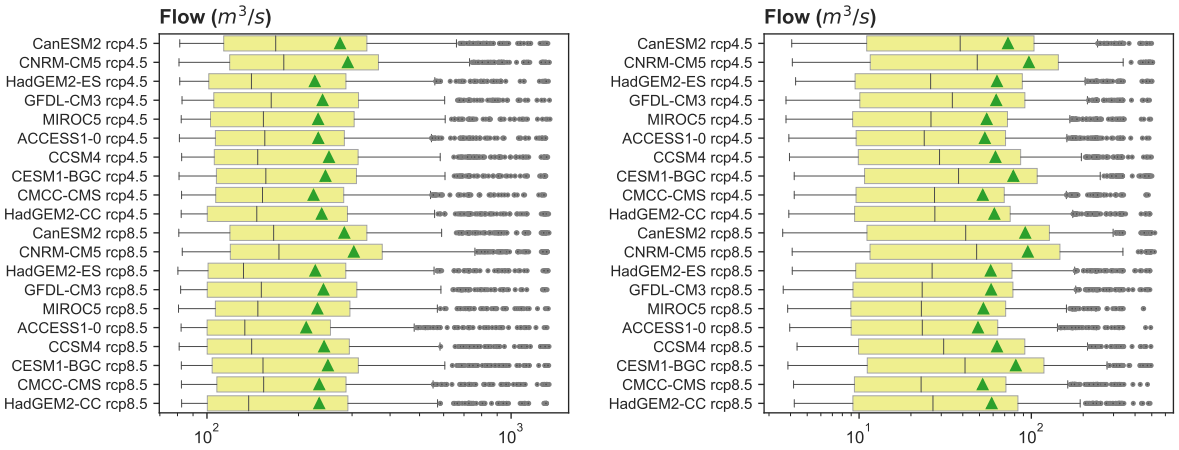

(a) Sacramento River at Shasta

(b) Kings River at Pine Flat

Figure 4.11: Routed flow predictions under 20 climate scenarios

4.5 Reservoir Inflows

Projected climate scenarios cover a wide range of hydrologic conditions, from wetter to drier, with all scenarios warmer, resulting in a variety of reservoir inflow scenarios. With climate change, probabilities of extreme events and variability of inflows are predicted to increase. Table 4.3 statistical properties of overall average reservoir inflows under future projected (2015-2100) and historical (1922-2014) climates. Because of increased and more frequent extreme events, all projections have greater maximum inflows, and most drier scenarios have greater standard deviations than historical climate. Most projected scenarios are wetter than historical climate, with the wettest scenario (CNRM-CM5 rcp 8.5) having monthly average inflow of 118 m^3/s, while the driest scenario (ACCESS1-0 rcp 8.5) has 69 m^3/s average inflow.

Table 4.3: Statistical properties of monthly average reservoir inflow (m^3/s) under projected (2015-2100) and historical (1922-2014) climates

Hydrology[1]	**Climate Scenario**	**Mean**	**Std. Dev.**	**Min**	**25%**	**50%**	**75%**	**Max**
wetter	CNRM-CM5 rcp 8.5	118	133	12	25	63	168	924
	CNRM-CM5 rcp 4.5	114	121	12	27	68	163	890
	CanESM2 rcp 8.5	111	129	11	26	61	154	1041
	CanESM2 rcp 4.5	101	106	12	25	62	140	817
	CESM1-BGC rcp 8.5	94	98	11	22	57	137	638
	CESM1-BGC rcp 4.5	89	90	12	22	54	130	598
	CCSM4 rcp 8.5	84	91	12	21	52	118	674
	HadGEM2-CC rcp 4.5	84	92	11	21	51	112	740
	CCSM4 rcp 4.5	84	88	12	21	49	118	551
	HadGEM2-CC rcp 8.5	83	91	11	20	50	112	755
	GFDL-CM3 rcp 4.5	82	75	12	21	57	121	487
	HadGEM2-ES rcp 4.5	80	85	12	20	47	113	621
	GFDL-CM3 rcp 8.5	80	80	12	19	48	116	576
	HadGEM2-ES rcp 8.5	80	91	11	19	46	104	711
	Historical	79	74	11	22	50	113	511
drier	MIROC5 rcp 4.5	79	76	12	21	53	115	570
	ACCESS1-0 rcp 4.5	78	81	11	21	51	106	675
	CMCC-CMS rcp 8.5	78	82	12	22	46	106	581
	MIROC5 rcp 8.5	76	76	11	20	49	108	614
	CMCC-CMS rcp 4.5	74	73	11	21	49	102	542
	ACCESS1-0 rcp 8.5	69	72	11	19	46	90	567

[1]Wetter or drier hydrology compared to mean historical reservoir inflow

Climate change will alter timing of reservoir inflows in addition to magnitude. Average reservoir inflows shown in Figure 4.12-(a) suggest a wetter winter and drier summer in all scenarios. Variability between winter and summer inflows increases. Although some wet scenarios predict winter flows up to 2.5 times greater than historical averages, most scenarios and the ensemble average predict about 50% increase in winter runoff peak and roughly 20% decrease in summer runoff. Figure 4.12-(b) shows monthly average reservoir inflows for historical period and early (2015-2039), mid (2040-2069) and end (2070-2100) of the century under medium (RCP 4.5) and high (RCP 8.5) emission scenarios. Monthly average inflows peak in May mostly due to snowmelt runoff under historical climate. As the climate changes, snowmelt runoff decreases and winter rainfall increases, and peak flows shift to winter, potentially causing floods and increasing summer water shortages. These changes slow down with RCP 4.5 scenarios and remain unchanged in the mid and end of the century. With RCP 8.5 scenario, snowmelt recession in spring and winter precipitation further increase until the end of the century.

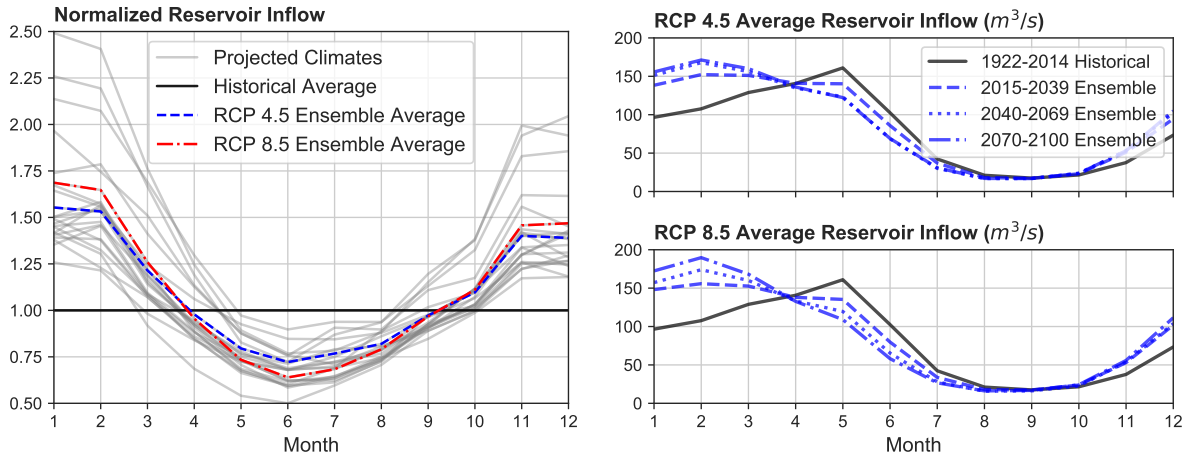

(a) Reservoir inflow ($Q_{projected}/Q_{historical}$)

(b) Historical average inflow and ensemble averages inflow for beginning, mid and end of the century

Figure 4.12: Monthly average reservoir inflow projections with ensemble averages (2015-2100) normalized to historical average (1922-2014) and shift in ensemble average inflow

4.6 Results

The LP hydropower optimization model developed in Chapter 2 is run with monthly time-steps for 20 future climate scenarios from 2015 to 2100 and for the historical climate from 1922 to 2014 with historical monthly average (2010-2018) energy prices (Figure 4.2-(a)). Ensemble average results are compared to historical average operations. Modeling results include hydropower load and generation, reservoir storage, capacity evaluation of hydropower plants and implications for run-of-river plants and presented below.

4.6.1 Hydropower Load and Generation

Hydropower load is usually favorable in energy systems with mixed generation sources due to its lower operating costs and greater operating flexibility than fossil-fueled generations (Hamlet et al., 2002; Madani et al., 2014). But hydropower generation strictly depends on water availability affected by climatic and hydrologic changes. These changes vary temporally and spatially. Figure 4.13 shows load-duration curves of ten modeled plants categorized into three hydrologic regions: Cascade Range (CR); Northern Sierras (NS); and Southern Sierras (SS). CR plants have higher hydropower loads at all durations under projected climate scenarios. But differences are greater for peak loads close to the plant capacities between durations 10 and 40%. Plants in this region generate power about 10% of time at the capacity. Reliabilities of peak loads of NS plants slightly decrease with climate change, except for Oroville, which sees an increase in duration of peak loads but decrease in smaller loads. As a smaller-storage plant, Englebright historically generates electricity at about 40% of time at its capacity, with a small reduction under RCP 8.5 ensemble average. Loads at plant capacities decrease slightly for SS plants, but ensemble average loads at around duration of 50% increase. Also, due to lower baseflow

of SS plants, they do not generate about 20% of time. Standard deviations of hydropower loads across climate scenarios increase from north to south.

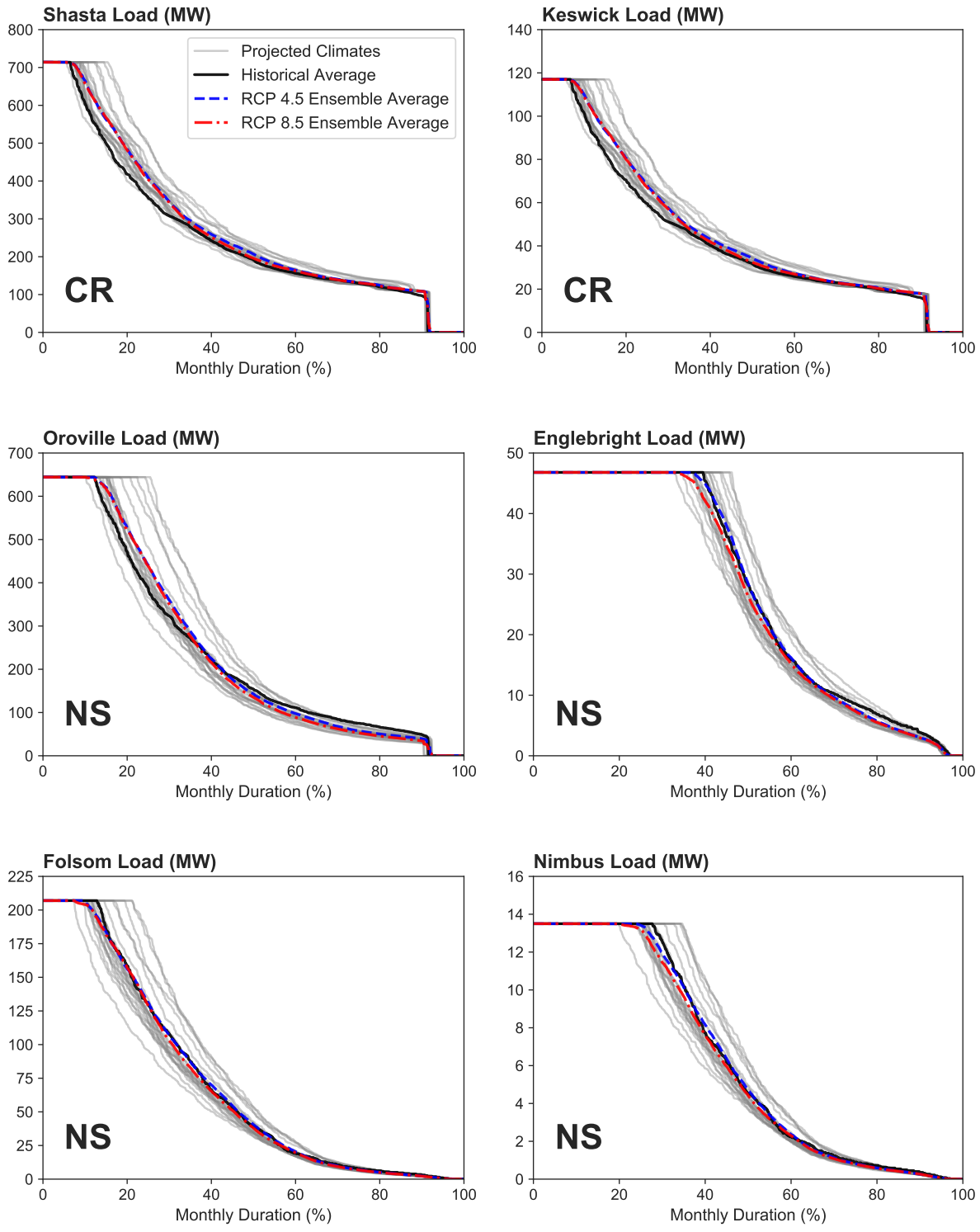

Figure 4.13: Load-frequency (reliability) curves of modeled hydropower plants under historical and projected climates for all months. Historical climate is from 1922 to 2014, and projected climates are from 2015 to 2100. (CR: Cascade Range, NS: Northern Sierras, SS: Southern Sierras)

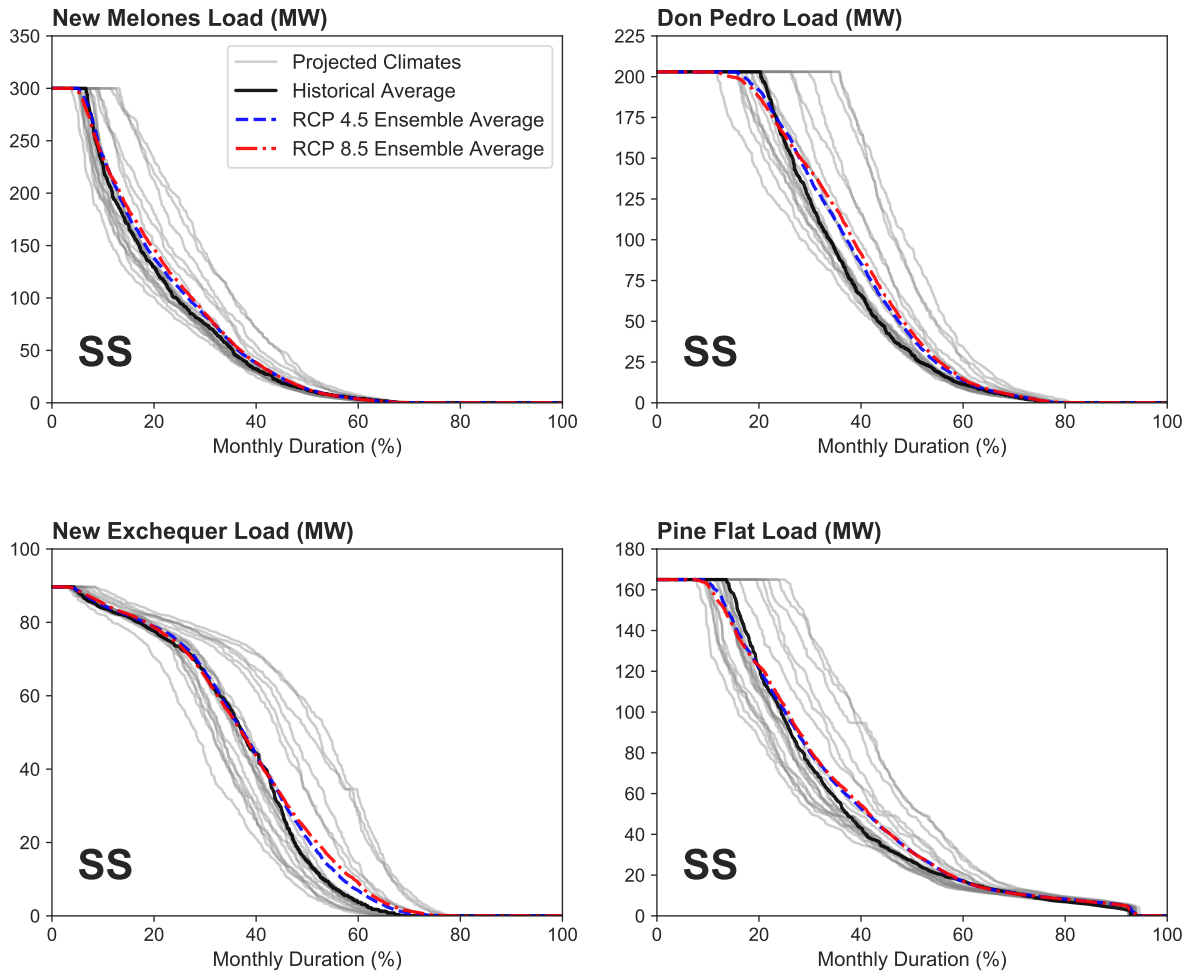

Figure 4.13: Load-frequency (reliability) curves of modeled hydropower plants under historical and projected climates for all months. Historical climate is from 1922 to 2014, and projected climates are from 2015 to 2100. (CR: Cascade Range, NS: Northern Sierras, SS: Southern Sierras)

Climate change effects on magnitude of hydropower generation are limited, especially comparing ensemble and historical averages, but temporal changes are more significant. Figure 4.14 shows monthly average hydropower generation (GWh/month) under historical (1922-2014) and future climate conditions (2015-2100), with ensemble average of RCP 4.5 and 8.5 scenarios. Generation significantly decreases in spring and early summer due to snowmelt recession. Peak generation shifts to March rather than April and May. While some wet scenarios bring peak hydropower generation close to 140 GWh, the ensemble average peak is about 10 GWh more than the historical monthly average peak. With operational flexibility from having large storage capacity, reservoir can capture some winter peak flows to maximize energy generation and revenue to make up some of the lost energy generation in spring. RCP 8.5 ensemble average generation is slightly lower in spring due to less water availability. Although winter inflows are higher in RCP 8.5 scenarios, RCP

4.5 and 8.5 ensemble average hydropower generation are mostly the same due to reservoir storage capacity and excess water is spilled.

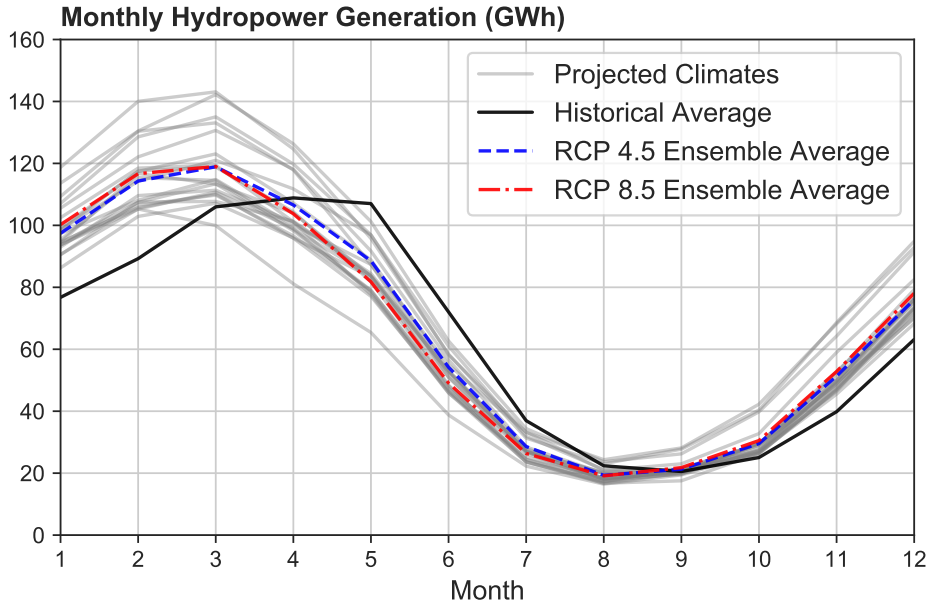

Figure 4.14: Average monthly historical hydropower generation and climate ensemble

Monthly average hydropower generation (% of historical) for each plant and climate scenario is shown in Figure 4.15, where darker green and blue are greater generation and lighter green and yellow are less generation than historical. Wet scenarios, such as CanESM2, CNRM-CM5, and CESM1-BCG, result is much higher hydropower generation, especially in SS plants, where average generation increases up to 50%. Also, for such wet cases, changes in Oroville's generation is similar to changes in CR plants, operating more like mostly rainfall-driven plants. Climate scenarios have less effect on CR plants, with average generation close to historical levels. Also, some NS plants, such as Englebright and Nimbus, are less affected, because of their lower storage capacities. Generation variances are much higher in SS plant among climate scenarios. Overall, under projected climates, almost all plants have slightly more generation than historical operations, with some exceptions, such as ACCESS1-0 rcp 8.5.

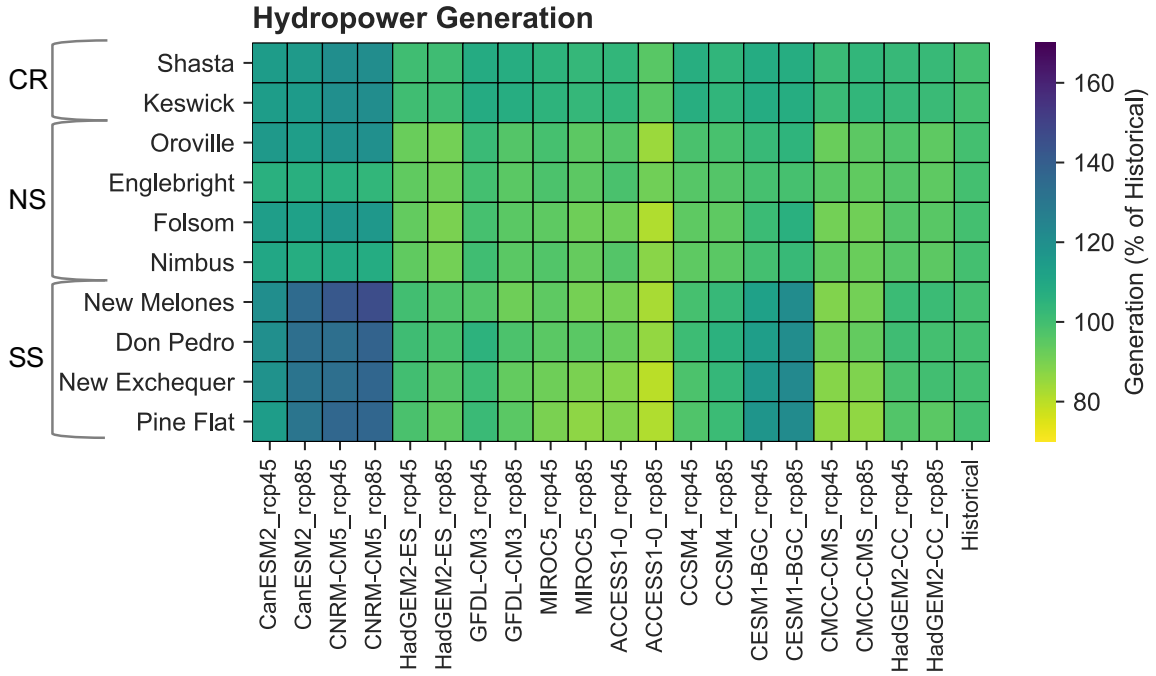

Figure 4.15: Monthly overall average hydropower generation (% of historical) of modeled plants under 20 climate scenarios normalized to historical generation (CR: Cascade Range, NS: Northern Sierras, SS: Southern Sierras)

Hydropower generation changes depend on water availability. Figure 4.16 shows relative changes between historical and ensemble average hydropower generation and water availability (Equation 4.2). If monthly water availability increases with climate change, generation increases, but less than the percent increase in the water availability (below red line), because generation is limited by plant turbine and storage capacities and some excess water is spilled, even though plants optimize their operations to capture additional inflow. If monthly water availability increases by 100% (wet months, January-March), generation only increases by 25%. Reduced water availability decreases generation, but with adaptation, percent reduction in generation is less than percent reduction in water availability (above red line). In this case, if monthly water availability decreases by 75% (dry months, August-October), generation decreases by about 60%. Adaptation capability from having storage capacity is discussed in the next section.

$$\Delta f_i(\%) = \frac{f_{ensemble,i} - \widehat{f}_{historical}}{\widehat{f}_{historical}} 100, \forall i \in \{1, 2, ...12\} \tag{4.2}$$

where $f_{ensemble,i}$ is ensemble average hydropower generation or water availability (inflow) for each month i, and $\widehat{f}_{historical}$ is historical overall monthly average hydropower generation or water availability.

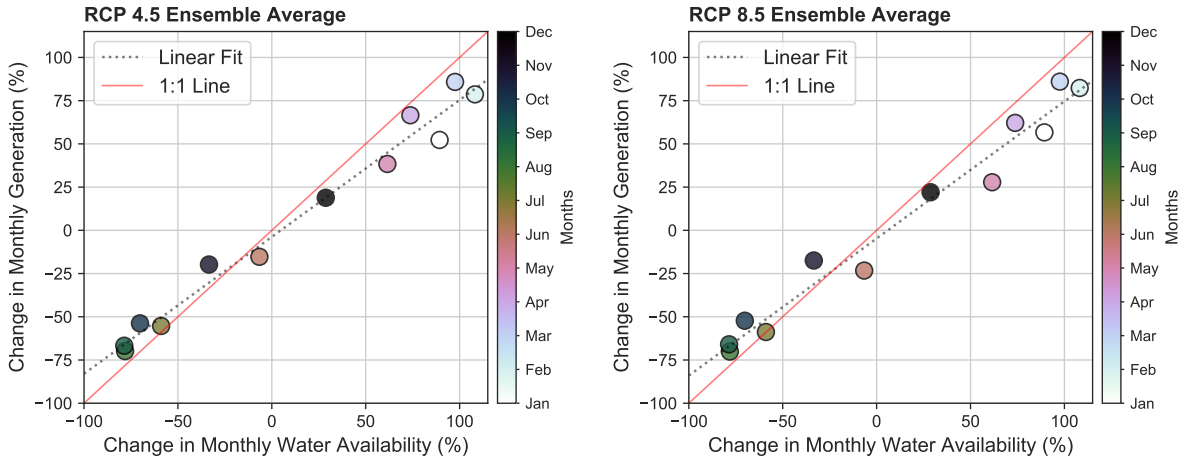

(a) RCP 4.5 ensemble average

(b) RCP 8.5 ensemble average

Figure 4.16: Change (%) in monthly generation and water availability between historical (1922-2014) and ensemble (2015-2100) 4.5 and 8.5 average climates (across 12 months)

4.6.2 Reservoir Storage

Reservoirs add flexibility to water resources operations. They also help maximize meeting water and energy demands by storing water when demand is lower and water supply is higher and releasing when demand is higher and water is scarcer. Shifts in timing and magnitude of water availability with climate change significantly change reservoir operations. Peak storage shifts to May with climate change rather than historical peak occurring in July (Figure 4.17-(a)). Climate change increases storage in winter with increased inflows under climate change. Summer and fall storage, however, is lower than historical average. Because of wetter winters and late falls, dry season storage is lowered for more hydropower generation with an anticipation to fill reservoirs later during the year. Flood pools are not dynamically represented and the physical reservoir capacity is kept constant across months. In some wet scenarios, higher winter storage increases frequency of hitting flood pool.

Spills are penalized with a small persuasion cost to minimize foregone energy in the hydropower optimization model (Equations 2.12 and 2.21). If a plant's reservoir capacity is full and inflow exceeds turbine release capacity, it spills the excess water. Figure 4.17-(b) shows change in monthly average spills (m^3/s) under projected climate scenarios. All projected scenarios result in more spills than for the historical climate, while spills only slightly decreases in a few drier scenarios in May an June. Increased winter inflows result in spills differences up to 25 m^3/s in the wettest scenario with an ensemble average of 10 m^3/s in January and February. Spills are higher with RCP 8.5 ensemble average in winter and slightly lower in spring.

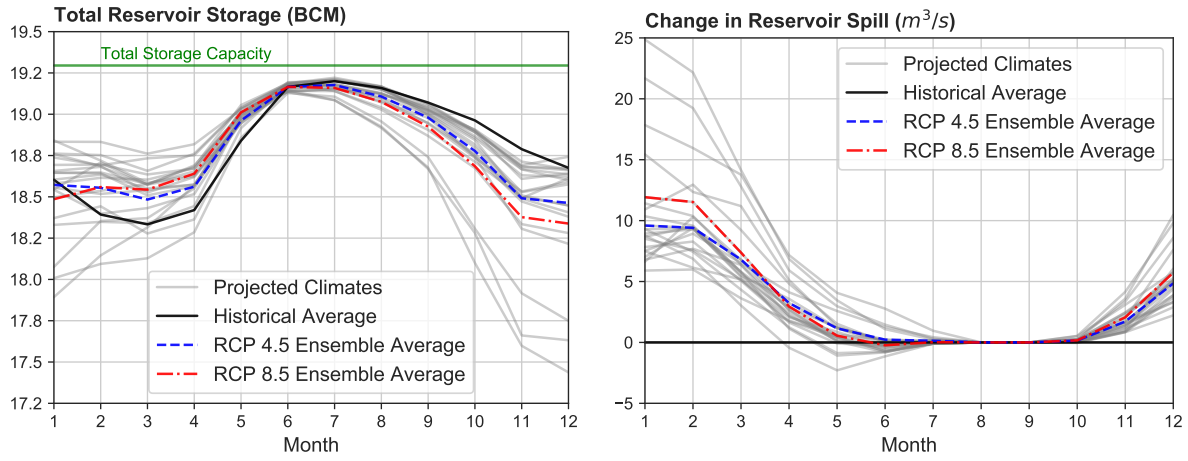

(a) Reservoir storage

(b) Change in reservoir spill

Figure 4.17: Monthly average reservoir storage (BCM) and change in spill (m^3/s) under historical and projected climates

Figure 4.18 shows how adaptability changes with storage capacity. Adaptability is measured with standard deviation of monthly hydropower generation across projected scenarios and historical climate. It illustrates storage capacity (MCM) on the x-axis and range of standard deviation of monthly average generation under different climate conditions (boxplot) and historical climate (star) on the y-axis. As storage capacity increases, with operational flexibility, plants can better adapt to changed (wetter or drier) climates, resulting in greater standard deviations. Plants with smaller storage capacities, however, have little room to make operational adjustments and have less adaptability. The purpose of reservoirs is to regulate temporal water availability and demand mismatch. As this variability increases with climate change, the role of reservoirs become more important, especially with large storage capacity, such as Shasta and Oroville, which have more variability with climate change than historical hydrology. Operations of smaller plants cannot be affected as much by climatic changes.

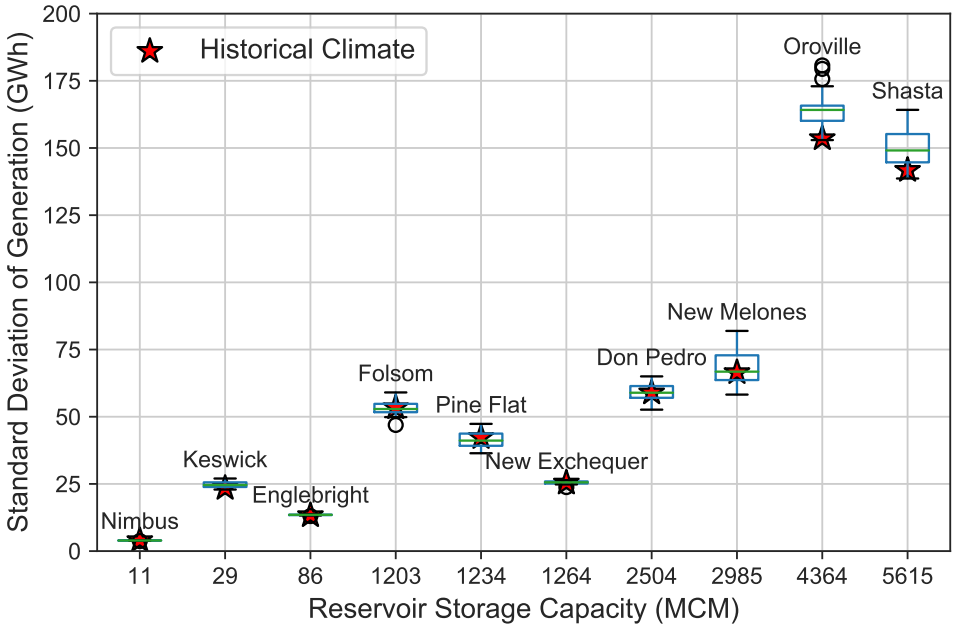

Figure 4.18: Adaptability of hydropower plants with different storage capacities under climate change. Boxplot shows range of standard deviations of monthly hydropower generation under 20 projected climates (2015-2100) and star shows standard deviation of generation under historical climate (1922-2014). Note: X-axis is not on scale

4.6.3 Hydropower Revenue

The hydropower optimization model maximizes hydropower revenue across all plants and time-steps (Equation 2.21). With a price-taking approach, energy prices are assumed exogenous and hydropower operations do not affect energy prices, eliminating second-order effects. Table 4.4 shows monthly average hydropower revenue ($M/month) and change in revenue (%) from 10 modeled plants under the projected climate scenarios and historical climate. This revenue increases proportionally with wetness of the scenario, limited by plant capacities. Wetter climate scenarios have revenue increases of 10-25% compared to historical climate. Drier climates result in revenue decreases of 1-11%. Because of big variations of average revenue among projected climates, ensemble average revenues are 21.46 and 21.26 million dollars, while ensemble median revenues are 20.71 and 20.45 million $ under rcp 4.5 and rcp 8.5 respectively. Ensemble average revenues are greater than historical average revenue of 20.54 million dollars by 4.5% and 3.5%, but ensemble median is only 0.8 % greater under rcp 4.5 and 0.4% less under rcp 8.5. Here monthly average energy prices are used to separate price effects and evaluate only hydrologic effects on hydropower generation (Figure 4.2). Although monthly distribution does not change, other variables, such as petroleum and natural gas may significantly change energy prices, resulting in different hydropower revenues, but revenue differences should be similar.

Table 4.4: Monthly average hydropower revenue in million dollars per month and change in revenue (%) under projected and historical climate scenarios

	Revenue[1] (10^6\$)		**ΔRevenue** (%)	
Scenario	rcp 4.5	rcp 8.5	rcp 4.5	rcp 8.5
CNRM-CM5	25.54	25.64	24.3	24.8
CanESM2	23.85	24.45	16.1	19
CESM1-BGC	22.17	22.78	7.9	10.9
GFDL-CM3	21.42	20.61	4.3	0.3
CCSM4	20.86	20.88	1.6	1.7
HadGEM2-CC	20.56	20.29	0.1	-1.2
MIROC5	20.5	19.93	-0.2	-3
HadGEM2-ES	20.07	19.84	-2.3	-3.4
ACCESS1-0	20.03	18.19	-2.5	-11.4
CMCC-CMS	19.64	19.97	-4.4	-2.8
Ensemble Average	21.46	21.26	4.5	3.5
Ensemble Median	20.71	20.45	0.8	-0.4
Historical Average	20.54		0	

[1]Revenue is not adjusted for inflation

Figure 4.19 shows how monthly average revenue across projected climates change with changes in water availability using Equation 4.2, with f representing overall average monthly revenue and water availability for each scenario. Hydropower revenue increases with water availability as more hydropower is generated, but limited by plant turbine and storage capacities. If water availability increases by 50%, revenue increases by only 25% because excess water is either spilled or used lower-valued months. As water availability decreases, limited water is used in higher-valued months, reducing negative impacts.

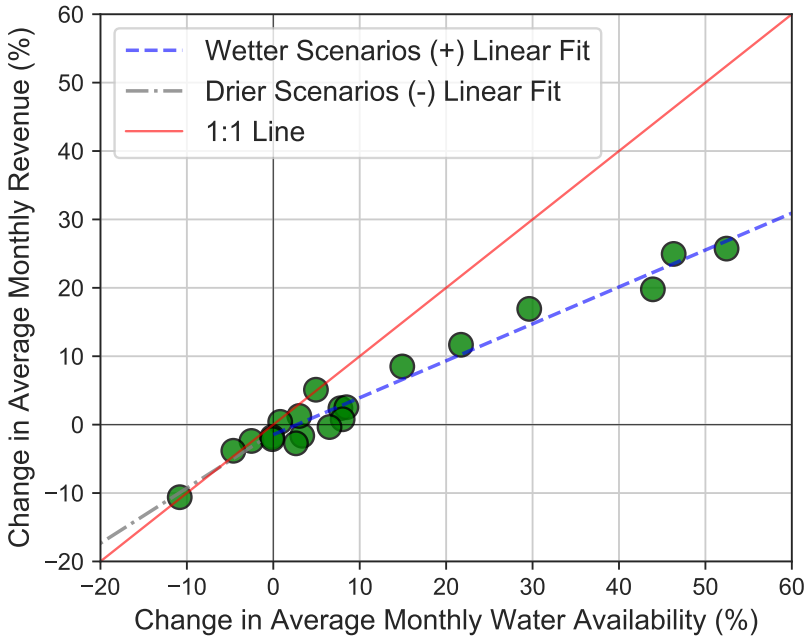

Figure 4.19: Change (%) in monthly generation and water availability between historical (1922-2014) and projected (2015-2100) climates (across 20 climate scenarios)

Figure 4.20 shows monthly revenue difference between ensemble average and historical average climates. Overall, revenue increases in fall and winter, and decreases in spring and summer. Increased fall and winter runoff help compensate for revenue losses from reduced snowmelt runoff in spring and summer, resulting in an average net increase of 1.3 million $ per year in medium emission (rcp 4.5) and 1.1 million $ per year in high emission (rcp 8.5) scenarios. With solar energy, if hydropower generation is allocated to higher-valued hours, as discussed in Chapter 3, benefits can be increased and losses can be minimized, resulting in more net revenue.

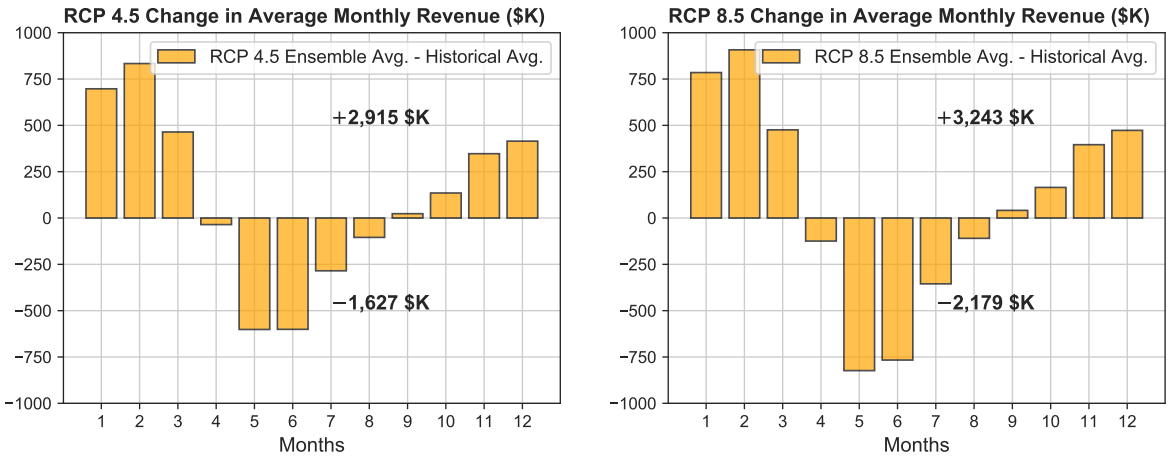

(a) RCP 4.5 revenue change

(b) RCP 8.5 revenue change

Figure 4.20: Change in monthly hydropower revenue ($K) for each month (Ensemble average minus historical average)

4.6.4 Capacity Evaluation and Investment

Expanding turbine capacity is evaluated for historical and projected climates by using dual variables (Lagrange multipliers) on capacity constraints. In mathematical optimization (linear and nonlinear programming), each constraint including lower bounds, upper bounds, and mass balances (Equations 2.22, 2.23, and 2.24), have an associated dual variable or Lagrange multiplier. A dual variable shows the change to the objective function (Equation 2.21) if there were one more unit (m^3/s) of that constraint (turbine capacity), shown in Equation 4.3. Since the objective function is revenue here, it shows the direct benefit of expanded turbine capacity in a specific time and location. Table 4.22 shows monthly average dollar values from one m^3/s turbine release capacity expansion for each plant under projected climates. Nimbus, New Melones, Don Pedro, and New Exchequer have the most benefit from expanded turbine capacity with historical and projected climates. Except for Don Pedro, their benefits slightly increase with climate change. Keswick, Englebright, Folsom, and Pine Flat show small benefit from expanding turbine capacity, while some climates have spiked benefits. Frequency of marginal benefits is also important. Figure 4.21 shows monthly frequencies (%) and ensemble average monthly benefits of those additional turbine releases. Most plants provide benefits during a small duration of time. Don Pedro, New Melones, and New Exchequer have longest durations and benefit from expanded turbine releases at about 25, 34, and 37% of time, respectively, making their turbine expansion more favorable. These dual values only show the systemwide benefit. For a complete analysis, the cost of expansion should be explored for plants that could benefit from expansion, and a complete cost-benefit study should be performed.

$$\lambda_{ij} = \frac{\partial z_{ij}}{\partial u_{ij}}, \forall (i,j) \in A \tag{4.3}$$

where λ is Lagrange Multiplier, z is objective function, and u is right-hand-side constant of upper bound constraint on a turbine link (i, j).

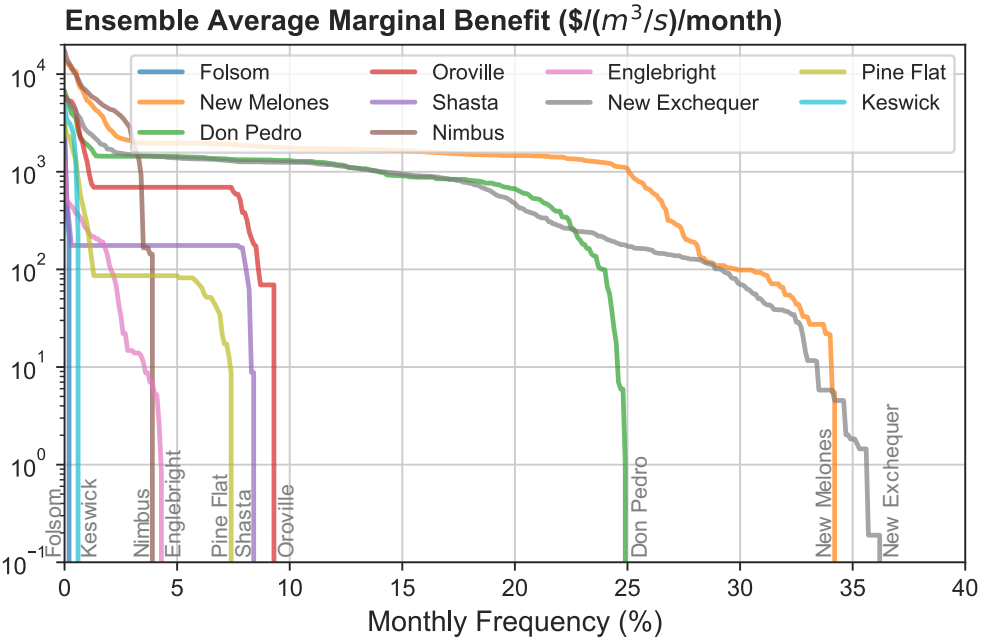

Figure 4.21: Monthly frequencies (%) of total ensemble average monthly marginal benefits of additional turbine releases ($/($m^3$/s)/month)

Higher discount rates reduce future value of money and the value of postponing investment decisions (Andersson et al., 2014). Figures 4.22 shows expected annual present value benefits (Equation 4.6) of capacity expansion ($/($m^3$/s)/year) for low, medium, and high real discount (or interest) rates (1, 2.5, and 5%, respectively) with a return period of 50 years. With the nominal discount rate $i_{nominal}$ and the inflation rate $e_{inflation}$, the real (inflation corrected) discount rate i_{real} is:

$$i_{real} = i_{nominal} - e_{inflation} \tag{4.4}$$

Annual average expected value benefit (EVB) of capacity expansion (dual value, λ) for each turbine capacity constraint for N number of months in the modeling period is:

$$EVB = \frac{12}{N} \sum_{k=1}^{N} \lambda_k \tag{4.5}$$

With the real discount rate i and the investment return period n, the expected present value benefit (EPVB) of annual average expected value benefit (EVB) for a turbine investment becomes:

$$EPVB = EVB \left(\frac{1 - (1+i)^{-n}}{i} \right) \tag{4.6}$$

Expected present value benefit of turbine capacity expansion differ across scenarios and hydropower plants. As the real discount rate increases, expected present value benefit of turbine capacity expansion decreases. There are macroeconomic (discount rate) uncertainties affecting profitability of turbine capacity expansion investments, besides hydrologic uncertainties. Increased macroeconomic uncertainties with higher discount rates can outweigh hydrologic uncertainties. New Melones benefits the most from turbine capacity expansion, more than 250 thousand $ per year from 1 m^3/s turbine release capacity expansion. As discount rate increases, not only these benefits, but also EPV variability across projected scenarios decrease.

Figure 4.22: Expected present value benefits ($\$K/(m^3/s)$/year) of additional turbine releases with 50 year return for low (1%), medium (2.5%), and high (5%) interest rates

Figure 4.23 shows ensemble average monthly benefit of storage capacity expansion ($/MCM/month) for 10 modeled reservoirs, considering only hydropower objectives. Most reservoirs show either no benefit or benefit in a small duration of months for some extreme

events. Out of 10 reservoirs, only Englebright significantly benefits from expanding storage capacity in about one third of months, and no benefit in remaining months. Considering water supply benefits and environmental constraints, Nover et al. (2019) evaluate capacity expansion of most California reservoirs and show that a few Cascade Range and Northern Sierras reservoir could benefit from expanded capacity under climate change, but cost of expansion could substantially reduce these benefits.

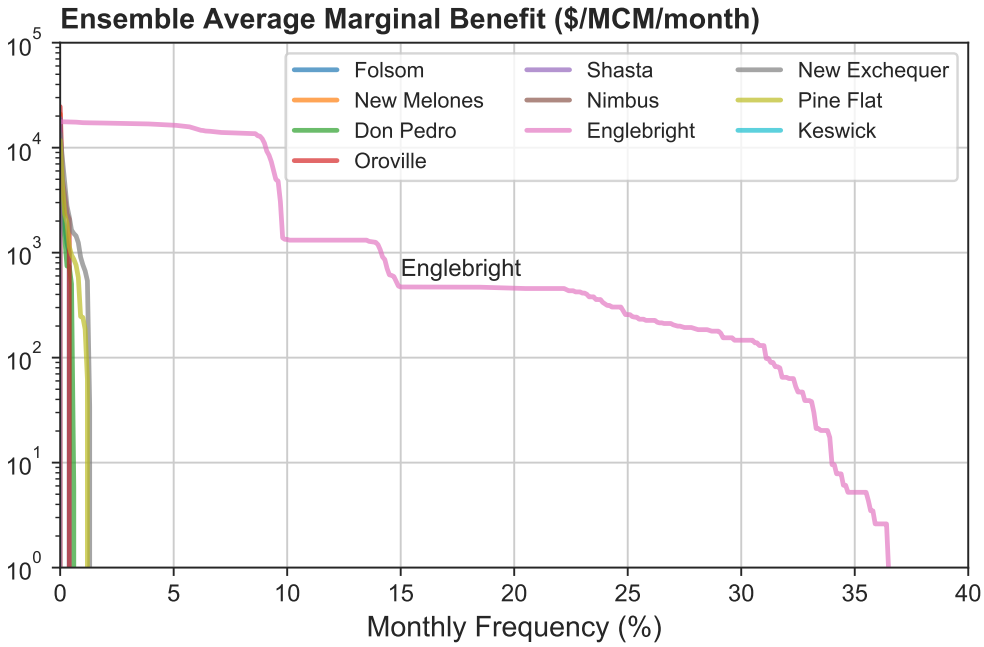

Figure 4.23: Monthly durations (%) of total ensemble average monthly marginal benefits of additional reservoir storage ($/MCM/month)

4.6.5 Implications for Run-of-River Plants

Constant head, low-storage also called 'run-of-river' plants operate continuously depending on water availability and usually help supply base load. Lacking storage capacity, they have little room to optimize their operations. Thus, their adaptability to changing climate is limited and more affected by timing and magnitude of water availability, especially when it decreases. Given constant head (h), run-of-river hydropower generation $G(t)$ over time period Δt is:

$$G(t) = \eta \rho g h Q(t) \Delta t \tag{4.7}$$

where all parameters (overall efficiency η, density of water ρ, gravitational constant g, and head h) are constant, except for plant inflow $Q(t)$. So, any change in plant inflow affects hydropower generation proportionately.

$$G(t) = \psi Q(t) \tag{4.8}$$

where ψ represents all constants ($\eta\rho gh\Delta t$). If β (%) change occur on plant inflow $Q(t)$ in time-step t, then hydropower generation with a change of $\Delta G(t)$ becomes:

$$G(t) + \Delta G(t) = \begin{cases} \min(G(t) + \beta\psi Q(t), \text{Plant Capacity}), & \text{if } \beta \text{ is positive} \\ G(t) - \beta\psi Q(t), & \text{otherwise} \end{cases} \tag{4.9}$$

Plants with large storage capacities lessen water shortage effects and get the most benefit from increased water availability with adaption (Figure 4.24). Plants with small-storage capacities and high-heads (located on high elevations), however, lack of adaptation capabilities. If water availability decreases, their generation reduce equally. If water availability increases, they can only utilize this up to their plant capacity, spilling the remaining. Their capability of utilizing these increased water availability also is less than plants with large-storage capacities.

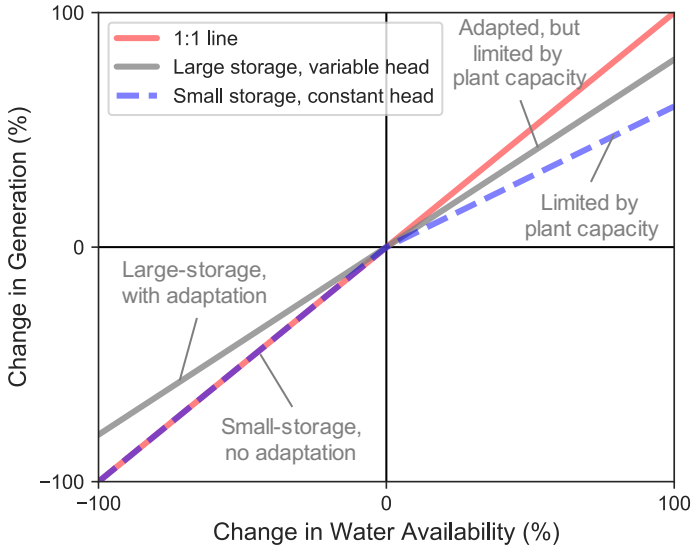

Figure 4.24: Change in water availability vs. change in hydropower generation for small-storage, high-head plants (conceptual)

Given the assumption above, small-storage, high-head hydropower generation reduces in spring and summer in all regions CR, NS, and SS, with reduced inflow (Figures 4.25). The largest generation reductions occur in NS region, about 40% in rcp 4.5 and about 60% in rcp 8.5 in June and July. Summer hydropower generation from run-of-river plants in SS region fall about 30% in rcp 4.5 and about 40% in rcp 8.5. Plants in these regions benefit from increased fall and winter water availability, but this option will be limited by plant capacities. Also, using Equation 4.9 and monthly changes, operators in these regions can determine how their run-of-river hydropower generation would be impacted by climate change.

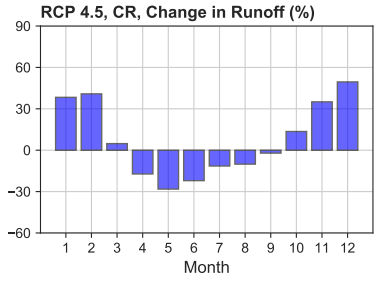

(a) Cascade Range

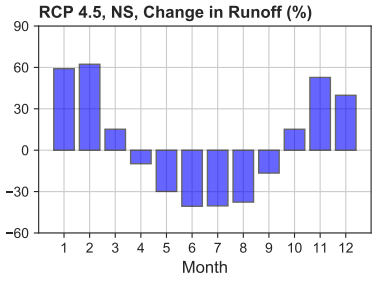

(b) Northern Sierras

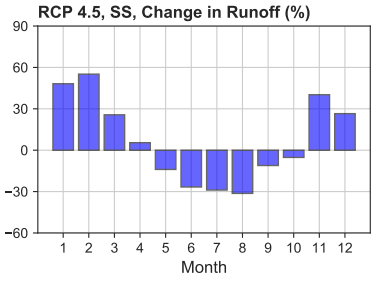

(c) Southern Sierras

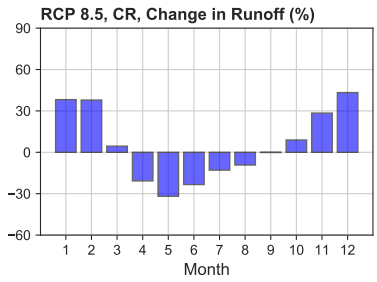

(d) Cascade Range

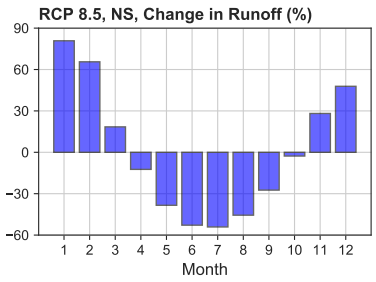

(e) Northern Sierras

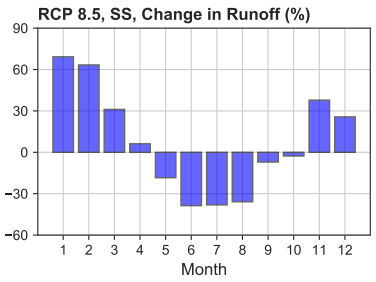

(f) Southern Sierras

Figure 4.25: Rcp 4.5 and rcp 8.5 ensemble average (2015-2100) and historical average (1922-2014) monthly runoff change (%)

4.7 Summary

Results are summarized on a parallel coordinates plot, where vertical axes represent the average percent change ($\Delta f = (f_{projected} - f_{historical})/f_{historical} * 100$) of parameter and horizontal lines are climate scenarios (Figure 4.26). Given projected precipitation and temperature changes under 20 climate scenarios, average reservoir inflow increases up to 50% in the wettest scenario and decreases by 10% in the driest scenario, with an RCP 4.5 ensemble average and median increase of 10 and 5%, and an RCP 8.5 ensemble average and median increase of 11 and 3%. Overall average change in reservoir storage is small compared to changes in other parameters, but there are considerable monthly temporal storage changes (Figure 4.17). Because of plant capacities (storage and turbine), increases in generation are smaller than increases in reservoir inflows. Capacity factor (shown for one year in Equation 4.10) is calculated as average generation divided by maximum possible generation and is an indicator of how much of plant capacity is exploited. Capacity factor (%) changes proportionally with generation, although both RCP 4.5 and 8.5 ensemble median capacity factors are slightly lower than historical average. With adaptations, revenue increases by 4.5% and 3.5% under RCP 4.5 and 8.5 ensemble average but does not change under ensemble medians of projected scenarios. Useful adaptations include improved winter flood forecast, less carry-over storage, and increased

turbine release capacity for some hydropower plants.

$$Capacity\ Factor(\%) = \frac{\sum_{m=1}^{12} \eta \rho g h Q(t) \Delta t}{8760 Capacity_{MW}} * 100 \tag{4.10}$$

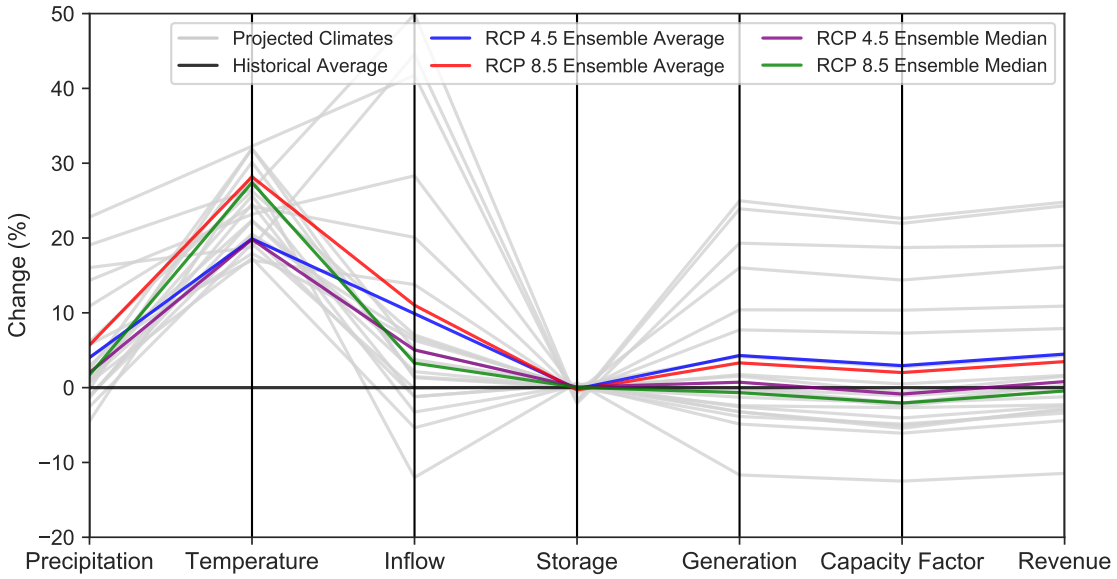

Figure 4.26: Summary of operations normalized to historical averages with each line representing a different climate scenario

4.8 Conclusions

Climate change shifts timing and magnitude of water availability with earlier snowmelt recession and slightly increased winter rainfall rather than snowfall. Monthly average peak runoff occurs in earlier and greater than the historical average. Summer water availability decreases about 25%, while frequency and variability of extreme events increase, especially in winter. Temperature increases about 1.7-2.5 ^oC, and precipitation changes varies with an ensemble average increase of 4-5 %. These effects also vary spatially. Sierras, where operations are historically snowmelt-driven, have the most dramatic changes, with runoff decreasing 20-40% in summer and increasing 40-60% in winter. Reservoir operations for hydropower changes significantly with climate change. Increased water availability increases hydropower generation in fall and winter, but spring and summer generation declines, shifting peak hydropower generation earlier in the season. Spills increase in the wet season, resulting in spilled energy. Plants with large-storage capacity have some adaptation capability and lessen effects of decreased water availability, and take most advantage of increased water availability, but this is limited by plant capacity. Lacking adaptability and flexibility from having large-storage, run-of-river plants see more impact from climate change, especially when water availability declines in spring and summer. Useful adaptations to climate change include 1) improved winter flood forecast and dynamic dedicated flood pool so that more storage is used for hydropower and less energy

is lost with spills; 2) reduced (hedging) carry-over storage at the end of the dry season so that more hydropower is generated; 3) some plants benefit from expanded turbine release capacity, especially Don Pedro, New Melones and New Exchequer, but cost of expansion should be explored to evaluate net benefits. Storage capacity expansion provides little additional hydropower benefits, except for Englebright, under climate change. With optimization and adaptive management, negative consequences of climate change can be diminished.

Chapter 5

Optimizing Pumped-Storage Hydropower Operations

5.1 Introduction

Pumped-storage hydropower (PSH) plants pump water into an upper reservoir during low price (off-peak) hours, storing water in the form of energy, and generate hydropower during high price (on-peak) hours. A typical PSH layout is shown in Figure 5.1, where the lower reservoir is on a stream and the upper reservoir is off-stream at a higher elevation. Other layouts can have both upper and lower reservoirs are on streams. PSH operations are driven by hourly price variability and efficiencies. In energy systems without price variations, PSH are not economically feasible. Because some energy is lost with pumping and generation, some price gradient is needed to recover the cost of lost energy. With a price-taking approach, the basic operating rule is to decide when to pump water into an upper reservoir, and release back to the lower reservoir, generating energy. ASCE Hydropower Commitee (1989), Wood and Wollenberg (1996), Lu et al. (2004), Figueiredo and Flynn (2006), and Bozorg Haddad et al. (2014) discuss operational algorithms for PSH.

This chapter presents two algorithms for PSH operations. The first algorithm uses price-duration curves without taking water availability into account. Given a daily, weekly or monthly duration with hourly time-steps, the optimal operating duration (pumping or generation) without energy losses is 50%, meaning a PSH plant should pump if energy price is less than median price, at 50% duration, and generate if the price exceeds the median price without energy losses. However, energy losses or system inefficiencies affect this operating policy. Algorithm 1 optimizes PSH operations assuming there is enough water storage in lower and upper reservoirs to pump and generate at any time. A reduced analytical solution depending only on efficiencies and energy prices is provided. Algorithm 2 is modified from the hydropower reservoir operations model, developed in Chapter 2, and includes water availability and infrastructure capacities. Differences and similarities of presented and existing algorithms are discussed. The two algorithms are compared and results are presented. The second algorithm then is used to evaluate how energy prices transformed by solar energy affects optimal PSH hydropower operations. Given solar

affected energy price patterns with two peaks, water tends to be pumped during midnight and midday, and energy is generated during the morning and evening peak hours, with two daily operating cycles.

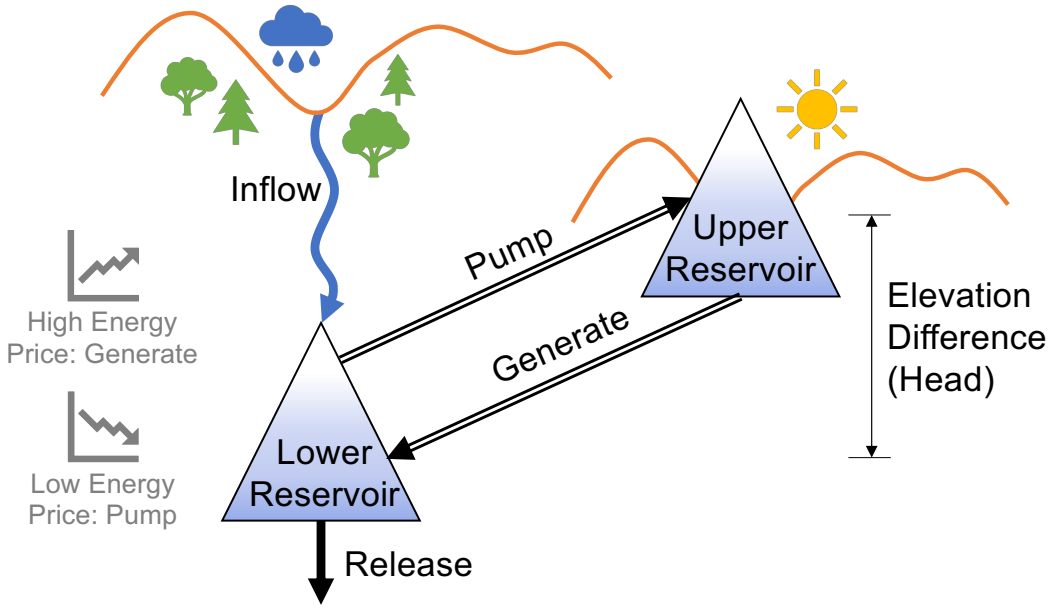

Figure 5.1: Pump and generation scheme between lower and upper reservoirs

5.2 Algorithm 1: Optimizing with a Price-Duration Curve

An optimal PSH operating policy maximizes net energy generation revenue (revenue minus pumping cost) (Equation 5.1). Price-duration curves can help optimize these PSH decisions. A price-duration curve (Figure 5.2) sorts energy prices, P, in descending order over a duration, H, between [0,1] or [0,100%] of the duration. The decision variable is the optimal operating duration that maximizes total net profit, difference between generation revenue and operating costs (Equation 5.5). Algorithm 1 finds the optimal operating duration given energy losses and prices. This algorithm implicitly considers water mass balance in the total duration by setting pumping, H_P, and generating, H_G, durations the same. Energy prices corresponding to optimal generating duration or greater, $P(H \geq H_G)$, are generating prices, and energy prices less than pumping duration, $P(H \leq H_T - H_G)$, are pumping prices. In other durations and energy prices, $P(H_T - H_G \leq H \leq H_G)$, operations are stopped.

$$Total\ Net\ Profit = \sum_{t=1}^{T} Generation\ Revenue_t - \sum_{t=1}^{T} Pumping\ Cost_t \qquad (5.1)$$

Net profit from T_G hours of hydropower generation and T_P hours of pumping is:

$$Total\ Net\ Profit = \int_0^{T_G} \eta_G \rho g h_G Q_G(t) p(t) dt - \int_0^{T_P} \frac{1}{\eta_P} \rho g h_P Q_P(t) p(t) dt \tag{5.2}$$

where η is efficiency, ρ is density of water, g is gravitational constant, h is head, Q is discharge, and p is energy prices. Indices G and P represent generation and pumping, respectively.

Duration H_i of a price p_i in an array of prices p is calculated with Equation 5.3. Energy prices are obtained from price-duration curves, and H is percent hours of operation, substituting Equation 5.4 into Equation 5.2 results in Equation 5.5.

$$H_i(\%) = \frac{rank(p_i)}{(count(p)+1)} * 100 \tag{5.3}$$

$$\int p(t)dt = \int P(H)dH \tag{5.4}$$

$$\max z = \int_0^{H_G} \eta_G \rho g h Q P(H) dH - \int_{H_T}^{H_T - H_G} \frac{1}{\eta_P} \rho g h Q P(H) dH \tag{5.5}$$

where z is the objective function to be maximized, H_G is optimal pumping duration, H_T is total duration (100%), and the difference $H_T - H_G$ is pumping duration (H_P). This concave objective function can be analytically solved to find optimal operating duration $H_G = H_P$. First-Order (Necessary) condition:

$$\frac{\partial z}{\partial H}\Big|_{H_G} = 0 \tag{5.6}$$

Taking the First-Order derivative of Equation 5.5 with respect to H, and numerically evaluating at point H_G yields:

$$\frac{\partial z}{\partial H} = P(H)\eta_G \rho g h Q\Big|_{H_G} - P(H)\frac{1}{\eta_P}\rho g h Q\Big|_{H_T - H_G} = 0 \tag{5.7}$$

With an assumption that generating and pumping heads and discharges are the same and $H_T = 100$, at the economic equilibrium, the reduced analytical solution of the objective function is:

$$\eta_G \eta_P = \frac{P(100 - H_G)}{P(H_G)} \tag{5.8}$$

Threshold prices that trigger pumping or generation are:

$$P_P^* \leq P_G^* \eta_G \eta_P \tag{5.9}$$

$$P_G^* \geq \frac{P_P^*}{\eta_G \eta_P} \tag{5.10}$$

where $P_P^* = P(100 - H_G)$ is pumping threshold price, and $P_G^* = P(H_G)$ is generation threshold price. This reduced analytical solution simplifies PSH operating rules and does not require a price-duration curve, with an assumption that pumping head and discharge equal generation head and discharge.

Given a concave objective function (Equation 5.5), the Second-Order condition of maximization is satisfied.

$$\frac{\partial^2 z}{\partial H^2}\Big|_{H_G} < 0 \tag{5.11}$$

The algorithm 1 numerically evaluates Equation 5.5 between [0,50%], and finds the optimal operating duration and corresponding pumping and generating prices ($argmax\{z\}$). Generation or pumping duration cannot exceed 50% as the total must be less than or equal to 100%. Equation 5.8 also can efficiently find pump and generate price pairs without integral calculations.

ASCE Electric Power Research Institute (EPRI) Guides suggest that for planning purposes, 70% overall cycle efficiency ($\eta_G \eta_P$) can be used for small plants ($\leq$ 300MW) and 75 % can be used for large plants (ASCE Hydropower Commitee, 1989) and provides an approximate energy balance ratio (Equation 5.12), similar to the reduced analytical solution above (Equation 5.8), if pumping to generation (or charge-to-discharge) ratio is 1. Figueiredo and Flynn (2006) used this approach for PSH modeling. Wood and Wollenberg (1996) also provides a similar method, where $generation\ (MWh) = \eta * pumping\ load\ (MWh)$ for the same volume of water.

$$Pumping\ Energy = 130\%\ Generating\ Energy \tag{5.12}$$

Lu et al. (2004) used energy balance instead of price duration curves used in algorithm 1, where the total stored (or ending) energy (E_T) with an initial energy (E_0) is:

$$E_T = E_0 + E_{in} - E_{out} \tag{5.13}$$

where

$$E_{in} = P_p t_p \eta,\ E_{out} = P_g t_g \tag{5.14}$$

where pumping is P_p MW for t_p hours, and generation is P_g MW for t_g hours, with an overall efficiency of η. If $E_T = E_0$, then Equation 5.13 becomes similar to the reduced analytical solution of algorithm 1 (Equation 5.8):

$$P_g t_g = \eta P_p t_p \tag{5.15}$$

5.2.1 Example

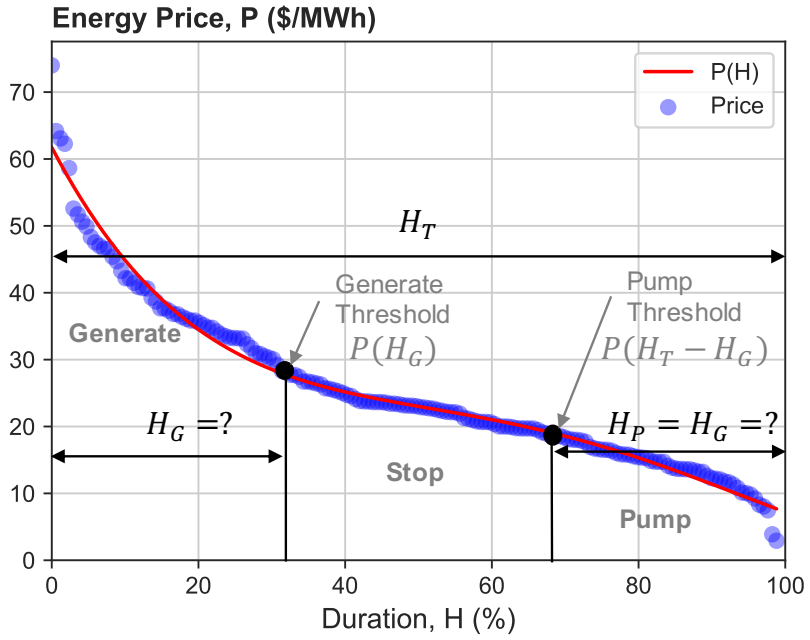

Figure 5.2: Price-duration curve of hourly energy prices for a week between May 1, and May 7, 2018

Algorithm 1 is run with energy prices for one week period (May 1-7, 2018) and parameters in Table 5.1. These parameters are arbitrarily chosen for the conceptual model. 1000 m^3/s of discharge capacity for pump and generator and 100 m of elevation difference between lower and upper reservoirs are assumed. Pumping occurs from lower to upper reservoir, and generation is from upper to lower reservoir. Pumping and generation efficiencies are constant (0.8 and 0.9).

Table 5.1: Parameters for algorithm 1

Parameter	**Lower Reservoir**	**Upper Reservoir**
Head (m)	100	100
Discharge Capacity (m^3/s)	1,000	1,000
Efficiency	0.8	0.9
Gravitational Constant (m/s^2)	9.81	
Density of Water (kg/m^3)	1,000	

Analytical solution of this unconstrained optimization problem includes evaluating the First-Order and Second-Order optimality conditions for the price-duration function $P(H)$ fitted to ordered observed energy prices (Figure 5.2). Fourth-degree polynomial $P(H)$ function for this example is:

$$P(H) = 1.547 * 10^{-06} H^4 - 0.00045 H^3 + 0.04506 H^2 - 2.095 H + 61.74 \quad (5.16)$$

Objective function z:

$$\begin{aligned}\max z = &\int_0^{H_G} 0.9 * 1000 * 9.81 * 100 * 1000 P(H) dH \\ &- \int_{100}^{100-H_G} \frac{1}{0.8} * 1000 * 9.81 * 100 * 1000 P(H) dH\end{aligned} \tag{5.17}$$

Substituting Equation 5.16 into Equation 5.17 yields:

$$\begin{aligned}\max z = &\int_0^{H_G} 0.9 * 9.81 * 10^8 (1.547 * 10^{-06} H^4 - 0.00045 H^3 \\ &+0.04506 H^2 - 2.095 H + 61.74) dH \\ &- \int_{100}^{100-H_G} \frac{1}{0.8} * 9.81 * 10^8 (1.547 * 10^{-06} H^4 - 0.00045 H^3 \\ &+0.04506 H^2 - 2.095 H + 61.74) dH\end{aligned} \tag{5.18}$$

First-Order condition given $\psi = 9.81 * 10^8$:

$$\begin{aligned}\frac{\partial z}{\partial H}\Big|_{H_G} = 0 = &0.9\psi (1.547 * 10^{-06} H_G^4 - 0.00045 H_G^3 \\ &+0.04506 H_G^2 - 2.095 H_G + 61.74) \\ -\frac{1}{0.8}\psi &(1.547 * 10^{-06} (100 - H_G)^4 - 0.00045 (100 - H_G)^3 \\ &+0.04506 (100 - H_G)^2 - 2.095 (100 - H_G) + 61.74)\end{aligned} \tag{5.19}$$

$H_G = 34$ satisfies Equation 5.19. Evaluating this point in the Second-Order condition satisfies that $H_G = 34$ is a maximum point.

$$\begin{aligned}\frac{\partial^2 z}{\partial H^2}\Big|_{H_G=34} &= 0.9\psi (6.2 * 10^{-6} H_G^3 - 0.0013509 H_G^2 + 0.09012 H_G - 2.095) \\ &-\frac{1}{0.8}\psi (6.2 * 10^{-6} H_G^3 - 0.0005055 H_G^2 + 0.00558 H_G - 0.404) \\ &= -3.084 * 10^8 - 3.097 * 10^8 < 0\end{aligned} \tag{5.20}$$

This example can also be solved numerically. Figure 5.3-(a) shows the objective function (Equation 5.5) evaluation results. As the operating duration ($H_G = H_P$) increases, hourly net profit increases first, then after a certain point, it starts to decrease and eventually becomes negative. At that maximum point $\partial z / \partial H = 0$, and corresponding duration is H_G^*. Then, using the optimal operating duration, generation $P(H_G^*)$ and pumping $P(100 - H_G^*)$ energy price thresholds are determined (Figure 5.3-(b)). If energy prices are at or above the generate threshold, energy is generated. Similarly, if prices are at or below the pump price, pumping is done. Operations are stopped when the prices are between these thresholds. For this example, the optimal operating duration of 34% corresponds to a generation threshold price of 27.4 \$/MWh and a pump threshold price of 19.5 \$/MWh.

These price thresholds also satisfy the reduced analytical solution (Equation 5.8), where $\eta_G\eta_P = 0.9 * 0.8 = 0.7$ and $P(66)/P(34) = 19.5/27.4 = 0.7$.

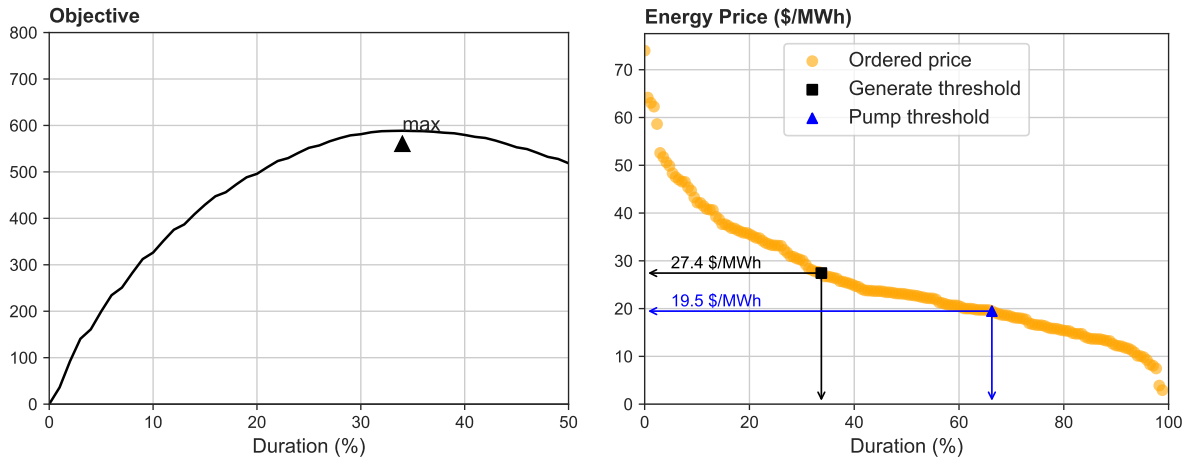

(a) Numerically finding H_G with function evaluation

(b) Optimal duration and prices

Figure 5.3: Simulation of the objective function and finding pump and generate threshold prices and durations

In algorithm 1, the optimal operating duration is determined solely by overall plant efficiency ($\eta_G\eta_P$). The magnitude of energy prices and the slope of the price-duration curve only affect the net total profit. Figure 5.4 simulates how optimal operating duration changes with overall plant efficiencies. If the overall efficiency is 1 (no energy losses), then optimal operating duration is 50%, and corresponding generate and pump thresholds are the median price. As the overall efficiency decreases, the optimal generate and pump durations decrease and the duration where operations are stopped increases. As the overall efficiency approaches to zero, only small generation duration with highest prices and pumping duration with the lowest prices become economically profitable.

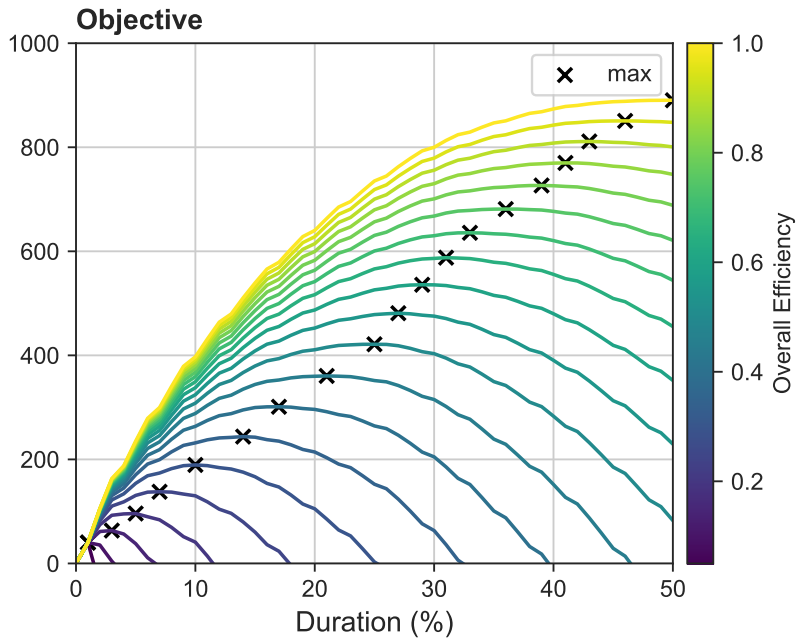

Figure 5.4: Simulating optimal operating durations and prices for a range of overall efficiencies $\eta_G\eta_P$

The biggest limitation of algorithm 1 is that water mass balance is conserved at the end of the period with an assumption that there is always enough water storage in the lower and upper reservoir to pump and generate. In the total duration with implicit representation, total volumes of pumping and generation releases are the same. But, the mass balance within the time-period does not necessarily work. Since the thresholds are constant, the model can suggest generation without pumping, which is why enough water availability is assumed. Also, it is assumed that pump and turbines releases are made at the capacity. With these assumptions, the resulting solution approximates the global optimal solution, which is discussed in the more numerical algorithm 2.

5.3 Algorithm 2: Optimizing with a Reservoir Operations Model

Algorithm 2 is modified from the hybrid LP-NLP hydropower reservoir operations model to represent PSH operations (Figure 5.5). This algorithm explicitly represents water mass balance, and pump and generate decisions can be between 0 and the pump or turbine capacity. In addition to when to pump and generate, which Algorithm 1 determines, algorithm 2 quantifies how much to pump and generate. The objective (Equation 5.21) is to maximize overall net hydropower revenue in all time-steps within lower bound, upper bound, and mass balance constraints (Equations 5.23, 5.24, and 5.25). Algorithm 2 is modeled with Pyomo (Hart et al., 2017) and solved with GLPK (Free Software Foundation, 2019), an open-source, large-scale mathematical programming solver. Given an concave objective function in the feasible range, the solver provides a globally optimum

solution.

$$\max_X \; z = \sum_i \sum_j b_{ij} X_{ij} \tag{5.21}$$

$$b_{ij} = \begin{cases} \eta_G \rho g h_G p_{ij} \Delta t, & \text{if } (i,j) \text{ is a generation link} \\ -(1/\eta_P) \rho g h_P p_{ij} \Delta t, & \text{if } (i,j) \text{ is a pump link} \\ 0, & \text{otherwise} \end{cases} \tag{5.22}$$

subject to:

$$X_{ij} \geq l_{ij}, \forall (i,j) \in A \tag{5.23}$$

$$X_{ij} \leq u_{ij}, \forall (i,j) \in A \tag{5.24}$$

$$\sum_i X_{ji} - \sum_i a_{ij} X_{ij} = 0, \forall j \in N \tag{5.25}$$

where X_{ij} represents flow (decision variable) over a link (i,j), from an origin node i to terminal node j representing different points in time and space. b_{ij} is unit benefit (\$ per flow) and positive for generation links and negative for pumping links (Equation 5.22). Generation and pumping efficiencies η_G and η_P and heads h_G and h_P are assumed constant. Δt is time difference and equal to 1 for hourly time-step. l_{ij} and u_{ij} are lower and upper bound constraints, and a_{ij} is amplitude representing losses.

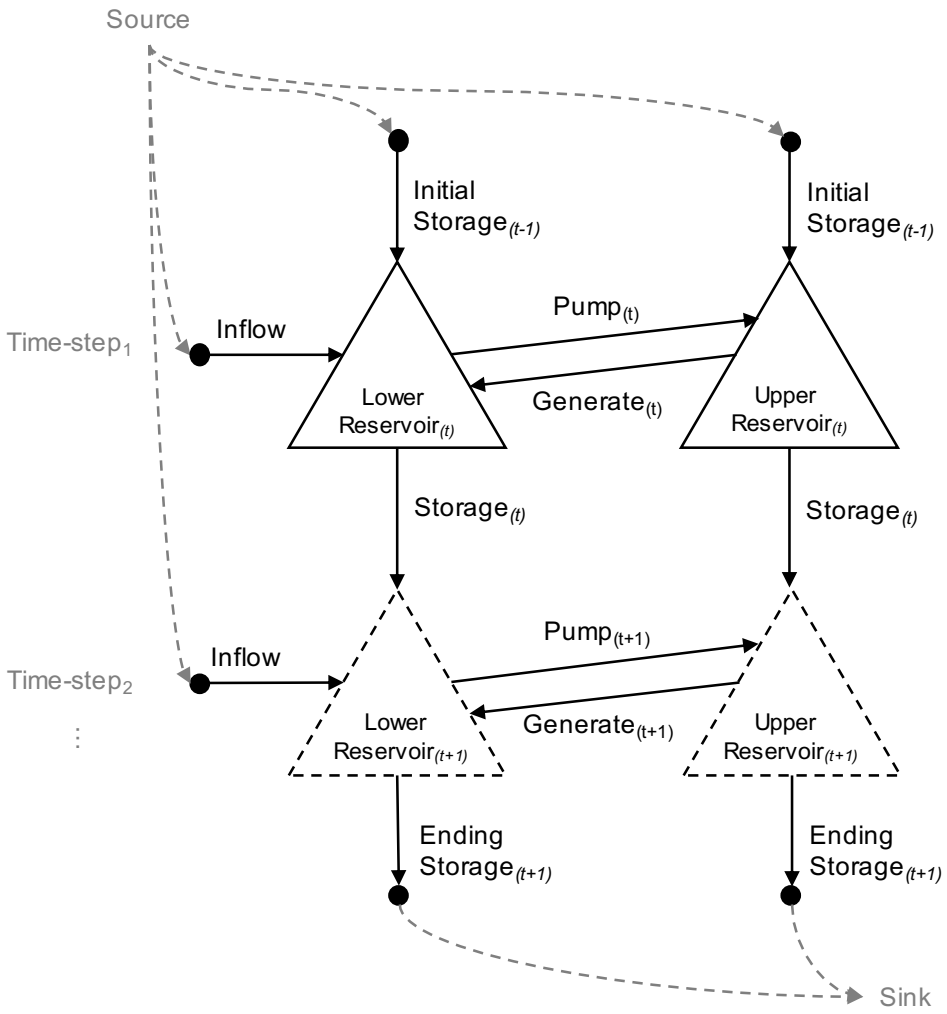

Figure 5.5: Generic network flow representation of the PSH model

5.3.1 Example

Table 5.2 shows parameters used for the algorithm 2. The same head, discharge capacity, and efficiency as algorithm 1 are assumed for a comparison between two algorithms. Lower reservoir has 5,000 MCM, and upper reservoir has 2,500 MCM of storage capacity, with no deadpool, initial and ending storage. Inflow for the lower reservoir (Figure 5.6) is obtained from CDEC station ORD, representing Sacramento River at Ord Ferry. May 1-7, 2018 inflows are extracted from the dataset.

Table 5.2: Parameters for algorithm 2

Parameter	**Lower Reservoir**	**Upper Reservoir**
Head (m)	100	100
Storage Capacity (MCM)	5,000	2,500
Initial and Ending Storage (MCM)	0	0
Deadpool (MCM)	0	0
Discharge[1] Capacity (m^3/s)	1,000	1,000
Release Capacity (m^3/s)	1,500	0
Efficiency	0.8	0.9
Gravitational Constant (m/s^2)	9.81	
Density of Water (kg/m^3)	1,000	

[1]Pump or generator discharge

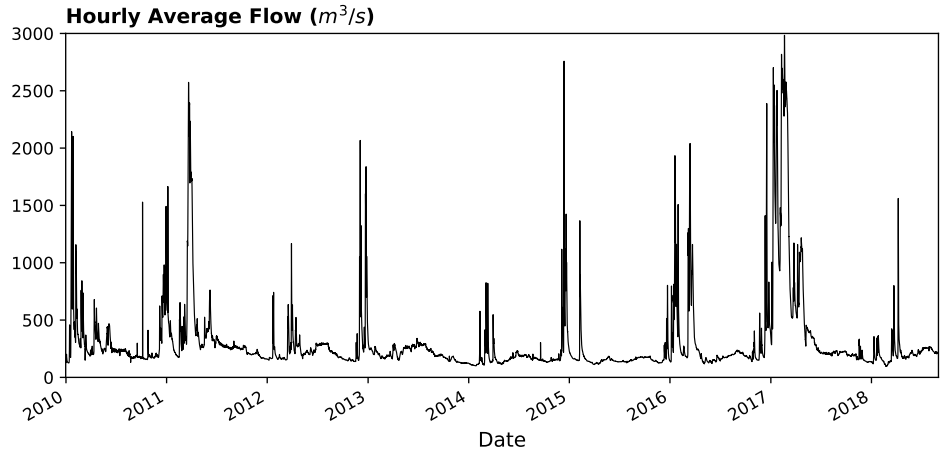

Figure 5.6: Hourly inflow for lower reservoir in algorithm 2. This flow data is Sacramento River at Ord Ferry (Data source: CDEC)

Figure 5.7-(a) shows hourly average net flow, generation minus pumping (m^3/s), and energy prices ($/MWh) over one week period (May 1-7, 2018). Pumping and generation occur twice a day given off-peak and on-peak energy price cycles. Water is usually pumped to the upper reservoirs during hours between 0-5 and 9-17. Energy is mostly generated during peak hours between 5-7 and 17-0. Water is pumped for longer periods than generation, which occurs in a smaller time-frame with greater intensity. Instead of setting pumping and generating thresholds, algorithm 1 can pump and generate different quantities depending on energy prices, although operations are mostly at pump and generation capacities (Figure 5.7-(b)). As energy prices increase, hydropower is generated by releasing water into the lower reservoir, and with lower energy prices water is pumped to the upper reservoir. To maximize overall net revenue (generation revenue minus pumping cost), generation releases reach the capacity at high energy prices. When energy prices are above 24 $/MWh, water is never pumped and only hydropower is generated (Fig-

ure 5.7-(b)). When energy prices are below 20 $/MWh, water is pumped to the upper reservoir without generation. Water is sometimes pumped and hydropower is sometimes generated for prices between 20 and 24 $/MWh. Unlike algorithm 1, operations are never stopped for any energy price, but rather mixed pumping and generation sometimes occur between thresholds.

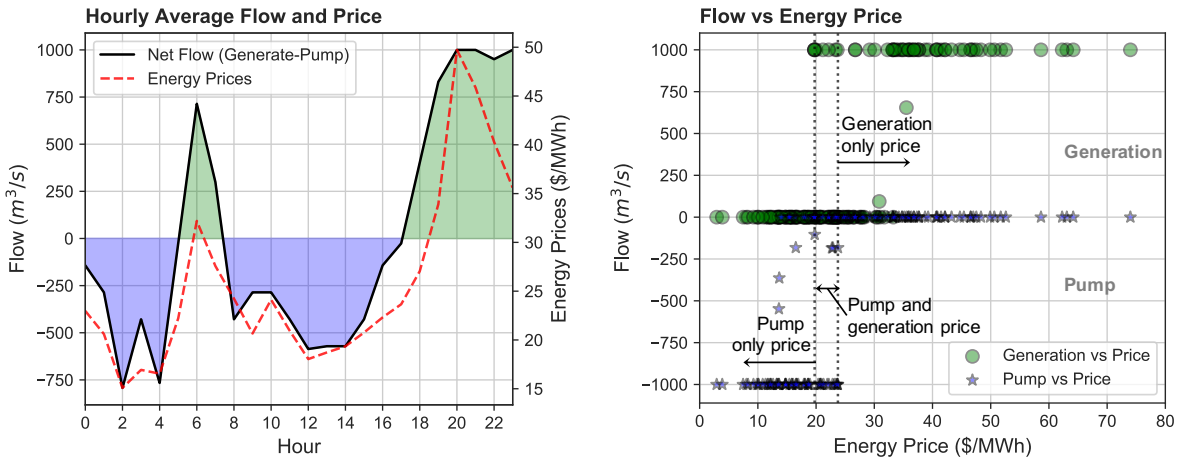

(a) Net flow (left) and energy prices (right)

(b) Flow vs. energy prices

Figure 5.7: Hourly average net flow (generation - pumping) (m^3/s) and energy prices ($/MWh)

Upper and lower storages change with pumping and generation (Figure 5.8). Storage in the upper reservoir increase with pumping before the morning and evening peak hours, which decreases the lower reservoir's storage. The upper reservoir has two daily peaks occurring between mode changes from pumping to generation (hours around 5 and 17). Since energy prices are much higher in the evening peak hours, the second peak of the upper reservoir, occurring hours around 15-18 is much greater. Generation discharges and streamflows increase storage of the lower reservoir, peaking when the operating mode changes from generation to pumping around hours 7 and 0. Although there is stream inflow into the lower reservoir, only the portion pumped is stored, and the remaining is released, because there is no benefit of storing water other than pumping.

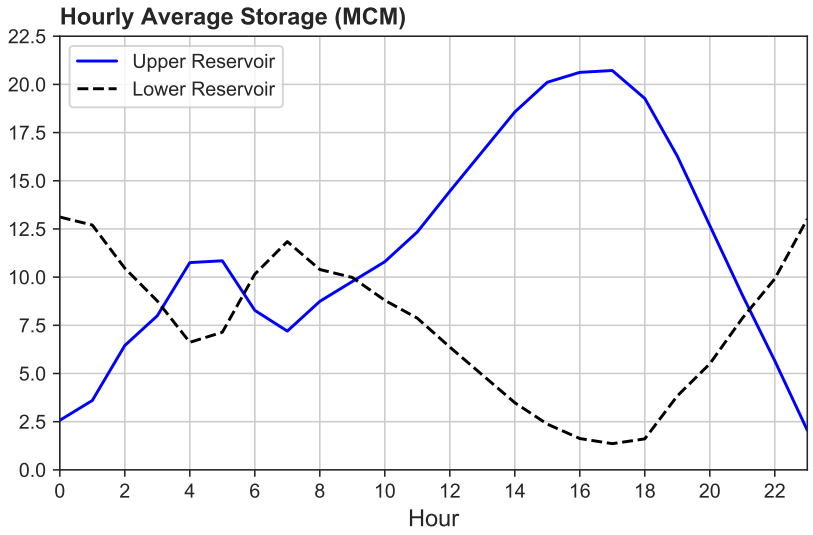

Figure 5.8: Average hourly storage (MCM) of upper and lower reservoirs

5.4 Comparing Algorithm 1 and 2

Algorithms 1 and 2 optimize short-term PSH operations with different approaches, both aiming to maximize net revenue and help meet peak energy demands. Algorithm 1 uses price-duration curves to find generation and pumping price thresholds, driven mostly by efficiencies, without considering reservoir inflows and water mass balance, assuming there is always enough water to pump and generate energy. This algorithm provides simple, fast, and approximate solutions to the problem, especially with the reduced analytical solution. Algorithm 2 uses reservoir operation optimization modeling to have a better and more flexible system representation. Algorithm 1 has a single decision variable, which is the optimal pumping or generating operating duration ($H^* = H_P = H_G$), while algorithm 2 has more than 3,000 decision variables in the one week period with an hourly time-step. Each storage (flow in time) and flow of a network link in a given time-step is a decision variable in algorithm 2. Figure 5.9 shows energy prices time-series (May 1-7, 2018) and compares pump and generate decisions of algorithm 1 and 2. After finding optimal duration, algorithm 1 creates pumping and generating price thresholds, and any prices below and above those constant lines determines PSH operating policy. However if operated at the capacity, this can result in water imbalances within the period if there is not enough water in the upper reservoir. For example, in Figure 5.9-(a), the total number of pumping hours in first 72 hours is 17, while the total number of generating hours is 31. Algorithm 2 determines both pumping and generation timing and quantities and does not have a water imbalance problem. With this algorithm, water must be pumped first to generate energy later.

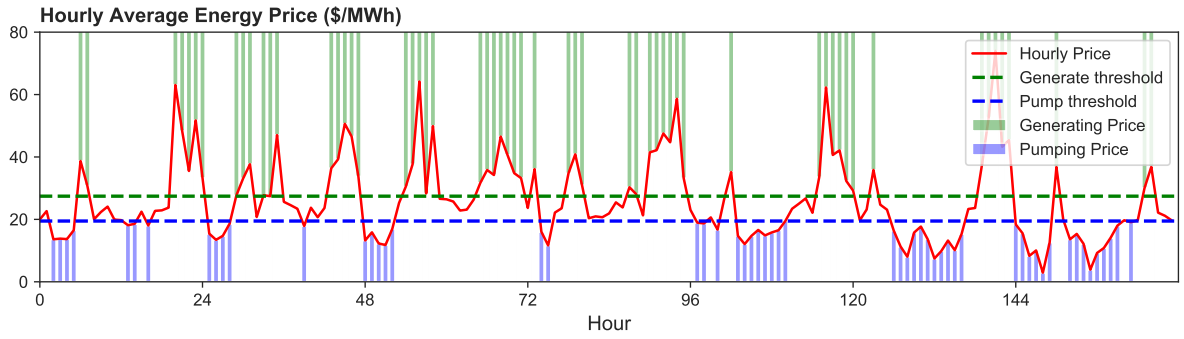

(a) Algorithm 1

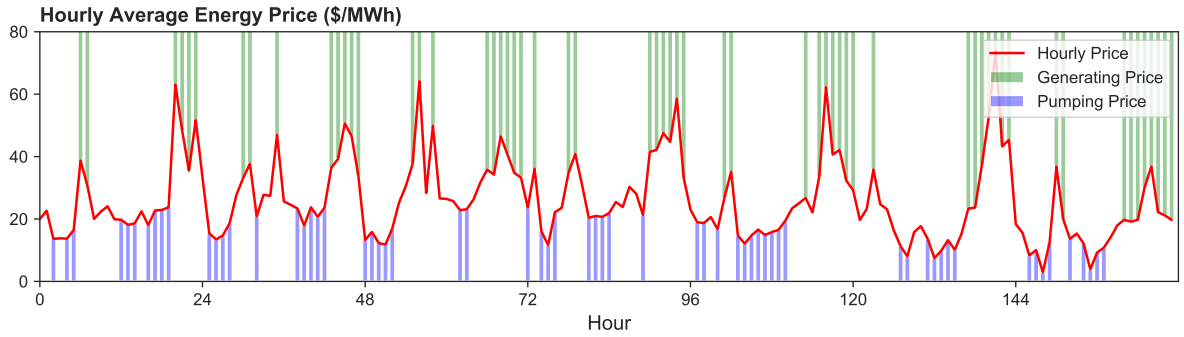

(b) Algorithm 2

Figure 5.9: Hourly energy price ($/MWh) time-series and pump-generate prices with Algorithms 1 and 2 for one week period (May 1-7, 2018)

Figure 5.10 compares cumulative generation revenues and pumping costs ($K) of algorithm 1 and 2. As algorithm 1 only determines pumping and generation timing, revenue is calculated using algorithm 2's objective function (Equation 5.21), assuming operations at plant capacities. In the first half of the period (hours 0-96), algorithm 1 has greater hydropower revenue and less pumping cost than algorithm 2, resulting in a more net profit (Figure 5.11). This is because algorithm 1 suggests more generation than pumping during this period, with slightly higher energy prices. After that, the cumulative net revenue remains around 1000 $K until the end of the period. Average change in cumulative revenue and cost in algorithm 2 is mostly constant. At the end of the modeling period, algorithm 1 and 2 have cumulative net benefits of 1,070 and 851 $K, respectively. If algorithm 1 is used, it should be considered as guidance for when to pump and generate, and operators should decide how much to pump and generate, accounting for mass balance. In addition, the reduced analytical solution of the algorithm 1 can be used to find minimum generating price given pumping price. For example, given overall efficiency ($\eta_G \eta_P$) of 0.72, if water is pumped into the upper reservoir with the average energy price of 18 $/MWh, the average generating price must be at least $18/0.72 = 25$ $/MWh to recover energy losses.

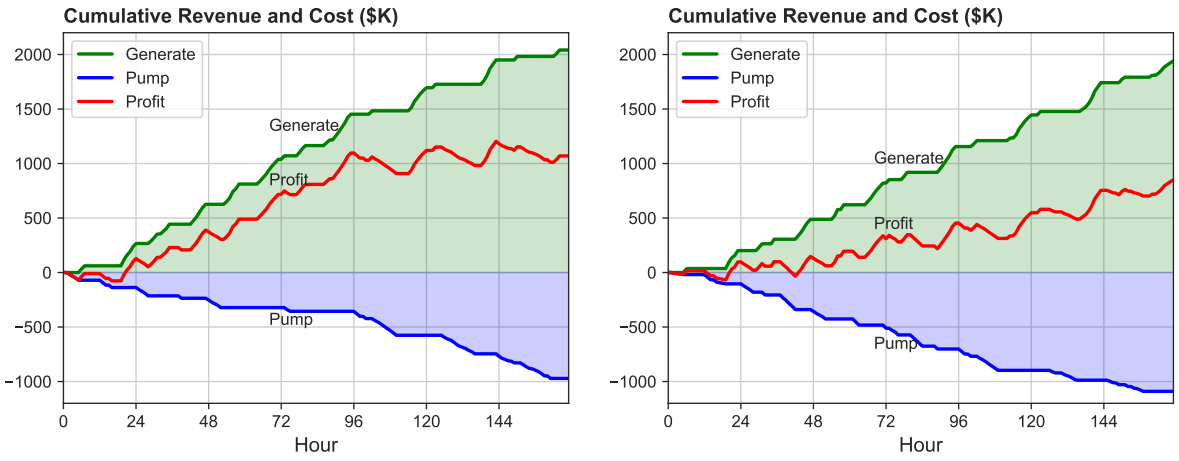

(a) Algorithm 1 (b) Algorithm 2

Figure 5.10: Cumulative generation revenue, pumping cost and net profit ($K) with Algorithms 1 and 2. Revenue and cost of algorithm 1 is calculated using objective function of algorithm 2

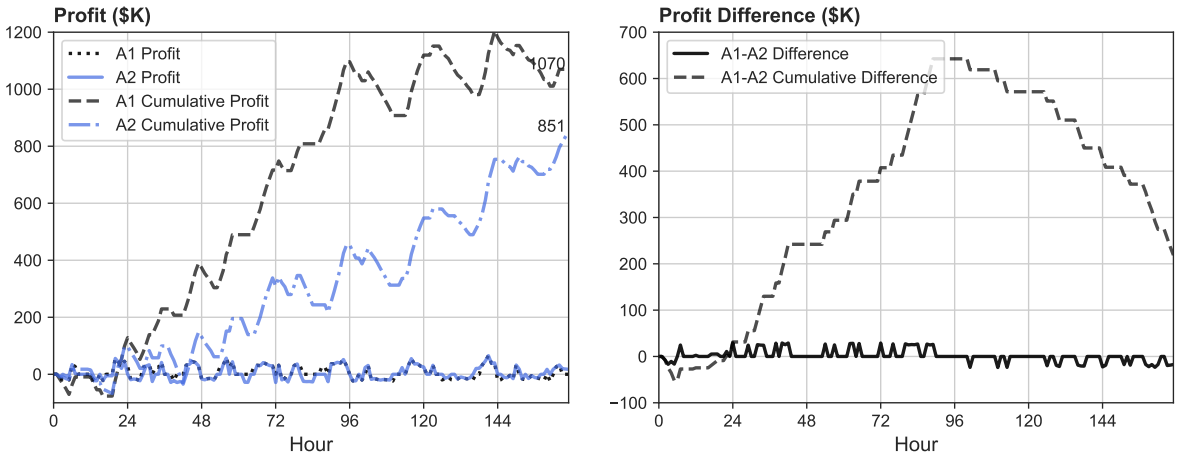

(a) Algorithm 1 and 2 profits (b) Algorithm 1 and 2 profit differences (A1-A2)

Figure 5.11: Comparison of hourly and cumulative hourly profits for algorithm 1 (A1) and algorithm 2 (A2). Profit of A1 is calculated using objective function of A2

Algorithms 1 and 2 converge when the hourly energy price pattern does not change across days. Algorithm 1 sorts energy prices and sets threshold prices but does not know when low and high prices occur. If energy prices are mostly higher in the first half of the period, then mostly lower (like this example), then differences between algorithm 1 and 2 decisions increase.

5.5 Solar Effects on PSH Operations

With deployment of solar energy to meet renewable goals, energy prices fall significantly during solar generation hours, between 9 and 18, resulting in two daily energy price peaks and lows, shown in Figure 5.12. With this new price pattern, PSH pumping and generating twice a day become more profitable, instead of a single daily pump and generate cycle without solar generation. Effects of the new energy price pattern transformed by solar energy on short-term hourly PSH operations are evaluated using algorithm 2. As discussed in Chapter 3 (Figure 3.8), the negative energy prices shifts to daytime due to solar generation is favorable for PSH operations, increasing pumping during negative price hours. Hourly overall average of inflows are used to eliminate hydrologic variations (Figure 5.6). The model is run with energy prices of each year and overall lower reservoir inflow separately from 2010 through 2018. Pump and storage decisions, lower and upper reservoir storage, and generation revenues and pumping costs are presented.

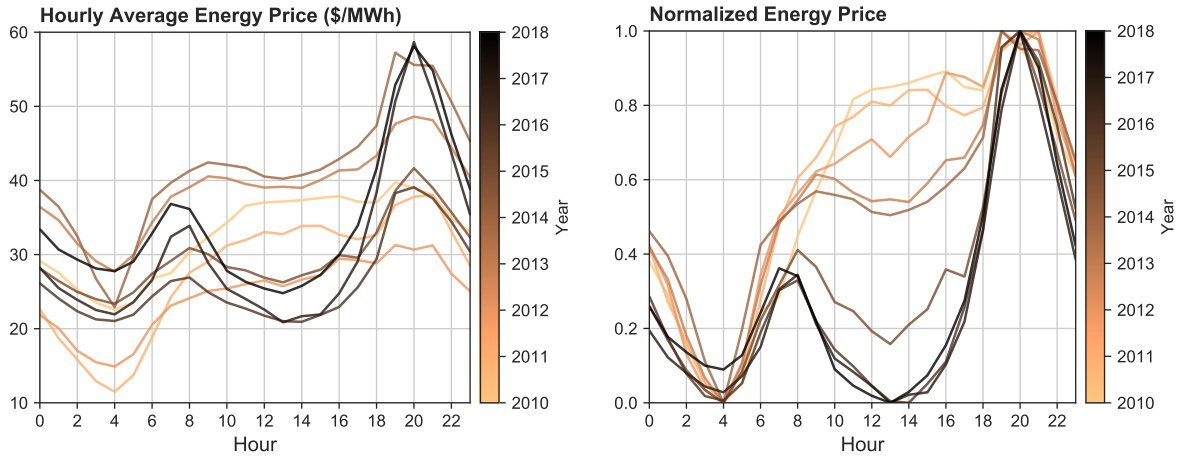

(a) Hourly average price ($/MWh)

(b) Normalized price

Figure 5.12: Hourly average and normalized energy prices from 2010 to 2018

5.5.1 Optimal Pump and Generate Decisions

PSH operations are driven solely by energy prices and efficiencies. Water is pumped at low energy prices, and energy is generated if prices are high. This low and high energy price scheme changes as solar generation increases. Years from 2010 through 2013, pumping occurs only in hours between 0-8 (Figure 5.13-(a)). As solar generation increases and energy prices decrease between 9 and 18, water is also pumped during those hours with increasing amounts, reducing pumping between hours 0-8. Between years 2010 and 2012 (1-daily cycle), before the significant solar deployment, energy is generated for longer durations between 8-23, peaking around 19-20 (Figure 5.13-(b)). While peak generation hours are the same with slight extension, generation between 10-16 is significantly reduced in the following years, and starting 2016 (2-daily cycle) once energy prices are high enough, energy is generated between 7-9 in the morning peak. Figure 5.13-

(c) combines daily pump (negative) and generate (positive) flow (m^3/s) cycles. As solar generation increases, volumes of pumped before morning peak hours decrease, morning peak generation increases, and pumping before evening peak hours increases, forming two daily off-peak and on-peak pump and storage cycles.

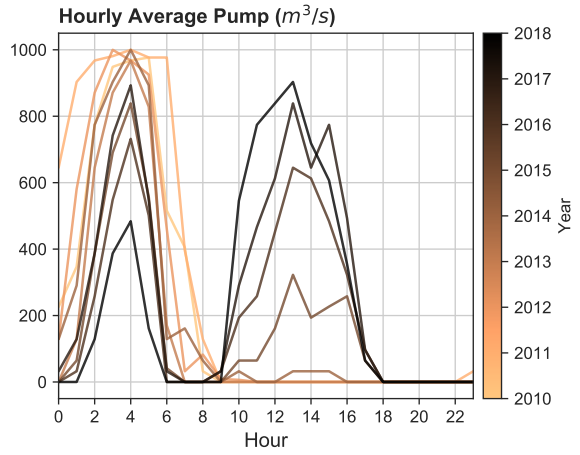

(a) Pumping hours

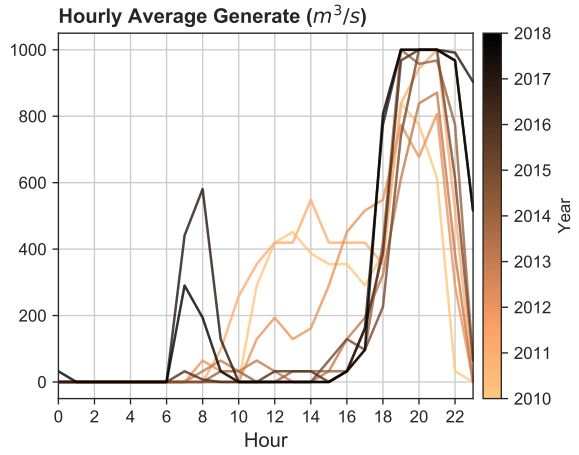

(b) Generation hours

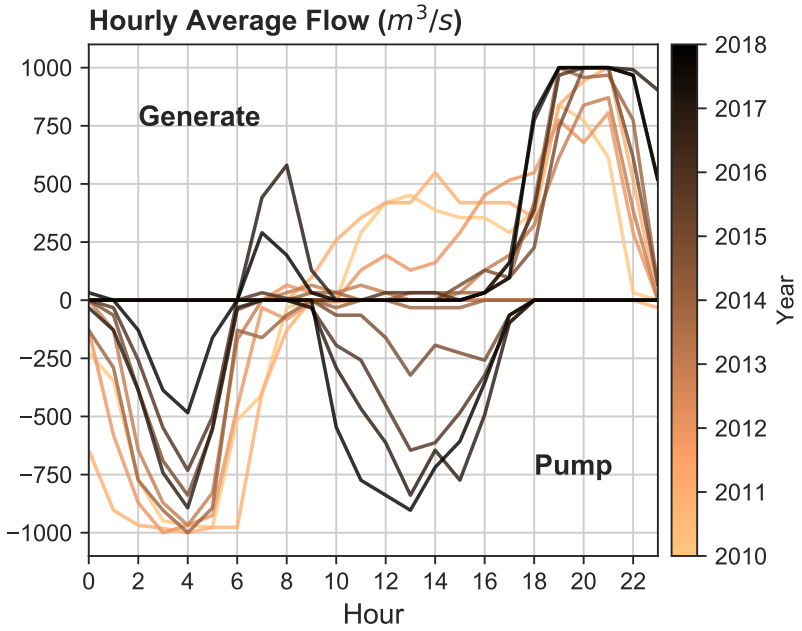

(c) Pumping (-) and generation (+) combined

Figure 5.13: Pump and generation discharges (m^3/s) and combined cycle

Figure 5.14 shows stacked percent hours of operation (pump, generate, and stop) for 1-daily (2010-2012) and 2-daily (2016-2018) cycles. With 1-daily cycle (Figure 5.14-(a)), water is mostly pumped into the upper reservoir between hours 0-8, then hydropower is

generated between hours 9-22. During transitioning hours between pumping and generation modes, such as 8-18 or 23, at about 90% of hours operations are stopped. With 2-daily cycle (Figure 5.14-(b)), water is mostly pumped between hours 0-6 and 10-16, generating hydropower in remaining hours. In this cycle, hydropower is generated at about 100% of time in hours 19-22.

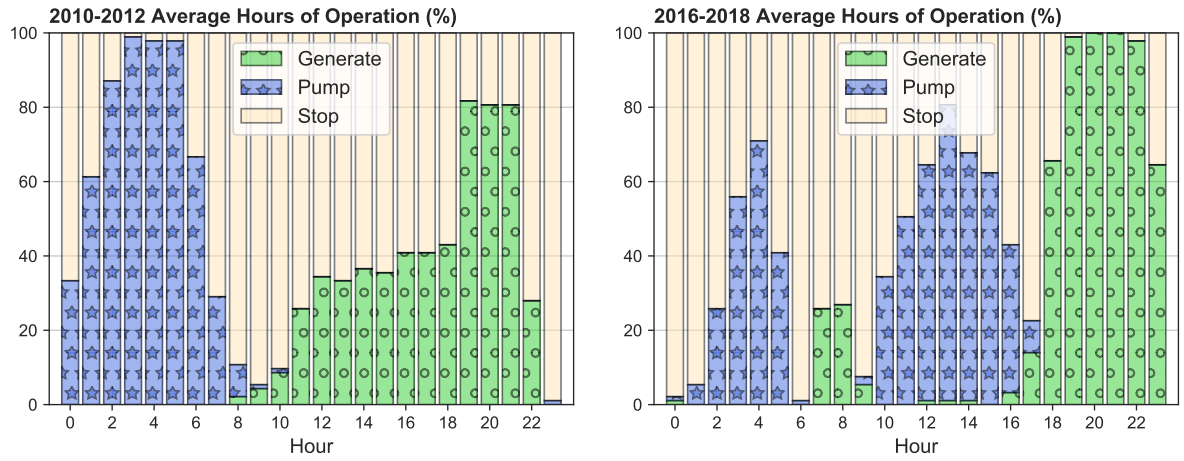

(a) 1-daily cycle (2010-2012)

(b) 2-daily cycle (2016-2018)

Figure 5.14: Hourly average stacked pumping, generation, and stopped hours (%)

5.5.2 Reservoir Storage

Energy price transformation reshapes upper and lower reservoirs' storage curves. In this PSH layout, water must be pumped into the upper reservoir to generate energy. Figure 5.15 hourly average (MCM) and normalized upper and lower reservoir storage between 2010 and 2018. The upper reservoir has single storage peaks years from 2010 through 2013, peaking hours around 6-8 before generation starts. With solar deployment, these hours become morning peak generation hours, and the storage peak shifts earlier, and second upper reservoir's storage peak arises, with a greater magnitude, around hours 15-18 before the evening peak generation starts. The lower reservoir has an opposite trend. Its storage increases with generation releases and stored inflow to be pumped later around hours 6-10, and the second peak occurs hours around 20-2. As solar deployment increases, the first lower storage peak increases, while the second decreases.

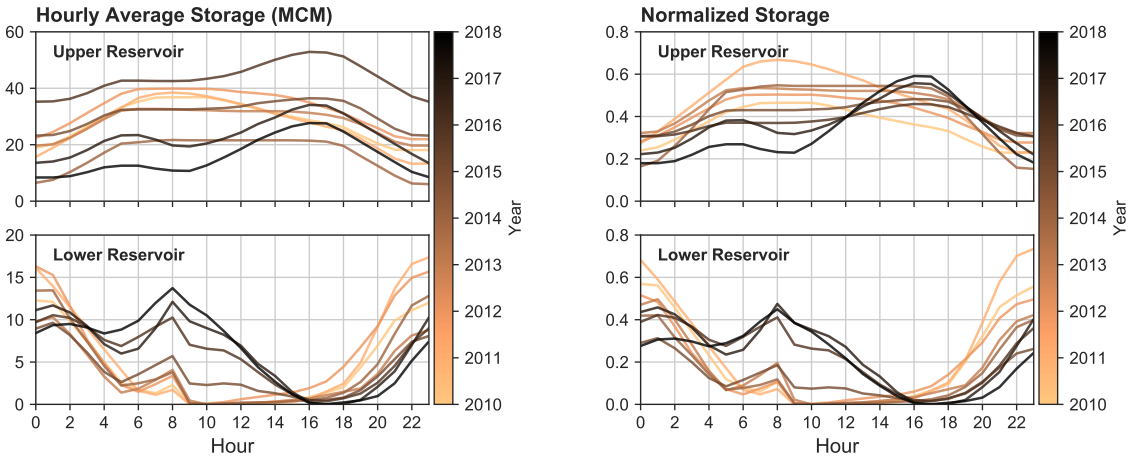

(a) Hourly average storage

(b) Normalized storage

Figure 5.15: Hourly average (MCM) and normalized storage for years from 2010 through 2018

5.5.3 Revenue and Cost

The model's objective is to maximize overall net benefits (hydropower revenue - pumping cost). Figure 5.16 hourly average hydropower revenues and pumping costs ($K) between 2010 and 2018 with adapted PSH operations to changed energy price scheme. Without solar generation effects (2010-2012), pumping costs are mostly from night hours, and generation revenue is from mid-day and evening peak hours. As solar generation increases hours between 10-18, reducing energy prices, these hours become pumping hours. Also, operations become less flexible compared to the pre-solar period of 2010-2012, focusing them in a smaller pump and generation periods, with sudden shifts between modes reflected in revenues and costs. Some transitioning hours have both pumping cost and generation revenue, which is due to averaging from longer periods. The model does not pump and generate at the same time.

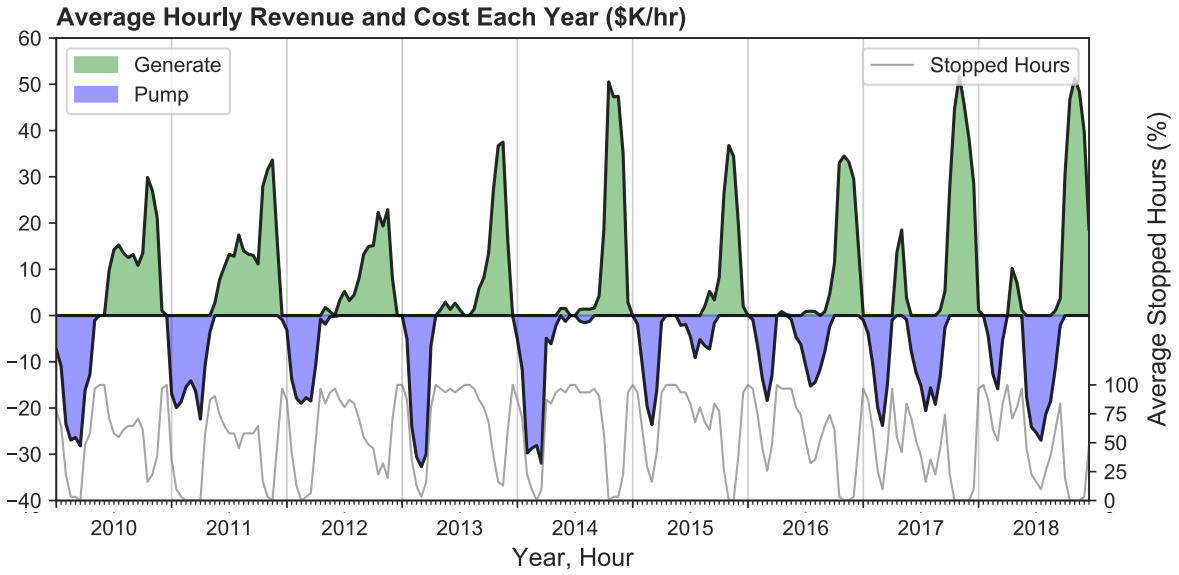

Figure 5.16: Generation revenue and pumping cost ($K) for years from 2010 through 2018

As energy prices change, hourly optimal PSH schedules and operating cycles change. Table 5.3 shows net hourly revenues ($/h) for different hours and average net daily profit ($/d). Years from 2010 through 2012 have a single daily off-peak when water is pumped, and one-peak when energy is generated. This cycle starts to transition in 2013. Generation and revenue starts to decrease in hour 13, which is the hour that solar generation peaks. Starting 2016, new two-daily off-peak and on-peak price cycle is completely formed. Although daily profits are slightly higher with 2-daily peak cycle, no significant trend is observed. There are several factors affecting daily revenue, including daily mean energy price (μ) and standard deviation (σ). Standard deviation increases the price range and has more impact than mean (compare daily net revenue of 2017 and 2018 or 2010 and 2011). When mean energy price is higher, more revenue is generated but pumping cost also increases, less affecting net revenue. Highest net revenue is generated when both daily energy price mean and standard deviation are higher.

Table 5.3: Average hourly and daily net revenue (generation revenue - pumping cost) and daily energy price mean (μ) and standard deviation (σ)

Cycle	Year	Hourly Average Net Revenue ($/h)				Daily Price ($/MWh)		Average Daily Net Revenue ($/d)
		Hour 4	Hour 8	Hour 13	Hour 20	μ	σ	
1 Daily Peak	2010	-26,375	-1,035	15,276	27,023	33	6	28,858
	2011	-14,103	-3,508	12,806	31,579	28	8	86,409
	2012	-17,766	-149	3,251	19,351	25	5	38,648
Transition	2013	-32,688	1,306	0	36,703	39	6	27,008
	2014	-28,092	-2,271	96	47,291	41	9	60,777
	2015	-23,620	0	-9,116	36,778	30	5	26,100
2 Daily Peak	2016	-18,369	196	-14,307	34,504	26	6	38,766
	2017	-23,804	18,509	-20,589	51,803	31	11	96,033
	2018	-15,866	7,051	-26,976	51,295	35	10	73,783

5.5.4 Summary

Results are summarized with normalized values for 1-daily (2010-2012) and 2-daily (2016-2018) peak cycles (Figure 5.17). As a dispatchable hydropower resource, PSH operations substantially change to adapt to new energy price pattern from solar energy generation. Between 2010 and 2012 with 1-daily cycle, the lower reservoir's storage peaks during hours between 20-2 with generation releases, while the upper reservoir's storage peaks between 6-10 hours. During this period, water is mostly pumped from hours 0 through 7, and energy is generated from 11 through 22, peaking around 20, which is also reflected in pumping costs and generation revenues. Between 2016 and 2018 after 2-daily cycle is established, upper reservoir's storage peak shifts to hours 13-18, with pumping from the lower reservoir. In this period, water is pumped twice a day; first during hours 2-5, then 10-16, the latter has much more volume and longer durations. Generation occurs in a shorter time-frame with a smaller amount between 7-8 during the morning peak, and with a much larger amount between 18-24 during the evening peak. In the 1-daily cycle period, there is roughly 3 hours between pumping and generation, and the mode changes gradually. In the 2-daily cycle period, however, this reduces to 1 hour with sudden mode changes.

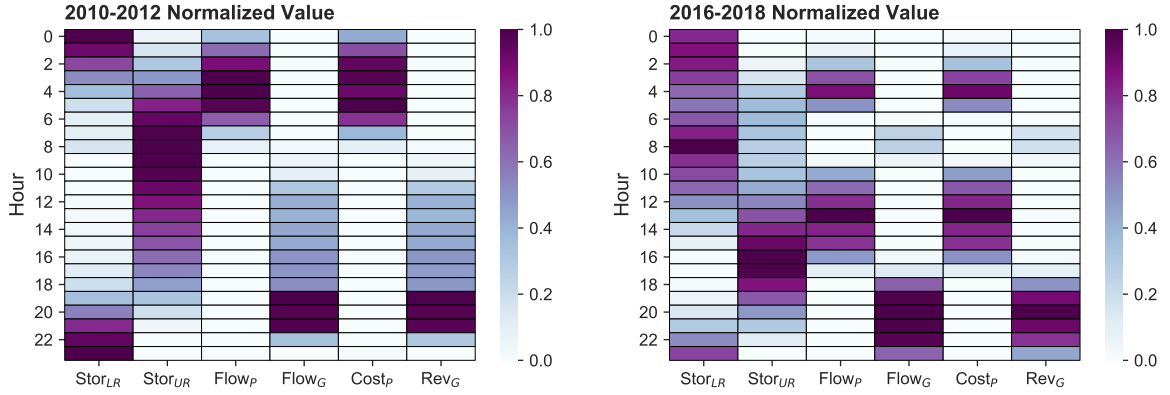

(a) 2010-2012 Average

(b) 2016-2018 Average

Figure 5.17: Summary of normalized hourly lower (LR) and upper (UR) reservoir storages, pumping (P) and generation (G) flows, and pumping costs and generation revenues for 1-daily (2010-2012) and 2-daily (2016-2018) cycles

5.6 Conclusions

Two algorithms are developed and compared for short-term PSH operations. Algorithm 1 employs a price-duration curve of a given period, such as daily, weekly, or monthly, with hourly time-step, and finds optimal pumping and generation durations and threshold prices. Pump or generate modes are triggered depending on these thresholds. An analytical solution to the problem is provided for the special case where pumping and generations discharges (1000 m^3/s) and head (100) with hourly energy prices for May 1-7, 2018. Algorithm 1 is driven by energy prices and efficiencies, without considering

water mass balance, assuming there is enough water storage in the lower and upper reservoirs to pump and generate. Algorithm 2 uses a reservoir systems modeling approach to determine pumping and generation quantities in addition to the timing, accounting for mass balance. Both algorithms have perfect energy price foresight and algorithm 2 has perfect hydrologic knowledge. Algorithm 1 and 2 decisions converge for cases where energy price fluctuations are low and the hourly price pattern repeats. The reduced analytical solution of algorithm 1 simplifies PSH operating rules if pumping and generation heads and discharges are the same. Then algorithm 2 is used to evaluate solar deployment effects and energy price transformations on PSH operations in California between 2010 and 2018. The model is run for each year in the range. Before the solar generation, the optimal PSH operating strategy is to pump into upper reservoir at night, and generate energy during daytime, peaking in the evening. However, as solar generation reduces energy prices between 9-18, these hours are no longer profitable for generation, but favorable for pumping, creating two-daily pumping and generation cycles.

Chapter 6

Overall Conclusions and Future Directions

This dissertation used hydropower reservoir optimization modeling to evaluate effects of changed energy prices from solar deployment on short-term hydropower operations and climate change impacts on long-term hydropower planning and management. Additional algorithms are developed and compared for pumped-storage hydropower (PSH) optimization, and energy price effects on PSH operation cycles are studied. Key concluding points, corresponding to each chapter, include:

1. Initialization with LP reduces NLP iterations and runtime by 80%. The developed hybrid LP-NLP hydropower optimization model can be efficiently used for short-term hydropower operations with hourly time-step and long-term hydropower planning with monthly time-step. LP model provides a good initial starting point for the NLP model. The number of NLP iterations and runtime can be significantly reduced with 'warmstart' from the LP solution. For long-term planning with a large number of decision variables, LP model is more favorable as NLP model's runtime increases exponentially. Besides, uncertainties in reservoir inflows outweigh accuracy losses from linearization in the long-term.

2. Solar energy development and changed energy price patterns substantially change dispatchable hydropower reservoir operations. Hours with more solar energy generation become less valuable, so hydropower is not generated during these hours, but stored for later use. In the wet season, energy is generated twice a day, during the morning and evening peak hours. In the dry season with less inflow and higher evening energy prices, operations mostly concentrate on the evening peak hours with increased ramping rates.

3. Climate change reduces snowmelt runoff in the spring and increases precipitation as rainfall in the winter, with increased intensities and frequencies. Hydropower plants with large-storage capacities capture some of increased winter inflows and increase hydropower generation. But, spring and early summer hydropower generations significantly reduce. Lacking storage capacity flexibility and adaptation, plants with

smaller storage capacity and run-of-river hydropower plants are more affected inflow uncertainties. Although the ensemble mean hydropower revenue is slightly higher, the ensemble median revenue is close to the historical average revenue, with current monthly average energy prices. Increased fall and winter hydropower revenues help compensate for reduced spring and summer revenues.

4. Two developed algorithms optimize PSH decisions of when to pump and generate to maximize net profit. The analytical solution (algorithm 1) provides fast and approximate solution to the PSH optimization problem of deciding when to pump and generate to maximize net revenue and help meet peak demands, while the numerical optimization solution (algorithm 2) is more detailed and provides a more complete solution. As a result of solar development and transformed energy prices, PSH pumping and generation cycles change. Water is pumped into the upper reservoir hours from 2 through 5 and 10 through 16, and energy is generated hours from 7 through 8 and 18 through 23.

Climate change affects hydropower revenue by shifting temporal and spatial water availability, increasing revenue in fall and winter and decreasing in spring and summer. Management policies also affect hydropower revenue. With solar generation, hydropower revenue increases during the morning and evening peak hours and decreases during hours when solar generation peaks. Combining management policies and climatic changes with optimization and adaptive management, limited spring and summer generation can be allocated to more valuable hours, reducing negative effects of climate change. PSH also benefits from increased solar generation. Increased price range and variability with more solar generation results in more PSH revenue.

The hybrid model, where the NLP model is initialized with LP solutions, reduces the NLP model's runtime by 80%, but this can be further reduced if a better initial solution is provided, with piecewise LP or successive LP, where objective function differences (Figure 2.4-(b)) are smaller than LP. With the current trend and management policies, solar generation will increase to meet RPS target of 50% by 2030. This will continue to deepen the belly of the 'duck curve,' reducing energy prices during solar generation hours. Quantifying effects of further increased solar generation on hydropower reservoir operation, including hydropower with large storage capacity and PSH, and identifying adaptations will be useful. With the new energy price scheme, the model suggests large pulse releases in a short duration of time. Compromising hydropower and ecological benefits will be worthy. Studying effects of climate change can be expanded to other regions to include more plants. Exploring these effects on different types of hydropower, such as run-of-river and PSH, will make this study more completel. Constant efficiencies are assumed for hydropower optimization modeling, but implementing varying efficiencies with release decisions can improve result accuracy, especially for PSH, where operations are directly affected by system efficiencies. Implementing limited hydrologic foresight with a sequential annual optimization can help better quantify hydropower generation during extreme hydrologic events, especially for long-term decisions. Variable head functions can be applied to PSH for better system representation. Algorithm 1 assumes the same operating duration and flow quantity for pumping and generation. But, it can be modified to

operate at different durations and flow quantities, which can minimize differences between two algorithms.

References

Afshar, A., Jemaa, F. B., & Mariño, M. A. (1990). Optimization of Hydropower Plant Integration in Water Supply System. *Journal of Water Resources Planning and Management*, *116*(5), 665–675. doi: 10.1061/(ASCE)0733-9496(1990)116:5(665)

Ahmad, A., El-Shafie, A., Mohd Razali, S. F., & Mohamad, Z. S. (2014). Reservoir optimization in water resources: A review. *Water Resources Management*, *28*(11), 3391–3405. doi: 10.1007/s11269-014-0700-5

Ahmadi, M., Haddad, O. B., & Loáiciga, H. A. (2014). Adaptive Reservoir Operation Rules Under Climatic Change. *Water Resources Management*, *29*(4), 1247–1266. doi: 10.1007/s11269-014-0871-0

Anderson, D., Moggridge, H., Warren, P., & Shucksmith, J. (2015). The impacts of 'run-of-river' hydropower on the physical and ecological condition of rivers. *Water and Environment Journal*, *29*(2), 268–276. doi: 10.1111/wej.12101

Andersson, A. M., Elverhøi, M., Fleten, S. E., Fuss, S., Szolgayová, J., & Troland, O. C. (2014). Upgrading hydropower plants with storage: Timing and capacity choice. *Energy Systems*, *5*(2), 233–252. doi: 10.1007/s12667-013-0112-2

ASCE Hydropower Commitee. (1989). *Civil Engineering Guidelines for Planning and Designing Hydroelectric Developments: Volume 5. Pumped Storage and Tidal Power*. New York: ASCE.

Barbour, E., Wilson, I. A., Radcliffe, J., Ding, Y., & Li, Y. (2016). A review of pumped hydro energy storage development in significant international electricity markets. *Renewable and Sustainable Energy Reviews*, *61*, 421–432. doi: 10.1016/j.rser.2016.04.019

Bazaraa, M. S., Jarvis, J. J., & Sherali, H. D. (2010). *Linear Programming and Network Flows* (Fourth ed.). Hoboken, New Jersey: John Wiley & Sons, Inc.

Bedsworth, L., Cayan, D., Franco, G., Fisher, L., & Ziaja, S. (2018). *Statewide Summary Report. California's Fourth Climate Change Assessment* (Tech. Rep. No. SUM-CCCA4-2018-013). California Energy Commission. Retrieved from `http://www.climateassessment.ca.gov`

Boehlert, B., Strzepek, K. M., Gebretsadik, Y., Swanson, R., McCluskey, A., Neumann, J. E., ... Martinich, J. (2016). Climate change impacts and greenhouse gas mitigation effects on U.S. hydropower generation. *Applied Energy*, *183*, 1511–1519. doi: 10.1016/j.apenergy.2016.09.054

Bozorg Haddad, O., Ashofteh, P.-s., Rasoulzadeh-Gharibdousti, S., & Mariño, M. A. (2014). Optimization Model for Design-Operation of Pumped-Storage and Hydropower Systems. *Journal of Energy Engineering*, *140*(2), 04013016. doi: 10.1061/(ASCE)EY.1943-7897.0000169

Bratrich, C., Truffer, B., Jorde, K., Markard, J., Meier, W., Peter, A., ... Wehrli, B. (2004). Green hydropower: A new assessment procedure for river management. *River Research and Applications*, *20*(7), 865–882. doi: 10.1002/rra.788

Braun, S., & Hoffmann, R. (2016). Intraday Optimization of Pumped Hydro Power Plants in the German Electricity Market. *Energy Procedia*, *87*, 45–52. doi: 10.1016/j.egypro.2015.12.356

Breiman, L. (2001). Random forests. *Machine Learning*, *45*(1), 5–32. doi: 10.1023/A:1010933404324

Brekke, L. D., Maurer, E. P., Anderson, J. D., Dettinger, M. D., Townsley, E. S., Harrison, A., & Pruitt, T. (2009). Assessing reservoir operations risk under climate change. *Water Resources Research*, *45*(4), 1–16. doi: 10.1029/2008WR006941

Bushnell, J. (2003). A Mixed Complementarity Model of Hydrothermal Electricity Competition in the Western United States. *Operations Research*, *51*(1), 80–93. doi: 10.1287/opre.51.1.80.12800

CAISO. (2018a). *Company Information and Facts.* Retrieved 2018-08-25, from `http://www.caiso.com/about/Pages/OurBusiness/Default.aspx`

CAISO. (2018b). *Locational marginal energy price data.* Retrieved 2018-02-26, from `http://www.caiso.com`

Cal-Adapt. (2018). *Climate and streamflow dataset.* Retrieved 2018-07-11, from `http://cal-adapt.org`

California Data Exchange Center. (2018). *Observed reservoir storage and elevation data.* Retrieved 2018-07-11, from `http://cdec.water.ca.gov`

California Energy Commision. (2017). *The 2017 Integrated Energy Policy Report* (Tech. Rep. No. CEC-100-2017-001-CMF). Sacramento, CA: California Energy Commission. Retrieved from `https://www.energy.ca.gov/2017_energypolicy/`

California Energy Commision. (2018). *Installed In-State Electric Generation Capacity and Generation by Fuel Type.* Retrieved 2018-05-10, from `http://www.energy.ca.gov/almanac/electricity_data/electric_generation_capacity.html`

Cayan, D. R., Maurer, E. P., Dettinger, M. D., Tyree, M., & Hayhoe, K. (2008). Climate change scenarios for the California region. *Climatic Change*, *87*(1). doi: 10.1007/s10584-007-9377-6

Chang, M. K., Eichman, J. D., Mueller, F., & Samuelsen, S. (2013). Buffering intermittent renewable power with hydroelectric generation: A case study in California. *Applied Energy*, *112*, 1–11. doi: 10.1016/j.apenergy.2013.04.092

Chatterjee, B., Howitt, R. E., & Sexton, R. J. (1998). The optimal joint provision of water for irrigation and hydropower. *Journal of Environmental Economics and Management*, *36*(3), 295–313. doi: 10.1006/jeem.1998.1047

Connell-Buck, C. R., Medellín-Azuara, J., Lund, J. R., & Madani, K. (2011). Adapting California's water system to warm vs. dry climates. *Climatic Change*, *109*(1), 133–149. doi: 10.1007/s10584-011-0302-7

Côté, P., & Leconte, R. (2016). Comparison of Stochastic Optimization Algorithms for Hydropower Reservoir Operation with Ensemble Streamflow Prediction. *Journal of Water Resources Planning and Management*, *142*(2), 04015046. doi: 10.1061/(ASCE)WR.1943-5452.0000575

Denholm, P., O'Connell, M., Brinkman, G., & Jorgenson, J. (2015). *Overgeneration from Solar Energy in California. A Field Guide to the Duck Chart* (Tech. Rep. No. NREL/TP-6A20-65023). National Renewable Energy Laboratory. Retrieved from `http://www.osti.gov/servlets/purl/1226167/` doi: 10.2172/1226167

Dettinger, M. (2016). Historical and Future Relations Between Large Storms and Droughts in California. *San Francisco Estuary and Watershed Science*, *14*(2), 1–21.

doi: 10.15447/sfews.2016v14iss2art2

Dogan, M. S., Fefer, M. A., Herman, J. D., Hart, Q. J., Merz, J. R., Medellín-Azuara, J., & Lund, J. R. (2018). An open-source Python implementation of California's hydroeconomic optimization model. *Environmental Modelling & Software*, *108*, 8–13. doi: 10.1016/j.envsoft.2018.07.002

Draper, A. J., Jenkins, M. W., Kirby, K. W., Lund, J. R., & Howitt, R. E. (2003). Economic-Engineering Optimization for California Water Management. *Journal of Water Resources Planning and Management*, *129*(3), 155–164. doi: 10.1061/(ASCE)0733-9496(2003)129:3(155)

Draper, A. J., Munévar, A., Arora, S. K., Reyes, E., Parker, N. L., Chung, F. I., & Peterson, L. E. (2004). CalSim: Generalized Model for Reservoir System Analysis. *Journal of Water Resources Planning and Management*, *130*(6), 480–489. doi: 10.1061/(ASCE)0733-9496(2004)130:6(480)

Eichman, J. D., Mueller, F., Tarroja, B., Schell, L. S., & Samuelsen, S. (2013). Exploration of the integration of renewable resources into California's electric system using the Holistic Grid Resource Integration and Deployment (HiGRID) tool. *Energy*, *50*(1), 353–363. doi: 10.1016/j.energy.2012.11.024

Faber, B. A., & Stedinger, J. R. (2001). Reservoir optimization using sampling SDP with ensemble streamflow prediction (ESP) forecasts. *Journal of Hydrology*, *249*, 113–133. doi: 10.1016/S0022-1694(01)00419-X

Feng, Z.-k., Niu, W.-j., Cheng, C.-t., & Wu, X.-y. (2017). Optimization of hydropower system operation by uniform dynamic programming for dimensionality reduction. *Energy*, *134*, 718–730. doi: 10.1016/j.energy.2017.06.062

Figueiredo, F. C., & Flynn, P. C. (2006). Using diurnal power price to configure pumped storage. *IEEE Transactions on Energy Conversion*, *21*(3), 804–809. doi: 10.1109/TEC.2006.877373

Forrest, K., Tarroja, B., Chiang, F., AghaKouchak, A., & Samuelsen, S. (2018). Assessing climate change impacts on California hydropower generation and ancillary services provision. *Climatic Change*. doi: 10.1007/s10584-018-2329-5

Free Software Foundation. (2019). *GNU Linear Programming Kit Reference Manual for GLPK Version 4.65.* Retrieved 2019-03-10, from `https://www.gnu.org/software/glpk/`

Garrido, J., Zafra, Á., & Vázquez, F. (2009). Object oriented modelling and simulation of hydropower plants with run-of-river scheme: A new simulation tool. *Simulation Modelling Practice and Theory*, *17*(10), 1748–1767. doi: 10.1016/j.simpat.2009.08.007

Grygier, J. C., & Stedinger, J. R. (1985). Algorithms for Optimizing Hydropower System Operation. *Water Resources Research*, *21*(1), 1–10. doi: 10.1029/WR021i001p00001

Hamlet, A. F., Huppert, D., & Lettenmaier, D. P. (2002). Economic Value of Long-Lead Streamflow Forecasts for Columbia River Hydropower. *Journal of Water Resources Planning and Management*, *128*(2), 91–101. doi: 10.1061/(ASCE)0733-9496(2002)128:2(91)

Hanak, E., & Lund, J. R. (2012). Adapting California's water management to climate

change. *Climatic Change*, *111*(1), 17–44. doi: 10.1007/s10584-011-0241-3

Hart, W. E., Laird, C. D., Watson, J.-P., Woodruff, D. L., Hackebeil, G. A., Nicholson, B. L., & Siirola, J. D. (2017). *Pyomo Optimization Modeling in Python* (Vol. 67). Cham: Springer International Publishing. doi: 10.1007/978-3-319-58821-6

Herman, J., Fefer, M., Dogan, M. S., Jenkins, M., & Lund, J. (2018). *Advancing Hydro-Economic Optimization to Identify Vulnerabilities and Adaptation Opportunities in California's Water System* (Tech. Rep. No. CCCA4-CNRA-2018-016). California Natural Resources Agency. Retrieved from `http://www.climateassessment.ca.gov`

Hui, R., Herman, J., Lund, J., & Madani, K. (2018). Adaptive water infrastructure planning for nonstationary hydrology. *Advances in Water Resources*, *118*(May), 83–94. doi: 10.1016/j.advwatres.2018.05.009

Karimanzira, D., Schwanenberg, D., Allen, C., & Barton, S. (2016). Short-Term Hydropower Optimization and Assessment of Operational Flexibility. *Journal of Water Resources Planning and Management*, *142*(2), 04015048. doi: 10.1061/(ASCE)WR.1943-5452.0000577

Kelman, J., Stedinger, J. R., Cooper, L. A., Hsu, E., & Yuan, S.-Q. (1990). Sampling stochastic dynamic programming applied to reservoir operation. *Water Resources Research*, *26*(3), 447–454. doi: 10.1029/WR026i003p00447

Kim, K., Park, T., Bang, S., & Kim, H. (2017). Real Options-Based Framework for Hydropower Plant Adaptation to Climate Change. *Journal of Management in Engineering*, *33*(3). doi: 10.1061/(ASCE)ME.1943-5479.0000496

Kim, Y., & Palmer, R. N. (1997). Value of seasonal flow forecasts in Bayesian stochastic programming. *Journal of Water Resources Planning and Management*, *123*(6), 327–335. doi: 10.1061/(ASCE)0733-9496(1997)123:6(327)

Kopytkovskiy, M., Geza, M., & McCray, J. E. (2015). Climate-change impacts on water resources and hydropower potential in the Upper Colorado River Basin. *Journal of Hydrology: Regional Studies*, *3*, 473–493. doi: 10.1016/j.ejrh.2015.02.014

Kougias, I., & Szabó, S. (2017). Pumped hydroelectric storage utilization assessment: Forerunner of renewable energy integration or Trojan horse? *Energy*, *140*, 318–329. doi: 10.1016/j.energy.2017.08.106

Labadie, J. W. (2004). Optimal Operation of Multireservoir Systems: State-of-the-Art Review. *Journal of Water Resources Planning and Management*, *130*(2), 93–111. doi: 10.1061/(ASCE)0733-9496(2004)130:2(93)

Labouret, A., & Villoz, M. (2010). *Solar Photovoltaic Energy* (Fourth ed.). London, United Kingdom: The Institution of Engineering and Technology.

Lanini, J. S., Dozier, A. Q., Furey, P. R., & Kampf, S. K. (2014). Stochastic Method for Examining Vulnerability of Hydropower Generation and Reservoir Operations to Climate Change: Case Study of the Dworshak Reservoir in Idaho. *Journal of Water Resources Planning and Management*, *140*(9). doi: 10.1061/(ASCE)WR.1943-5452.0000426

Lazzaro, G., & Botter, G. (2015). Run-of-river power plants in Alpine regions: Whither optimal capacity? *Water Resources Research*, *51*, 9127–9140. doi: 10.1002/2014WR016259

Lettenmaier, D. P., & Sheer, D. P. (1991). Climatic sensitivity of California water resources. *Journal of Water Resources Planning and Management*, *117*(1), 108–125. doi: 10.1061/(ASCE)0733-9496(1991)117:1(108)

Li, J. Q., Mariño, M. A., Ji, C. M., & Zhang, Y. S. (2009). Mathematical models of interplant economical operation of a cascade hydropower system in electricity market. *Water Resources Management*, *23*(10), 2003–2013. doi: 10.1007/s11269-008-9365-2

Li, J. Q., Zhang, Y. S., Ji, C. M., Wang, A. J., & Lund, J. R. (2013). Large-scale hydropower system optimization using dynamic programming and object-oriented programming: the case of the Northeast China Power Grid. *Water Science & Technology*, *68*(11), 2458. doi: 10.2166/wst.2013.528

Liang, X., Lettenmaier, D. P., Wood, E. F., & Burges, S. J. (1994). A simple hydrologically based model of land surface water and energy fluxes for general circulation models. *Journal of Geophysical Research*, *99*(D7), 14415. doi: 10.1029/94JD00483

Lin, Q. G., Huang, G. H., Li, G. C., & Li, J. B. (2013). Dynamic Planning of Water Resource and Electric Power Systems under Uncertainty. *Journal of Water Resources Planning and Management*, *139*(4), 407–417. doi: 10.1061/(ASCE)WR.1943-5452.0000285

Lu, N., Chow, J. H., & Desrochers, A. A. (2004). Pumped-storage hydro-turbine bidding strategies in a competitive electricity market. *IEEE Transactions on Power Systems*, *19*(2), 834–841. doi: 10.1109/TPWRS.2004.825911

Lund, J. R., & Ferreira, I. (1996). Operating Rule Optimization for Missouri River Reservoir System. *Journal of Water Resources Planning and Management*, *122*(4), 287–295. doi: 10.1061/(ASCE)0733-9496(1996)122:4(287)

Lund, J. R., & Moyle, P. (2013). Adaptive Management and Science for the Delta Ecosystem. *San Francisco Estuary and Watershed Science*, *11*(3), 0–6.

Madani, K., Guégan, M., & Uvo, C. B. (2014). Climate change impacts on high-elevation hydroelectricity in California. *Journal of Hydrology*, *510*, 153–163. doi: 10.1016/j.jhydrol.2013.12.001

Madani, K., & Lund, J. R. (2009). Modeling California's high-elevation hydropower systems in energy units. *Water Resources Research*, *45*(9), 1–12. doi: 10.1029/2008WR007206

Mariño, M. A., & Loaiciga, H. A. (1985). Dynamic model for multireservoir operation. *Water Resources Research*, *21*(5), 619–630. doi: 10.1029/WR021i005p00619

Martin, Q. W. (1983). Optimal Operation of Multiple Reservoir Systems. *Journal of Water Resources Planning and Management*, *109*(1), 58–74. doi: 10.1061/(ASCE)0733-9496(1983)109:1(58)

Medellín-Azuara, J., Harou, J. J., Olivares, M. A., Madani, K., Lund, J. R., Howitt, R. E., ... Zhu, T. (2008). Adaptability and adaptations of California's water supply system to dry climate warming. *Climatic Change*, *87*(S1), 75–90. doi: 10.1007/s10584-007-9355-z

Miller, N. L., Bashford, K. E., & Strem, E. (2003). Potential Impacts of Climate Change on California Hydrology. *Journal of the American Water Resources Association*, *39*(4), 771–784. doi: 10.1111/j.1752-1688.2003.tb04404.x

Mukheibir, P. (2013). Potential consequences of projected climate change impacts on hydroelectricity generation. *Climatic Change*, *121*(1), 67–78. doi: 10.1007/s10584-013-0890-5

Murk, N. B. (1996). *Application of HEC-PRM for Seasonal Reservoir Operation of the Columbia River System* (Tech. Rep. No. RD-43). Davis, CA: US Army Corps of Engineers, Hydrologic Engineering Center. Retrieved from `https://www.hec.usace.army.mil/publications/ResearchDocuments/RD-43.pdf`

Nover, D., Dogan, M. S., Ragatz, R., Booth, L., Medellín-Azuara, J., Lund, J., & Viers, J. (2019). Does More Storage Give California More Water? *JAWRA Journal of the American Water Resources Association*, 1-13. doi: 10.1111/1752-1688.12745

Olivares, M. A., & Lund, J. R. (2012). Representing Energy Price Variability in Long- and Medium-Term Hydropower Optimization. *Journal of Water Resources Planning and Management*, *138*(6), 606–613. doi: 10.1061/(ASCE)WR.1943-5452.0000214

Pereira, M. V. F., & Pinto, L. M. V. G. (1985). Stochastic Optimization of a Multireservoir Hydroelectric System: A Decomposition Approach. *Water Resources Research*, *21*(6), 779–792. doi: 10.1029/WR021i006p00779

Pérez-Díaz, J. I., Chazarra, M., García-González, J., Cavazzini, G., & Stoppato, A. (2015). Trends and challenges in the operation of pumped-storage hydropower plants. *Renewable and Sustainable Energy Reviews*, *44*, 767–784. doi: 10.1016/j.rser.2015.01.029

Pérez-Díaz, J. I., & Wilhelmi, J. R. (2010). Assessment of the economic impact of environmental constraints on short-term hydropower plant operation. *Energy Policy*, *38*(12), 7960–7970. doi: 10.1016/j.enpol.2010.09.020

PGE. (2019). *Electric Rates.* Retrieved 2019-02-22, from `https://www.pge.com/tariffs/electric.shtml#RESELEC`

Pick, J. B. (2017). *Renewable Energy: Problems and Prospects in Coachella Valley, California*. Cham, Switzerland: Springer International Publishing. doi: 10.1007/978-3-319-51526-7

Pierce, D. W., Cayan, D. R., & Thrasher, B. L. (2014). Statistical Downscaling Using Localized Constructed Analogs (LOCA)*. *Journal of Hydrometeorology*, *15*(6), 2558–2585. doi: 10.1175/JHM-D-14-0082.1

Pierce, D. W., Kalansky, J. F., & Cayan, D. R. (2018). *Climate, Drought, and Sea Level Rise Scenarios for the Fourth California Climate Assessment* (Tech. Rep. No. CNRA-CEC-2018-006). California Energy Commission. Retrieved from `www.climateassessment.ca.gov`

Rangarajan, S., & Simonovic, S. P. (1999). The Value of Considering Autocorrelation Between Inflows in the Stochastic Planning of Water Resource Systems. *Water Resources Management*, *13*, 427–442. doi: 10.1023/A:1008198130175

Rheinheimer, D. E., Bales, R. C., Oroza, C. A., Lund, J. R., & Viers, J. H. (2016). Valuing year-to-go hydrologic forecast improvements for a peaking hydropower system in the Sierra Nevada. *Water Resources Research*, *52*(5), 3815–3828. doi: 10.1002/2015WR018295

Rheinheimer, D. E., & Viers, J. H. (2015). Combined Effects of Reservoir Operations and Climate Warming on the Flow Regime of Hydropower Bypass Reaches of Cal-

ifornia's Sierra Nevada. *River Research and Applications*, *31*(3), 269–279. doi: 10.1002/rra.2749

Rheinheimer, D. E., Viers, J. H., Sieber, J., Kiparsky, M., Mehta, V. K., & Ligare, S. T. (2014). Simulating High-Elevation Hydropower with Regional Climate Warming in the West Slope, Sierra Nevada. *Journal of Water Resources Planning and Management*, *140*(5), 714–723. doi: 10.1061/(ASCE)WR.1943-5452.0000373

Srivastava, A. K., Kamalasadan, S., Patel, D., Sankar, S., & Al Olimat, K. S. (2011). Electricity markets: an overview and comparative study. *International Journal of Energy Sector Management*, *5*(2), 169–200. doi: 10.1108/17506221111145977

Swain, D. L., Langenbrunner, B., Neelin, J. D., & Hall, A. (2018). Increasing precipitation volatility in twenty-first-century California. *Nature Climate Change*, *8*(5), 427–433. doi: 10.1038/s41558-018-0140-y

Tang, G., Zhou, H., Li, N., Wang, F., Wang, Y., & Jian, D. (2010). Value of Medium-range Precipitation Forecasts in Inflow Prediction and Hydropower Optimization. *Water Resources Management*, *24*(11), 2721–2742. doi: 10.1007/s11269-010-9576-1

Tejada-Guibert, J. A., Johnson, S. A., & Stedinger, J. R. (1995). The Value of Hydrologic Information in Stochastic Dynamic Programming Models of a Multireservoir System. *Water Resources Research*, *31*(10), 2571–2579. doi: 10.1029/95WR02172

Tejada-Guibert, J., Stedinger, J., & Staschus, K. (1990). Optimization of Value of CVP's Hydropower Production. *Journal of Water Resources Planning and Management*, *116*(1), 52–70. doi: 10.1061/(ASCE)0733-9496(1990)116:1(52)

Trezos, T., & Yeh, W. W.-G. (1987). Use of stochastic dynamic programming for reservoir management. *Water Resources Research*, *23*(6), 983–996. doi: 10.1029/WR023i006p00983

Turgeon, A. (2007). Stochastic optimization of multireservoir operation: The optimal reservoir trajectory approach. *Water Resources Research*, *43*(5), 1–10. doi: 10.1029/2005WR004619

Vicuna, S., Dracup, J. A., & Dale, L. (2011). Climate change impacts on two high-elevation hydropower systems in California. *Climatic Change*, *109*, 151–169. doi: 10.1007/s10584-011-0301-8

Vicuna, S., Dracup, J. A., Lund, J. R., Dale, L. L., & Maurer, E. P. (2010). Basin-scale water system operations with uncertain future climate conditions: Methodology and case studies. *Water Resources Research*, *46*(4), 1–19. doi: 10.1029/2009WR007838

Vicuna, S., Maurer, E., Joyce, B., Dracup, J., & Purkey, D. (2007). The sensitivity of California water resources to climate change scenarios. *Journal of the American Water Resources Association*, *43*(2). doi: 10.1111/j.1752-1688.2007.00038.x

Viers, J. H. (2011). Hydropower relicensing and climate change. *Journal of the American Water Resources Association*, *47*(4), 655–661. doi: 10.1111/j.1752-1688.2011.00531.x

Wächter, A., & Biegler, L. T. (2006). On the implementation of an interior-point filter line-search algorithm for large-scale nonlinear programming. *Mathematical Programming*, *106*(1), 25–57. doi: 10.1007/s10107-004-0559-y

Wang, L., Wang, B., Zhang, P., Liu, M., & Li, C. (2017). Study on optimization of the short-term operation of cascade hydropower stations by considering output error.

Journal of Hydrology, *549*, 326–339. doi: 10.1016/j.jhydrol.2017.03.074

Wood, A. J., & Wollenberg, B. F. (1996). *Power Generation, Operation, and Control* (Second ed.). New York: John Wiley & Sons, Inc.

Wu, X., Cheng, C., Zeng, Y., & Lund, J. R. (2016). Centralized versus Distributed Cooperative Operating Rules for Multiple Cascaded Hydropower Reservoirs. *Journal of Water Resources Planning and Management*, *142*(11), 05016008. doi: 10.1061/(ASCE)WR.1943-5452.0000685

Wurbs, R. A. (1993). Reservoir System Simulation and Optimization Models. *Journal of Water Resources Planning and Management*, *119*(4), 455–472. doi: 10.1061/(ASCE)0733-9496(1993)119:4(455)

Yakowitz, S. (1982). Dynamic programming applications in water resources. *Water Resources Research*, *18*(4), 673–696. doi: 10.1029/WR018i004p00673

Yang, C.-J. (2016). Pumped Hydroelectric Storage. In *Storing energy* (pp. 25–38). Elsevier. doi: 10.1016/B978-0-12-803440-8.00002-6

Yeh, W. W.-G. (1985). Reservoir Management and Operations Models: A State-of-the-Art Review. *Water Resources Research*, *21*(12), 1797–1818. doi: 10.1029/WR021i012p01797

Zhao, T., Zhao, J., & Yang, D. (2012). Improved dynamic programming for hydropower reservoir operation. *Journal of Water Resources Planning and Management*, *140*(March), 365–374. doi: 10.1061/(ASCE)WR.1943-5452.0000343

Ziaja, S. F. P. (2017). Rules and Values in Virtual Optimization of California Hydropower. *Natural Resources Journal*, *57*(2), 329–360.